RIJKSUNIVERSITEIT TE GRONINGEN

TRITIUM BETA POLARIZATION

PROEFSCHRIFT

TER VERKRIJGING VAN HET DOCTORAAT IN DE
WISKUNDE EN NATUURWETENSCHAPPEN
AAN DE RIJKSUNIVERSITEIT TE GRONINGEN
OP GEZAG VAN DE RECTOR MAGNIFICUS DR. M. J. JANSSEN
IN HET OPENBAAR TE VERDEDIGEN OP VRIJDAG 21 OKTOBER 1977
DES NAMIDDAGS TE 4 UUR

DOOR

FRANCISCUS WILHELMUS JOZEF KOKS
geboren te Wezep

VRB drukkerijen bv - Groningen

PROMOTOR: Prof.dr. H. de Waard

REFERENT: dr. J. van Klinken

Tekeningen: *B. Kamps*

Lay-out: *Willy Smeenge*

This work was performed as part of the research program of the "Stichting voor Fundamenteel Onderzoek der Materie" (FOM) with financial support from the "Nederlandse Organisatie voor Zuiver Wetenschappelijk Onderzoek" (ZWO).

CONTENTS

SYNOPSIS

This thesis deals with an experimental investigation of the longitudinal polarization of β-particles at low velocities. The measurements were performed with β^--particles from the allowed decay of tritium.

In the years after the fall of parity in 1956, a firm belief has grown in the so called (V-λA)-form of the β-interaction and in the validity of the two-component neutrino theory with left-handed neutrinos. The latter theory implies the equality of the "parity-conserving" and the "parity-violating" coupling constants in the interaction hamiltonian: $C_V = C'_V$ for vector interaction and $C_A = C'_A$ for axial-vector interaction. A direct consequence is that the degree of longitudinal polarization of β^--particles from allowed decays is given, in essence, by the simple relation $P = -v/c$, where v is the velocity of the electrons and c is the velocity of light. This relation has been confirmed indeed by a number of precise experiments covering the energy range above about 120 keV, which corresponds to velocities above $0.6c$. However, for velocities $0.4 \lesssim v/c \lesssim 0.6$, where experimental difficulties become more and more serious, large and unexplained deviations have been reported, while, so far, no measurements were performed at energies below 40 keV ($v/c = 0.37$).

The aim of this investigation was to obtain accurate β-polarization results at lowest possible velocities of the β-particles in order to check whether or not there are real deviations from theory in the low-velocity region. The tritium decay was selected for this investigation because of its very low end-point energy of 18.6 keV ($v/c = 0.26$). In addition, the transition is of interest since it occurs between mirror nuclei, so that both Fermi and Gamow-Teller decay modes participate. Therefore, a sufficiently precise polarization result can be of significance for obtaining limits for both ratios C'_V/C_V and C'_A/C_A.

We performed polarization measurements at electron energies between 5.5 and 16.0 keV ($0.15 < v/c < 0.25$). After preselection of energy, the electrons were accelerated to a final energy of 79 keV. The degree of longitudinal polarization was measured by means of the Mott scattering method. We used an absolutely calibrated polarimeter. Instrumental asymmetries were reduced and corrected for with two detectors at forward scattering angles and in addition with a source of unpolarized electrons. It has been shown that depolarization in the source is small near the end-point energy.

The final result for the degree of longitudinal polarization of tritium β-particles with an average energy of 15.2 keV (v = $0.24c$) is

$$P(^3\mathrm{H}) = -(1.005 \pm 0.026)\ v/c.$$

Because of the good agreement of this result with the theoretical prediction we propose to disregard the previous deviating results for other allowed decays at velocities below $0.6c$. Our result gives the following limits for the coupling-constant ratios: $0.61 < C'_V/C_V < 1.65$ and $0.80 < C'_A/C_A < 1.26$. The limits for C'_V/C_V are of special interest, because they give a range which is narrower than the range previously deduced from all other relevant parity experiments combined.

Chapter 1 reviews the description of polarized electron beams and gives some features of the β-decay interaction, the two-component neutrino theory and β-polarization.

Chapter 2 deals with β-polarization measurements. The Mott scattering method is briefly described. The figure 2.2 presents a compilation of β-polarization results from the literature and includes also the results of the present investigation.

Chapter 3 gives some features of the β-decay of tritium relevant for our investigation. The consequences of its being a transition between mirror nuclei are discussed. A compilation of experimental results for the end-point energy is presented and the determination of the nuclear matrix elements is described.

Chapter 4 deals with the composition of the tritium sources and with measurements of their energy spectra with a double-focusing electron spectrometer. It is shown that the influence of source contamination and of penetration of tritium in the backing is negligible.

In Chapter 5 we describe the apparatus and the basic features of two different arrangements. Details are given only for the arrangement used for the main measurements. The energy calibration with conversion lines and the experimental determination of the efficiency of the polarimeter are outlined.

Chapter 6 deals with depolarization in the source. The depolarization by the aluminium source backing was calculated using measured back-scattering probabilities from the literature. The depolarization by the titanium layer of the source was determined experimentally by placing various foils in front of the source.

Chapter 7 describes the experimental procedure and the data analysis. An extensive table with results of the measurements at various energy settings is presented (table 7.1). The final result for $P(^3H)$ is compared with the theoretical prediction and with other polarization results.

In Chapter 8 the procedure for obtaining limits for C'_V/C_V and C'_A/C_A is presented with a tentative discussion of the confidence level for the results.

A part of this thesis has been published, in a more condensed form, in ref. Kok76.

[illegible]

[illegible] by the aluminium source backing was calculated [illegible] probabilities [illegible] the source was deter-
mined experimentally by placing various foils in front of the source.

[illegible] Chapter 4 [illegible]

[illegible] Chapter 5 [illegible] for the results.

A part of this thesis has been published, in a more condensed form, [illegible]

[illegible]

CHAPTER 1 THEORY

1.1. Electron polarization

The idea that an electron has an intrinsic angular momentum or *spin* was first proposed in 1926 by Uhlenbeck and Goudsmit to explain the splitting of energy levels observed in spectra of hydrogen like atoms. The existence of electron spin is borne out by vast experimental evidence. It is manifested in a very direct way in a Stern-Gerlach experiment, where the electron spin causes a spatial splitting of an atomic beam in an inhomogeneous magnetic field.

In this section we briefly describe how the spin state of single electrons and of an electron beam can be characterized. For a detailed account on electron polarization we refer to the review article of Tolhoek (Tol56) and to the text books of Rose (Ros61) and of Kessler (Kes76).

The spin state of a non-relativistic electron can be completely characterized with a two-component *spinor*

$$\chi = \begin{pmatrix} c_1 \\ c_2 \end{pmatrix} \tag{1.1}$$

where c_1 and c_2 are complex numbers, which usually depend on the space coordinates of the electron; $|c_1|^2$ and $|c_2|^2$ are the probabilities that the component of the electron spin along a chosen reference axis is found to be $+\hbar/2$ ("spin up") or $-\hbar/2$ ("spin down"), respectively; normalization requires $|c_1|^2 + |c_2|^2 = 1$.

The electron spin is represented by the vector operator $\vec{S} = \frac{1}{2}\hbar\vec{\sigma}$, where $\vec{\sigma}$ is the Pauli spin operator. The components of $\vec{\sigma}$ can be represented by the Pauli spin matrices

$$\sigma_x = \begin{bmatrix} 0 & 1 \\ 1 & 0 \end{bmatrix}, \quad \sigma_y = \begin{bmatrix} 0 & -i \\ i & 0 \end{bmatrix}, \quad \sigma_z = \begin{bmatrix} 1 & 0 \\ 0 & -1 \end{bmatrix}. \tag{1.2}$$

Here the z-axis of a cartesian coordinate system was chosen as reference axis. Thus, the spinors $(\ 1\ 0\ )^T$ and $(\ 0\ 1\ )^T$ are eigenstates of σ_z with eigenvalues +1 and -1, respectively. Properties of the Pauli spin matrices are discussed in standard text books on quantum mechanics.

The spin state of the electron can also be characterized by a three-dimensional unit vector, the so called *polarization vector* $\vec{P}$. By definition, the components of $\vec{P}$ are the expectation values of the corresponding components of the Pauli spin operator:

$$\vec{P} = \langle\vec{\sigma}\rangle. \tag{1.3}$$

From the general expression for the expectation value of an operator A,

$$\langle A\rangle = \chi^* A\chi, \tag{1.4}$$

where $\chi^* = (c_1^* \; c_2^*)$, c_i^* denoting the complex conjugate of c_i, it is immediately verified that the three real numbers P_x, P_y and P_z are given by:

$$\begin{aligned} P_x &= \langle\sigma_x\rangle = 2\,\mathrm{Re}(c_1^* c_2), \\ P_y &= \langle\sigma_y\rangle = 2\,\mathrm{Im}(c_1^* c_2), \\ P_z &= \langle\sigma_z\rangle = |c_1|^2 - |c_2|^2. \end{aligned} \tag{1.5}$$

It turns out that the spinor χ is an eigenstate with eigenvalue +1 of the operator $\vec{\sigma}\cdot\vec{P} = \sigma_x P_x + \sigma_y P_y + \sigma_z P_z$:

$$(\vec{\sigma}\cdot\vec{P})\chi = \chi. \tag{1.6}$$

This implies that a measurement of the spin along the direction $\vec{P}$ gives always the result "spin up". Hence, the unit vector $\vec{P}$ may legitimately be said to point in the direction of the spin of the electron.

We briefly mention a third method to characterize the spin state of the electron, namely by means of the *density matrix* ρ, defined as:

$$\rho = \chi\chi^* = \begin{bmatrix} |c_1|^2 & c_1 c_2^* \\ c_1^* c_2 & |c_2|^2 \end{bmatrix} \tag{1.7}$$

Combination of eqs. 1.5 and 1.7 yields

$$\rho = \tfrac{1}{2}(1 + \vec{\sigma}\cdot\vec{P}). \tag{1.8}$$

It can be directly verified that trace $\rho = 1$, where the trace of a matrix is the sum of the diagonal elements, and that

$$\vec{P} = \text{trace}\ (\rho\vec{\sigma}) = \text{trace}\ (\vec{\sigma}\rho). \tag{1.9}$$

The density matrix concept offers an elegant method for calculating the expectation value of any operator: eq. 1.4 can be written as

$$\langle A\rangle = \text{trace}\ (\rho A) = \text{trace}\ (A\rho). \tag{1.10}$$

Of course, the elements of ρ depend on the choice of the coordinate system. If one chooses the z-axis along $\vec{P}$, so that $\vec{\sigma}\cdot\vec{P} = \sigma_z$, the density matrix becomes according to eqs. 1.2 and 1.8:

$$\rho = \begin{bmatrix} 1 & 0 \\ 0 & 0 \end{bmatrix}. \tag{1.11}$$

The polarization vector and density matrix concepts are the most suitable for describing a polarized beam of electrons because the spin state of such a beam can only be characterized by a spinor when all electrons are identically prepared, so that each of the electrons can be described with the same spinor (pure state). If this is not the case it is more convenient to use ensemble averages of the polarization vectors $\vec{P}_i$ or density matrices ρ_i which describe the spins of the N "individual" electrons:

$$\overline{\vec{P}} = \frac{1}{N}\sum_{i=1}^{N} \vec{P}_i = \frac{1}{N}\sum_{i=1}^{N} \langle\vec{\sigma}\rangle_i, \tag{1.12}$$

$$\overline{\rho} = \frac{1}{N}\sum_{i=1}^{N} \rho_i = \tfrac{1}{2}(1 + \vec{\sigma}\cdot\overline{\vec{P}}). \tag{1.13}$$

The ensemble average of the expectation value of an operator can be written as (see eq. 1.10):

$$\langle\bar{A}\rangle = \frac{1}{N}\sum_{i=1}^{N}\langle A\rangle_i = \frac{1}{N}\sum_{i=1}^{N}\text{trace}\,(\rho_i A) = \text{trace}\,(\bar{\rho}A). \qquad (1.14)$$

Thus, all physically relevant information concerning the spin state of an electron beam is contained in $\bar{\vec{P}}$ or $\bar{\rho}$. For convenience we omit in the following the averaging bars.

The magnitude of $\vec{P}$, $\mathcal{P} = |\vec{P}|$, is called the *degree of polarization* of the beam: $0 \leq \mathcal{P} \leq 1$. It is important to note that usually $\vec{P}$ is not a unit vector, as for a single electron. A beam is called completely polarized, partially polarized or unpolarized if $\mathcal{P} = 1$, $0 < \mathcal{P} < 1$ or $\mathcal{P} = 0$, respectively.

If one chooses the coordinate system so that $\vec{P}$ lies along the positive z-axis, the density matrix of the beam can be written as:

$$\rho = \tfrac{1}{2}(1 + \mathcal{P}\sigma_z) = (1 - \mathcal{P})\begin{bmatrix} \frac{1}{2} & 0 \\ 0 & \frac{1}{2} \end{bmatrix} + \mathcal{P}\begin{bmatrix} 1 & 0 \\ 0 & 0 \end{bmatrix} \qquad (1.15)$$

The matrix in the first term on the right-hand side is the density matrix of an unpolarized beam (eq. 1.13 with $\bar{\vec{P}} = 0$); according to eq. 1.11 the second matrix is the density matrix of a completely polarized beam with polarization vector $\vec{P}/\mathcal{P}$. Thus, a partially polarized beam with polarization vector $\vec{P}$ can be considered as an incoherent superposition of an unpolarized beam with relative intensity $(1 - \mathcal{P})$ and a completely polarized beam with polarization vector $\vec{P}/\mathcal{P}$ and relative intensity $\mathcal{P}$.

The degree of polarization P_n relative to a direction determined by a unit vector $\hat{n}$, is defined as the expectation value of the operator $\vec{\sigma}\cdot\hat{n}$, averaged over the ensemble:

$$P_n = \langle\vec{\sigma}\cdot\hat{n}\rangle = \vec{P}\cdot\hat{n} \qquad (1.16)$$

(ensemble averaging bars are omitted). P_n can also be written as

$$P_n = \frac{N_\uparrow - N_\downarrow}{N_\uparrow + N_\downarrow}, \qquad (1.17)$$

where $N_\uparrow$ and $N_\downarrow$ are the numbers of electrons found with spin up and spin down, respectively, with respect to $\hat{n}$.

The *degree of longitudinal polarization* P_L of an electron beam is defined as in eq. 1.16, taking for $\hat{n}$ the unit vector $\hat{p} = \vec{p}/p$, where $\vec{p}$ is the momentum vector of the electrons and $p = |\vec{p}|$:

$$P_L = \langle\vec{\sigma}\cdot\hat{p}\rangle = \vec{P}\cdot\hat{p}. \tag{1.18}$$

For a longitudinally polarized beam, that is a beam for which the polarization vector is parallel or anti-parallel to the direction of motion, holds: $P_L = \mathcal{P}$ or $-\mathcal{P}$, respectively.

A beam of electrons is called transversely polarized when the polarization vector is perpendicular to the direction of motion of the electrons.

For the description of relativistic electrons one has to use Dirac theory and four-component spinors. The interpretation of the polarization vector should be somewhat modified in that case. However, $\vec{P}$ can be considered as the spin direction in the coordinate system in which the electron is transformed to rest (To156).

We have to remark that we use in the following the symbol P instead of P_L to denote the degree of longitudinal polarization of electrons. Furthermore, we sometimes use, for convenience, "the polarization of the electrons" or "the degree of polarization of the electrons" instead of the rather unwieldy expression "the degree of longitudinal polarization of the electrons".

1.2. Beta decay

1.2.1. General

In β-decay a neutron is converted in a proton under emission of an electron and an antineutrino (β^--decay): $n \rightarrow p + e^- + \bar{\nu}$; or, a proton is converted into a neutron under emission of a positron and a neutrino (β^+-decay): $p \rightarrow n + e^+ + \nu$. These decays involve four fermions (spin-½ particles), namely two hadrons (p,n) and two leptons ($e^-, e^+, \nu, \bar{\nu}$). Usually the hadrons involved in β-decay are constituents of a nucleus.

Since the strength of the β-decay interaction is much smaller than that of the electromagnetic interactions or of the strong interactions between nuclei, this β-decay interaction is classified as a *weak interaction*. Surveys on experimental and theoretical features of β-decay and weak interactions were given, for example, by Tolhoek (Tol63), by Wu and Moszkowski (Wu66) and by Schopper (Sch66). In this section we present some features which are of relevance for the investigation described in this thesis.

Beta-decay theory started in 1934 when Fermi (Fer34) derived a theoretical expression for the continuous energy distribution of the emitted electrons. He started from the first order perturbation theory expression

$$w_{if} = \frac{2\pi}{\hbar} |\mathcal{H}_{if}|^2 \frac{dn}{dW}, \tag{1.19}$$

where w_{if} is the probability per unit of time that a transition occurs between an initial state i and a final state f; $\mathcal{H}_{if} = \langle f|H|i\rangle$ is the matrix element of the interaction hamiltonian between initial and final state; the quantity dn/dW is the density of final states, taken at the total decay energy W_o of the transition. Fermi postulated that this decay energy is shared statistically between an electron and a neutrino on the basis of available phase space. The existence of neutrinos was hypothesized three years earlier by Pauli.

The probability per unit of time that a β-active nucleus decays under emission of an electron with total energy between W and $W + dW$ becomes:

$$w(W)dW = \frac{1}{2\pi^3 c^5 \hbar^7} |\mathcal{H}_{if}|^2 \, p \, W \, F(Z,W) \, (W_o - W)^2 \, dW. \tag{1.20}$$

Here, p is the momentum of the electron. The Fermi function F accounts for the electromagnetic interaction between the emitted electron and the daughter nucleus: it depends on W and on the atomic number of the daughter nucleus. Extensive tables of F have been published. In the recent tables of Behrens and Jänecke (Beh69) the influence of the finite size of the nucleus and of screening by atomic electrons on $F(Z,W)$ has been taken into account.

The transition matrix element $\mathcal{H}_{if}$ is calculated by integrating the interaction density over the volume of a nucleon and summing over all nucleons of the nucleus:

$$\mathcal{H}_{if} = \sum_{k=1}^{A} \int H_k \, d\tau_k . \tag{1.21}$$

Fermi constructed his theory by assuming that β-interaction is analogous to electromagnetic interaction. Using basically the same idea, but allowing for the possibility of non-conservation of parity (see below), one assumes nowadays that the generalized form of the interaction density can be written (in conventional notation) as

$$H = g \sum_i (C_i H_i^{\text{even}} + C_i' H_i^{\text{odd}}) . \tag{1.22}$$

We omitted the index k. The summation extends over five possible types of interaction to be discussed below;.

$$H_i^{\text{even}} = (\tilde{\psi}_p, O_i \psi_n)\ (\tilde{\psi}_e, O_i \psi_\nu) + \text{h.c.}, \tag{1.23}$$

$$H_i^{\text{odd}} = (\tilde{\psi}_p, O_i \psi_n)\ (\tilde{\psi}_e, O_i \gamma_5 \psi_\nu) + \text{h.c.}. \tag{1.24}$$

Here, ψ_p, ψ_n, ψ_e and ψ_ν are four-component wave functions of proton, neutron, electron and neutrino, respectively; the adjoint wave function $\tilde{\psi}$ is defined as $\tilde{\psi} = \psi^* \gamma_4$, where ψ^* is the hermitian conjugate of ψ and γ_4 is a Dirac matrix (see below). Creation and annihilation operators have been omitted. The abbreviation h.c. denotes hermitian conjugate. Further features of the above equations are explained in the following.

The real constant g in eq. 1.22 determines the absolute strength of the β-interaction. The relative strengths of the various contributions are determined by the coupling constants C_i and C_i', which may be complex. By convention, these numbers are normalized such that $\sum_i |C_i|^2 + |C_i'|^2 = 1$. The 16 linearly independent operators O_i can be grouped into five classes according to their transformation properties. The operators are chosen such that H_i^{even} transforms as a scalar under Lorentz transformations.

The operator γ_5 (see below) effects that the terms H_i^{odd} are pseudoscalars. According to the transformation character of $(\tilde{\psi},O_i\psi)$ one discerns scalar (S), polar-vector (V), tensor (T), axial-vector (A) and pseudoscalar (P) interaction. The corresponding interaction operators can be expressed in terms of the five 4×4 Dirac matrices, which are, in the notation used by Schopper (Sch66),

$$\gamma_k = i\begin{bmatrix} 0 & -\sigma_k \\ \sigma_k & 0 \end{bmatrix}, \quad \gamma_4 = \begin{bmatrix} -1 & 0 \\ 0 & 1 \end{bmatrix}, \quad \gamma_5 = \begin{bmatrix} 0 & 1 \\ 1 & 0 \end{bmatrix} \tag{1.25}$$

(k = 1, 2, 3), where $\sigma_1 = \sigma_x$, $\sigma_2 = \sigma_y$ and $\sigma_3 = \sigma_z$ are the 2×2 Pauli spin matrices (eq. 1.2) and 1 denotes the 2×2 unit matrix. The operators O_i can be expressed as: $O_S = 1$, $O_V = \gamma_\mu$, $O_T = \gamma_\mu\gamma_\nu$, $O_A = \gamma_\mu\gamma_5$ and $O_P = \gamma_5$ (μ,ν = 1, 2, 3, 4; $\mu \neq \nu$). The number of independent operators is 1, 4, 6, 4 and 1, respectively.

In 1956 it was proposed by Lee and Yang (Lee56) that parity is not conserved in weak interactions, i.e. the mirror image of a process does not necessarily occurs with the same probability as the process itself. In quantum mechanics this implies that the expectation values of certain observables are not invariant for the parity operation P (i.e. space inversion). The first experimental evidence of violation of parity conservation in β-decay has been given by Wu et al. (Wu57) by measuring the β-asymmetry of polarized ^{60}Co nuclei. Before 1956 only the scalars H_i^{even} were taken into account in the β-interaction hamiltonian. The addition of the pseudoscalars H_i^{odd} has been proposed by Lee and Yang. It can be shown that parity conservation is equivalent to $C_i = 0$ or $C_i' = 0$ for all i. Besides space inversion one may consider time reversal T (not to be confused with tensor interaction) and charge conjugation C. Time-reversal invariance means that, for instance, a reversal of all velocities in a physical process does not change the observables. Time-reversal invariance holds in β-decay if all C_i and C_i' are real numbers. Charge conjugation implies that the observables are not changed if all particles are substituted by their antiparticles. The β-interaction is invariant under charge conjugation if all C_i are real and all C_i' are imaginary numbers or vice versa. One assumes nowadays on the basis of experimental evidence that the β-decay interaction is invariant under the combined CP-operation and under the T-operation and therefore also under the combined CPT-operation.

We summarize the situation concerning the β-interaction by stating that the experiments are compatible with:

i) time-reversal invariance: C_i and C'_i real.

ii) two-component neutrino theory with left-handed neutrinos: $C_i = C'_i$ (see subsect. 1.2.3).

iii) V,A-interaction, implying that only vector and axial-vector interactions occur: the coupling constants for the other interaction forms are identically zero.

iv) the ratio between the coupling constants of the vector and the axial-vector contributions to the interaction is constant: $\lambda = C_A/C_V \approx -1.25$ (see subsect. 1.2.2).
The conditions iii) and iv) are often combined by speaking of (V-λA)-interaction.

v) lepton conservation. This condition implies that, for example, emission of an electron is always accompanied by emission of an antineutrino: the probability that a neutrino is emitted is zero. If this was not the case an additional set of, in principle, 10 complex coupling constants would be needed, as discussed by Pauli (Pau57).

Under these five conditions the β-interaction can be completely characterized with the aid of only two real numbers viz. the interaction constant g (see eq. 1.22) and the ratio $\lambda = C_A/C_V$.

The accuracy with which the above conditions have been checked experimentally is rather poor in most cases. The reason for this is that the experiments are often difficult and furthermore that their experimental results are often insensitive for deviations from the conditions given above (e.g. for electron polarization results; see subsect. 1.2.3). In addition, information obtained about certain coupling constants is seldom independent of assumptions about the remaining coupling constants: for example, for deriving values for C'_V/C_V or C'_A/C_A from electron polarization results one usually assumes that the other coupling constants are exactly zero.

We mention in this context a study of Paul (Pau70) who performed a least-squares adjustment of the β-decay coupling constants using a large amount of experimental data from literature and assuming time-reversal invariance, lepton conservation, $C_S = C'_S$, $C_T = C'_T$ and $C_P = C'_P = 0$. Paul reported $C_S/C_V = -0.001 \pm 0.006$ and $C_T/C_A = -0.0004 \pm 0.0003$, without assumptions on C'_V/C_V, C'_A/C_A and C_A/C_V [†], and further $C'_V/C_V = 0.82 {}^{+0.40}_{-0.13}$ and $C'_A/C_A = 1.10 \pm 0.06$, independent of C_S, C_T [††]. Paul, however, was confronted with the unfortunate situation that the internal (a priori) and external (a posteriori) errors of his results are largely different. The above error limits, quoted from Paul's article, are external errors, which are about 2.4 times smaller than the internal ones. As Paul himself remarks in a later publication in cooperation with Kropf (Kro74) about a similar subject, it is safer to use as final error estimate the larger of the internal and external errors. This implies that the above errors should be enlarged with a factor 2.4 (see also sect. 8.1).

1.2.2. Allowed decay

An important category of β-decays, to which we restrict ourselves in the subsequent discussion, is the so called *allowed decay*. For this decay mode the orbital angular momentum of the emitted leptons is zero. This implies that the wave functions of the electron and the neutrino can be assumed, in good approximation, to be constant over the nuclear volume. If the initial nuclei are unpolarized and if one averages over the possible directions and spin orientations of the emitted leptons, so that parity-violating terms vanish, one obtains for the transition matrix element (Jac57)

$$|\mathcal{H}_{if}|^2 = g^2\ \xi\ (1 + b\ \frac{m_e c^2}{W}), \qquad (1.26)$$

† This at least is stated in the abstract of Paul's article. Table 2 (adjustment IV S) of his article, however, suggests that $C'_V/C_V = C'_A/C_A = 1$ has been taken for obtaining these results.

†† Similarly table 2 (adjustment III S) of Paul's article suggests that $C_S = C'_S = C_T = C'_T = 0$ has been used.

where

$$\xi = |M_{\mathrm{F}}|^2 \left(|C_{\mathrm{S}}|^2 + |C'_{\mathrm{S}}|^2 + |C_{\mathrm{V}}|^2 + |C'_{\mathrm{V}}|^2\right) + \\ + |M_{\mathrm{GT}}|^2 \left(|C_{\mathrm{T}}|^2 + |C'_{\mathrm{T}}|^2 + |C_{\mathrm{A}}|^2 + |C'_{\mathrm{A}}|^2\right) \tag{1.27}$$

and

$$b\,\xi = \pm 2(1 - \alpha^2 Z^2)^{\frac{1}{2}} \times \\ \mathrm{Re}\left[|M_{\mathrm{F}}|^2 \left(C_{\mathrm{S}}C_{\mathrm{V}}^{*} + C'_{\mathrm{S}}C'^{*}_{\mathrm{V}}\right) + |M_{\mathrm{GT}}|^2 \left(C_{\mathrm{T}}C_{\mathrm{A}}^{*} + C'_{\mathrm{T}}C'^{*}_{\mathrm{A}}\right)\right]. \tag{1.28}$$

Here, $\alpha = e^2/(\hbar c) \simeq 1/137$ is the fine-structure constant and $m_e c^2$ the electron rest energy. The nucleon wave functions have been treated non-relativistically and lepton conservation is assumed. Here and throughout this section the upper sign in an expression refers to β^--decay and the lower one to β^+-decay. The allowed nuclear matrix elements M_{F} (Fermi matrix element) and M_{GT} (Gamow-Teller matrix element) are of the form $\int \psi_f^* O_i \psi_i \, d\tau$ with $O_i = 1$ and $\vec{\sigma}$, respectively; ψ_i and ψ_f denote the initial and final state of the nucleus, respectively, while the integration runs over the nuclear volume. It can be shown that M_{F} is non-zero only if: $\pi_i = \pi_f$, $J_i = J_f$ and $T_i = T_f$ (Fermi selection rules), where π, J and T denote the parity, spin and isospin of the nuclear states, respectively. This case corresponds to the emission of two leptons with opposite spins, so that the total angular momentum carried away from the nucleus by the lepton pair is zero. Similarly, M_{GT} is non-zero only if: $\pi_i = \pi_f$, $\Delta J = |J_f - J_i| = 0$ or 1 (no $0 \rightarrow 0$) and $\Delta T = |T_f - T_i| = 0$ or 1 (Gamow-Teller selection rules). This case corresponds to the emission of two leptons with parallel spins, so that the total angular momentum carried away from the nucleus is one unit. Transitions for which both Fermi and Gamow-Teller decay modes participate are called mixed allowed transitions: $\pi_i = \pi_f$, $\Delta J = 0$ (no $0 \rightarrow 0$) and $\Delta T = 0$. It has to be remarked that the above isospin selection rules are not very severe (Sch66).

The values of the nuclear matrix elements M_{F} and M_{GT} can be calculated accurately only in a limited number of cases. For a β-transition between members of an isospin multiplet the Fermi matrix element can be calculated without reference to details of the nuclear structure if it is assumed that the wave functions of the initial and final state are identical. Then the value of M_F depends only on the isospin quantum numbers T and T_3 of the states involved. One obtains (Sch66):

$$|M_F|^2 = T(T+1) - T_3^i T_3^f. \qquad (1.29)$$

Well known cases are pure Fermi $0^+ \to 0^+$ transitions like the decays of ^{14}O, ^{10}C, ^{26}Al and ^{34}Cl and mirror transitions like the decays of n, ^{3}H, ^{7}Be, ^{11}C and ^{19}Ne. For the $0^+ \to 0^+$ transitions one has $T = 1$ and $T_3^i = 0$ or $T_3^f = 0$. Thus, eq. 1.29 gives $|M_F|^2 = 2$. For the mirror transitions $T = \frac{1}{2}$ and $T_3^{i,f} = \frac{1}{2}, -\frac{1}{2}$ or $-\frac{1}{2}, \frac{1}{2}$, so that $|M_F| = 1$ (for more details on mirror transitions see ch. 3). Slight modifications are expected since the assumption on which eq. 1.29 is based, namely that initial and final state wave functions are identical, is not exactly true. Since the parent nucleus contains one proton more or less than the daughter nucleus, their wave functions will be slightly different (imperfect overlap). Furthermore, the states involved are no pure isospin states when the nuclear forces are charge dependent. This results in isospin impurities and in a reduction of the Fermi matrix element. The influence of these effects was discussed by, for example, Blin-Stoyle (Bli73). According to the CVC-theory (Conserved Vector Current theory; see standard text books) the Fermi matrix element is not affected by the exchange of virtual pions that carry the strong interaction between the nucleons.

In general, the Gamow-Teller matrix element M_{GT} is sensitive to details of the nuclear structure. Furthermore, it is affected by strong interactions according to the PCAC-theory (Partially Conserved Axial vector Current theory; see standard text books). The only case for which M_{GT} is accurately known is the mixed allowed mirror decay of the free neutron. Here, $|M_{GT}|^2 = 3$ (see ref. Wu66). In sect. 3.5 we briefly mention an attempt to check the validity of the PCAC-theory by comparison of experimental and theoretical M_{GT}-values for the tritium decay, the second-simplest β-decay.

It is seen from eqs. 1.27 and 1.28 that only scalar (S) and (polar) vector (V) interactions can participate in Fermi transitions, while Gamow-Teller transitions can only be induced by tensor (T) and axial-vector (A) interactions. Pseudoscalar interaction can not contribute (in first order) to allowed transitions. The term b is called the Fierz term. If this term is non-zero, the transition matrix element for allowed decays would be energy dependent. Accurate shape measurements, however, fail to indicate this. The Fierz term must therefore be small: all measurements are in agreement with $b = 0$. This agrees with results of electron-neutrino directional correlation investigations for allowed transitions. These show that vector and axial-vector interactions contribute dominantly to the transition probability (see also subsect. 1.2.3).

The total decay probability per unit of time w_t of a β-active nucleus is obtained by integration of eq. 1.20 over the energy. For an allowed decay with $b = 0$ the nuclear matrix is independent of energy, so that

$$w_t = \int_{m_e c^2}^{W_o} w(W)\mathrm{d}W = \frac{|\mathcal{H}_{if}|^2}{2\pi^3 c^5 \hbar^7} \int_{m_e c^2}^{W_o} p\, W\, F(Z,W)\, (W_o - W)^2\, \mathrm{d}W. \quad (1.30)$$

The integral on the right-hand side, often abbreviated as f, was tabulated, for example, by Behrens and Jänecke (Beh69). As a measure for the magnitude of the nuclear matrix elements the ft-value or comparative half-life is introduced, where t denotes the half-life of the decay: $t = T_{\frac{1}{2}} = (\ln 2)/\omega_t$. Using eqs. 1.26 and 1.27, assuming time-reversal invariance and neglecting the Fierz term, the ft-value for an allowed decay can be written as:

$$ft = \frac{2\pi^3 c^5 \hbar^7 \ln 2}{g^2} \times \frac{1}{(C_S^2 + C_S'^2 + C_V^2 + C_V'^2)\,|M_F|^2 + (C_T^2 + C_T'^2 + C_A^2 + C_A'^2)\,|M_{GT}|^2}. \quad (1.31)$$

Values for the constant g can be obtained from measured ft-values for decays with known matrix elements M_F and M_{GT}. Recently, Hardy and Towner (Har75) and Raman, Walkiewicz and Behrens (Ram75) analysed all available data on pure Fermi transitions. They obtained $ft(0^+ \rightarrow 0^+) = 3081.7 \pm 1.9$ sec and 3088.6 ± 2.1 sec, respectively. The difference is mainly due to a different approach for obtaining isospin impurity corrections. With eq. 1.31, the value $ft(0^+ \rightarrow 0^+) = 3085 \pm 5$ sec, a compromise between the two results, yields $g(C_S^2 + C_S'^2 + C_V^2 + C_V'^2)^{\frac{1}{2}} = (1.4123 \pm 0.0008)\times10^{-49}$ erg·cm³. Kropf and Paul (Kro74) analysed available data on the neutron decay and deduced $ft(\mathrm{n}) = 1093.3 \pm 16.5$ sec. Comparison of $ft(0^+ \rightarrow 0^+)$ and $ft(\mathrm{n})$ gives

$$\lambda^2 = \frac{C_T^2 + C_T'^2 + C_A^2 + C_A'^2}{C_S^2 + C_S'^2 + C_V^2 + C_V'^2} = \frac{1}{3}\left[\frac{2\,ft(0^+ \rightarrow 0^+)}{ft(\mathrm{n})} - 1\right]. \quad (1.32)$$

Upon inserting the above values for $ft(\mathrm{n})$ and $ft(0^+ \rightarrow 0^+)$ one obtains $|\lambda| = 1.244 \pm 0.011$. A negative sign of λ follows from experiments with polarized neutrons. From such experiments Kropf and Paul (Kro74) derived $\lambda = C_A/C_V = -1.263 \pm 0.016$, assuming V,A-interaction and $C_V'/C_V = C_A'/C_A = 1$. A weighted average gives: $\lambda = -1.25 \pm 0.01$ (for V,A-interaction with $C_V'/C_V = C_A'/C_A = 1$).

1.2.3. Electron polarization and two-component neutrino theory

Longitudinal polarization of the emitted β-particles requires the expectation value $\langle\vec{\sigma}\cdot\vec{p}\rangle$ to be non zero (see eq. 1.18). Since $\vec{p}$ is a polar vector and $\vec{\sigma}$ is an axial vector, $\langle\vec{\sigma}\cdot\vec{p}\rangle$ is a pseudoscalar which is expected to be zero if parity conservation holds. The existence of longitudinal electron polarization in β-decay, therefore, is a very direct manifestation of parity-non-conservation of the β-interaction.

If the nuclei are unpolarized and if one averages over directions and spin orientations of the neutrinos the interaction given in eq. 1.22 yields for the probability that in an allowed decay the β-particle is emitted with spin either parallel or anti-parallel to its momentum (Jac57; Cur57):

$$w(W,\vec{\sigma}) \sim p\,W\,F(Z,W)\,(W_o - W)^2\,\xi\,(1 + b\,\frac{m_e c^2}{W} + G\,\frac{\vec{\sigma}\cdot\vec{p}}{W}). \quad (1.33)$$

Here, ξ and b are given by eqs. 1.27 and 1.28, respectively, and

$$G\,\xi = 2|M_F|^2 \left[\pm\, \mathrm{Re}(C_S C_S'^* - C_V C_V'^*) + \frac{\alpha Z m_e c^2}{p}\, \mathrm{Im}(C_S C_V'^* + C_S' C_V^*) \right]$$
$$+\, 2|M_{GT}|^2 \left[\pm\, \mathrm{Re}(C_T C_T'^* - C_A C_A'^*) + \frac{\alpha Z m_e c^2}{p}\, \mathrm{Im}(C_T C_A'^* + C_T' C_A^*) \right]. \tag{1.34}$$

The terms containing the fine-structure constant α disappear when time-reversal invariance holds i.e. when the coupling constants are all real. The above expression for G and the expressions for ξ and b (eqs. 1.27 and 1:28) are valid if lepton conservation is assumed. In eq. 1.33 the influence of finite nuclear size, screening by atomic electrons and higher-order transitions is not taken into account. These influences are briefly discussed in sect. 2.2.

From eq. 1.33 one obtains for the degree of longitudinal polarization of β-particles emitted in allowed decays:

$$P = \frac{w(W,\vec{\sigma}) - w(W,-\vec{\sigma})}{w(W,\vec{\sigma}) + w(W,-\vec{\sigma})} = \frac{v}{c} \cdot \frac{G}{1 + b\, m_e c^2/W}. \tag{1.35}$$

Longitudinal polarization experiments (see sect. 2.2) indicate that for electrons $P = -v/c$ and for positrons $P = +v/c$. If these relations could be verified with infinite accuracy, one could conclude: $C_V' = C_V$, $C_A' = C_A$, $C_S' = -C_S$ and $C_T' = -C_T$, where the coupling constants may be complex. For this particular combination $b \equiv 0$, and $G \equiv -1$ for electrons and $+1$ for positrons.

If time-reversal invariance is assumed the expression for P reduces for V,A-interaction (which implies $b \equiv 0$) to

$$P = \mp \frac{v}{c}\, \frac{2C_V C_V' \,|M_F|^2 + 2C_A C_A' \,|M_{GT}|^2}{(C_V^2 + C_V'^2)\, |M_F|^2 + (C_A^2 + C_A'^2)\, |M_{GT}|^2}. \tag{1.36}$$

The polarization of the emitted leptons is closely related to that of the emitted (anti)neutrinos. In the conventional Dirac theory for relativistic fermions, a four-component wave function describes the four internal degrees of freedom of the particle: two components for the two possible spin orientations, the other two for the particle-antiparticle distinction. Guided by experimental evidence on parity violation Lee and Yang (Lee57) proposed a two-component theory for neutrinos. In this theory the spin of a neutrino is always parallel to its momentum, while the antineutrino spin is opposite to its momentum (or vice versa). Thus, the number of internal degrees of freedom is reduced to two, so that a two-component spinor suffices to describe the particle. Such a theory was discussed already in 1929 by Weyl (Wey29); it was rejected, however, since it violated space-inversion invariance. In two-component neutrino theory the rest mass of the neutrino is zero. Otherwise a definite intrinsic polarization (helicity) would be impossible: if the neutrino has a finite rest mass one can always transform to a reference frame in which the momentum of the particle and hence also its helicity is reversed. Experimentally an upper limit for the neutrino rest mass of 55-60 eV has been found by Bergkvist[†] (Ber72; see subsect. 3.2), which is indeed close to zero.

Lee and Yang derived that the general β-decay Hamiltonian as given in subsect. 1.2.2, leads, in combination with a zero neutrino rest mass, to two-component neutrinos if either $C_i' = C_i$ for all i, or $C_i' = -C_i$ for all i. The first case corresponds to left-handed neutrinos and right-handed antineutrinos; the second case to the reversed handedness. Goldhaber et al. (Gol58) found experimentally that the helicity of neutrinos emitted in electron capture is negative (left-handedness). A similar direct determination of the helicity of neutrinos or antineutrinos emitted in β^+- or β^--decay has not been performed so far. However, by applying angular momentum conservation on the combined results of electron and positron polarization measurements and of recoil experiments it can be concluded that in β-decay the emitted neutrino is also left-handed, while the antineutrino is right-handed. Thus, these experimental results select $C_i' = C_i$.

With $C_i' = C_i$ the two-component neutrino prediction for the longitudinal electron polarization for allowed decays (eq. 1.35) becomes $P = -v/c$ for pure V,A-interaction, $P = v/c$ for pure

---

† Bergkvist assumed V,A-interaction with $C_V'/C_V = C_A'/C_A = 1$. He concluded from the coupling-constant data given by Paul (Pau70; see remarks in subsect. 1.2.1) that possible deviations of the above conditions will be too small to be of concern in his neutrino-mass experiment.

S,T-interaction and values between $-v/c$ and v/c when combinations of V,A- and S,T-interaction are present. Clearly two-component left-handed neutrinos and an electron polarization of exactly $-v/c$ are compatible only if $C'_V = C_V$, $C'_A = C_A$ and $C'_S = C_S = C'_T = C_T = 0$.

The most direct test to determine if the two-component neutrino theory holds in β-decay is of course the measurement of the neutrino helicity itself. Such an experiment, as performed by Goldhaber et al. (Gol58), is extremely difficult and it allows no accurate check of the condition $C'_i = C_i$. For more accurate checks one has to turn to electron and positron polarization measurements. In chapter 8 we derive limits for the ratios C'_V/C_V and C'_A/C_A from the longitudinal polarization measurements on β^--particles from tritium, described in this thesis.

2.1. The Mott scattering method

Various methods are available for measuring the polarization of electron or positron beams. The measurements may be direct, taking advantage of polarization dependent cross sections, e.g. Møller and Bhabha scattering on polarized electrons, Mott scattering on heavy nuclei and, especially for positrons, annihilation with polarized electrons or positronium formation. The measurements may also be indirect, transferring the longitudinal polarization of the β-particles to circular polarization of γ-radiation e.g. by bremsstrahlung; this circular polarization is then detected. For a detailed account of these methods we refer to reviews of, for example, Tolhoek (Tol56), Kofoed-Hansen and Christensen (Kof62), Frauenfelder (Fra68), Wu and Moszkowski (Wu66) and Schopper (Sch66).

We briefly describe the Mott scattering method, which was used for the experiment described in this thesis. It is the best method available for electron polarization measurements in the energy region below about 500 keV. The method is based on the spin dependence of the scattering of electrons by the Coulomb field of a nucleus. The physical mechanism that underlies this spin dependence is the spin-orbit interaction between the magnetic moment connected with the spin of the electron and the magnetic field caused by the motion of the nuclear charge (as seen in the rest frame of the electron). The attractive potential between electron and nucleus due to the Coulomb interaction, is influenced by the relative orientation of this magnetic field and the magnetic moment of the electron.

Mott (Mot29,32) was the first to give a relativistic quantum-mechanical treatment of single scattering of electrons by atomic nuclei. He showed that initially unpolarized electrons become transversely polarized after the scattering. The spin orientation is perpendicular to the plane of scattering. The degree of transverse polarization, usually denoted as S, depends on the scattering angle θ, the energy E of the electrons and the atomic number Z

of the nuclei. The function S is commonly called the Mott (asymmetry) function or the Sherman function (see later).

If, on the other hand, the electrons are initially transversely polarized with degree of polarization P_T, the differential scattering cross section is asymmetric:

$$\frac{d\sigma}{d\Omega}(\theta,\phi) = \frac{d\sigma_o}{d\Omega}(\theta)\left[1 - P_T S(\theta)\sin\phi\right], \qquad (2.1)$$

where $d\sigma_o/d\Omega$ is the polarization independent differential cross section, θ is the polar angle of scattering and ϕ is the azimuthal angle of scattering relative to the plane of the initial momentum $\vec{p}$ and polarization vector $\vec{P}$ of the electrons. Eq. 2.1 gives

$$\frac{I(\theta,\phi+\pi) - I(\theta,\phi)}{I(\theta,\phi+\pi) + I(\theta,\phi)} = P_T S(\theta)\sin\phi, \qquad (2.2)$$

where I denotes the observed intensity at the indicated angles. Thus, a measurement of the scattering asymmetry yields a value for P_T. The largest asymmetry is observed in the plane perpendicular to the initial momentum and polarization vector of the electrons ($\phi = 90^o$ or 270^o). The asymmetry in this plane is usually denoted as the "left-right asymmetry":

$$\delta \equiv \frac{L - R}{L + R} = P_T S(\theta), \qquad (2.3)$$

where "left" is defined as the direction of the vector $\vec{P}\times\vec{p}$.

The scattering cross section and the Mott function can be written as

$$\frac{d\sigma_o}{d\Omega} = |f|^2 + |g|^2 \text{ and } S = i(fg^* - gf^*)/(|f|^2 + |g|^2). \qquad (2.4)$$

The complex scattering amplitudes f and g depend on θ, E and Z. These amplitudes, with the aid of which Coulomb scattering of polarized electrons can be completely described, are obtained by solving the Schrödinger equation for the scattering process and are usually expressed in terms of partial wave expansions (Ros61).

The function S has been calculated, on the basis of eq. 2.4, for various values of θ, E and Z by Sherman (She56) for scattering by a point nucleus and, more recently, including screening by atomic electrons, by Lin (Lin64), by Holzwarth and Meister (Hol64) and by Bühring (Büh68). Values for S have been obtained from double-scattering experiments by, amongst others, Mikaēlyan et al. (Mik63), Nelson and Pidd (Nel59) and van Klinken (Kli66a). In such experiments an initially unpolarized beam is scattered twice, choosing similar conditions for the first and second scattering. Then, in the limit of zero scatterer thicknesses, the observed asymmetry becomes essentially S^2. Figs. 2.1a and b illustrate the dependence of S from θ and E for electron scattering on gold nuclei. Calculated and measured values agree reasonably well at electron energies above about 100 keV; at lower energies, however, large discrepancies exist (see also ref. Boe71).

For measuring β-polarization by Mott scattering one has to transform the longitudinal polarization to a transverse one. This can be achieved with electrostatic deflection over about 90° (as was used for this work), with Coulomb scattering by low-Z scatterers or with crossed electric and magnetic fields ("Wien filter"). Details may be found in the mentioned reviews.

In an actual experiment the theoretical quantity S in eq. 2.3 has to be replaced by an effective S-value, to be denoted as S_{an}, which includes effects of plural and multiple scattering in foils of finite thickness, of finite solid angles and of backscattering by walls. This polarimeter efficiency S_{an} may be obtained from a double-scattering experiment, as was done for this work, or it may be derived from calculated S-values (see a discussion in the subsequent section).

Optimum conditions for electron polarization analysis by means of Mott scattering are: a high-Z foil, for example of gold, as scatterer; backward-angle scattering over about 105°-125°, and electron energies in the range 50 - 500 keV. The foil should be thin, because S_{an} decreases with increasing foil thickness due to plural and multiple scattering. Since scattered intensities increase approximately linearly with increasing foil thickness, an optimum foil thickness can be found (see ref. Kli66a for details).

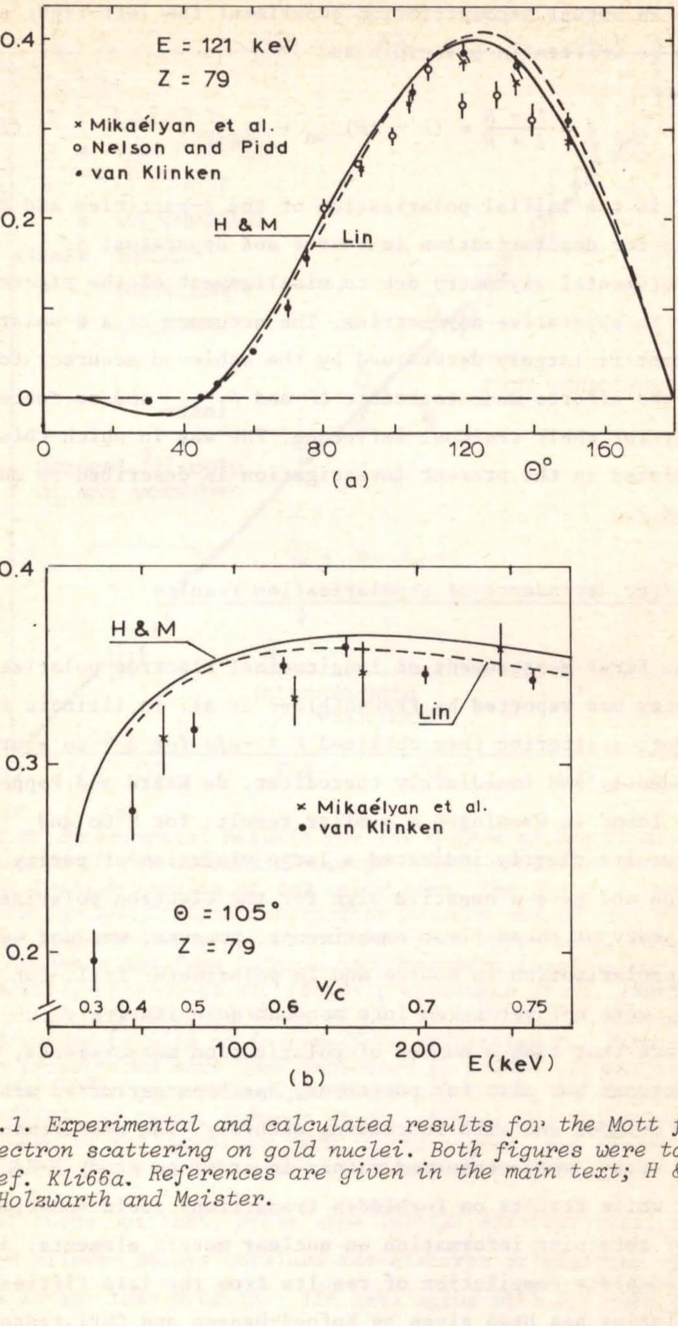

Fig. 2.1. Experimental and calculated results for the Mott function for electron scattering on gold nuclei. Both figures were taken from ref. Kli66a. References are given in the main text; H & M denotes Holzwarth and Meister.

In an actual β-polarization experiment the left-right asymmetry can be written in principle as

$$\delta = \frac{L - R}{L + R} = (P - \Delta P)S_{an} + \delta_{instr}. \qquad (2.5)$$

Here, P is the initial polarization of the β-particles and ΔP accounts for depolarization in source and apparatus; δ_{instr} is the instrumental asymmetry due to misalignment of the electron beam or to apparative asymmetries. The accuracy of a β-polarization experiment is largely determined by the achieved accuracy for S_{an} and by the efforts made to reduce ΔP and δ_{instr} and to correct properly for their residual influence. The way in which this was accomplished in the present investigation is described in chapters 5, 6 and 7.

2.2. Energy dependence of β-polarization results

The first measurement of longitudinal electron polarization in β-decay was reported by Frauenfelder et al. in Illinois (Fra57). Using Mott scattering they obtained $P \simeq -v/c$ for a ^{60}Co source. Independently and immediately thereafter, de Waard and Poppema (Waa57) found in Groningen a similar result for ^{60}Co and ^{32}P. These results clearly indicated a large violation of parity conservation and gave a negative sign for the electron polarization. The accuracy of these first experiments, however, was not yet high; depolarization in source and in polarimeter foil, for example, were not yet taken into account quantitatively.

Since that time a number of polarization measurements, mostly for electrons but also for positrons, has been performed with various methods and with increasing accuracy. The measurements on allowed decays were performed mainly in order to study β-decay theory, while results on forbidden transitions could sometimes be used for obtaining information on nuclear matrix elements. A fairly complete compilation of results from the late fifties and early sixties has been given by Kofoed-Hansen and Christensen (Kof62). Schopper (Sch66) compiled data on allowed decays obtained before 1965.

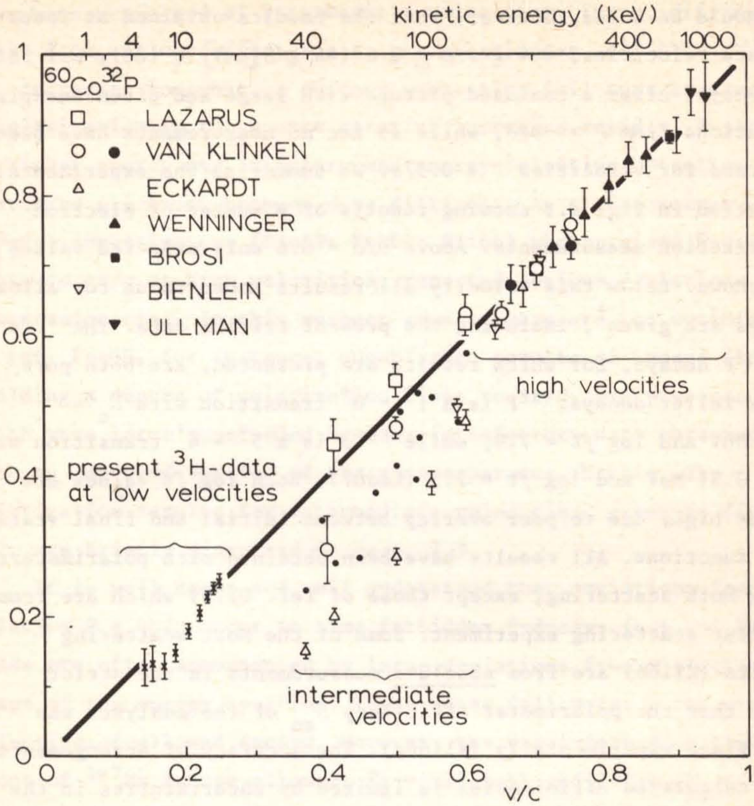

Fig. 2.2. Experimental results for the degree of longitudinal polarization P for allowed β^--decays. The compilation includes the present tritium results at low velocities. The factor Λ, which accounts for the Coulomb interaction between the emitted electron and the daughter atom, has been taken from ref. Beh69. Data with error brackets are from Lazarus and Greenberg (Laz70), van Klinken (Kli66), Eckardt et al. (Eck64), Wenninger et al. (Wen67), Brosi et al. (Bro62), Bienlein et al. (Bie59) and Ullman et al. (Ull61). Some results at intermediate velocities for first-forbidden transitions have been indicated by points without error brackets: ^{147}Pm data from refs. Kli66 and Eck64; ^{198}Au data from refs. Kli66 and Ava62. Eckardt et al. (Eck64) did not correct their results for depolarization in the source (see remark in sect. 7.3). The straight line represents the relation $P = -\Lambda v/c$.

It turns out that, after some initial discrepancies, all data on allowed decays obtained for electron or positron velocities larger than $0.6c$ ($E > 128$ keV) agree with $P = -v/c$ for electrons and $P = +v/c$ for positrons. Thus, a firm belief in the validity of these relations for the whole velocity range has grown.

It should be noted, however, that the results obtained at intermediate velocities, $0.4 \lesssim v/c \lesssim 0.6$ ($46 \lesssim E[\text{keV}] \lesssim 128$), all for β^--decays, offer a confused picture with large and often unexplained deviations from $P = -v/c$, while so far no measurements have been reported for velocities $v < 0.37c$. We summarize the experimental situation in fig. 2.2 showing results of a number of electron polarization measurements. Above $v/c = 0.6$ only selected values are shown. Below this velocity all results known to us for allowed decays are given†, including the present tritium data. The ^{60}Co and ^{32}P decays, for which results are presented, are both pure Gamow-Teller decays: ^{32}P is a $1^+ \rightarrow 0^+$ transition with E_o = 1.71 MeV and log ft = 7.9, while ^{60}Co is a $5^+ \rightarrow 4^+$ transition with E_o = 0.31 MeV and log ft = 7.5 (Led67). Both log ft values are rather high, due to poor overlap between initial and final state wave functions. All results have been obtained with polarimeters using Mott scattering, except those of ref. Ull61 which are from a Møller scattering experiment. Some of the Mott scattering results (Kli66) are from absolute measurements in the strict sense that the polarimeter efficiency S_{an} of the analyser was determined experimentally (Kli66a). The accuracy of arrangements with calculated efficiencies is limited by uncertainties in the adopted S_{an}-values, perhaps more seriously than realized by some of the investigators. For the best theoretical Mott functions S for single scattering by gold nuclei (Lin64; Büh68) a computational error of 1% has been estimated. However, this computed value must be converted to the efficiency S_{an} of the actual polarimeter (see previous section). In our experience this procedure excludes accuracies better than 2 or 3% for polarization results based on calculated S_{an}-values. Within this accuracy the v/c-relation is followed very well for velocities above 0.6c. It is at lower energies that the situation becomes confusing.

Relatively few experiments, all using Mott scattering,

---

†Recently, we were informed about an investigation of Ryu (Ryu75) on the polarization of β^--particles emitted in the allowed decay of ^{45}Ca (E_O = 255 keV). Ryu reports that his results indicate a polarization less than 30% of v/c at an energy of 79 keV (v/c = 0.5). This very low value has not been included in the compilation of fig. 2.2.

have been performed at intermediate velocities. There, difficulties arise from various effects: e.g. the polarimeter efficiency S_{an} decreases somewhat, a thinner scattering foil must be used, depolarization in the source material increases rapidly, β-particles of higher energy may interfere and energy-selective detection of scattered electrons becomes more difficult. As a consequence several investigators (Bie59; Eck64; Kli66) who obtained P-values close to $-v/c$ at high velocities, reported serious deviations at lower velocities. In this respect some surveys are too optimistic. In ref. Fra68, for instance, unpublished results of Ladage (Lad61) yielding a degree of polarization close to $-v/c$, are presented†, which were later superseded by less satisfactory data obtained with an improved version of the same apparatus (Eck64). The polarization results for intermediate velocities given in fig. 2.2, are briefly discussed in sect. 7.3.

It is well known and well understood that deviations from the relation $P = -v/c$ occur in some forbidden β-decays (e.g. of RaE). These are often accompanied by large deviations from a statistical shape of the energy spectrum. These cases fall outside the present selection of allowed decays. However, the first-forbidden transitions of ^{147}Pm (shape-allowed; E_o = 225 keV) and ^{198}Au (E_o = 962 keV), that are expected to follow the v/c-relation, have been included in the compilation of fig. 2.2 (for clarity by points without error brackets).

For the decay of high-Z nuclei an appreciable deviation is expected at lower energies because of the Coulomb interaction between the emitted electron and the daughter atom. This effect is usually incorporated in a factor Λ by writing $P = -\Lambda v/c$. For electrons Λ is smaller than unity; the deviation from unity increases with decreasing energy. If necessary, we corrected the data of fig. 2.2, using tables of Behrens and Jänecke (Beh69). Finite nuclear size effects are accounted for in these tables under the assumption of a uniform charge distribution inside the nucleus. The deviation of Λ from unity is negligible for the

†Unfortunately, the result at the lowest energy in ref. Fra68 (p. 1451), that belongs to the superseded data of Ladage, has been attributed by a misprint to Ullman et al.

tritium (< 0.1%) and the ^{32}P ($\lesssim$ 0.2%) data. It amounts to 3.3% for ^{60}Co at v/c = 0.37, to 6% for ^{198}Au at v/c = 0.45 and to 9% for ^{147}Pm at v/c = 0.37.

The influence of second-forbidden matrix elements on the polarization is of order $(kR)^2 \approx 10^{-4}p'^2$ or $(v_N/c)(kR) \approx 10^{-3}p'$, depending on the type of matrix element concerned (Mor59). Here, v_N is the average velocity of the nucleons in the nucleus ($v_N/c \approx$ 0.1), R is the nuclear radius, k is the wave number of the emitted electron and p' is its momentum in units $m_e c$. The influence is negligible small for the data of fig. 2.2: $\lesssim 3\cdot10^{-4}$ for tritium, $\lesssim 2\cdot10^{-3}$ for ^{60}Co and $\lesssim 3\cdot10^{-3}$ for ^{32}P.

We concur with several investigators (Bie59; Eck64; Laz70) in feeling the need for reliable low-velocity data, because any real deviation from $P = -v/c$ would be in serious contradiction with the present theory of β-interaction. The aim of the present investigation is to obtain accurate polarization results at the lowest possible energies in order to check whether or not there are real deviations from the theory at low velocities.

In this context we remark that a factor v/c also occurs in equations describing related phenomena like β-asymmetry of polarized nuclei and β-γ circular polarization correlation (Sch66). The first parity experiments were the measurements of the β-asymmetry of polarized nuclei by Wu et al. (Wu57) on ^{60}Co and ^{58}Co, followed by measurements of Postma et al. (Pos57,58,60) on ^{58}Co and ^{52}Mn. These experiments cover β-velocities 0.4 < v/c < 0.8. Steffen (Ste59) and later Lobashov and Nazarenko (Lob62) investigated the v/c-dependence of the β-γ circular polarization correlation for ^{60}Co at electron velocities between 0.52c and 0.77c. These four groups found a rather satisfactory v/c-dependence of the observed effects, though with deviations of about 20% at velocities below ≈ 0.6c, where large corrections were needed (e.g. for the influence of scattering in source and apparatus).

CHAPTER 3 THE β-DECAY OF TRITIUM

3.1. Introduction

Tritium, the isotope of hydrogen with one proton and two neutrons was discovered in 1934 by Rutherford et al. (Rut34). It occurs in nature as a result of nuclear reactions induced by cosmic radiation: on 10^{18} atoms of ^1H, about one atom of ^3H is found (Kau54). Tritium is β^--active and decays as

$$^3H \rightarrow {}^3He + \beta^- + \bar{\nu}. \qquad (3.1)$$

The transition occurs between the ground states (fig. 3.1). Spin and parity of both states are $J^\pi = \frac{1}{2}^+$ (Led67), in accordance with the single-particle model of the nuclear shell theory: the ^3H and ^3He nuclei can be described as closed cores (N=Z=2) with a single hole in the $1s_{\frac{1}{2}}$ proton or neutron shell, respectively.

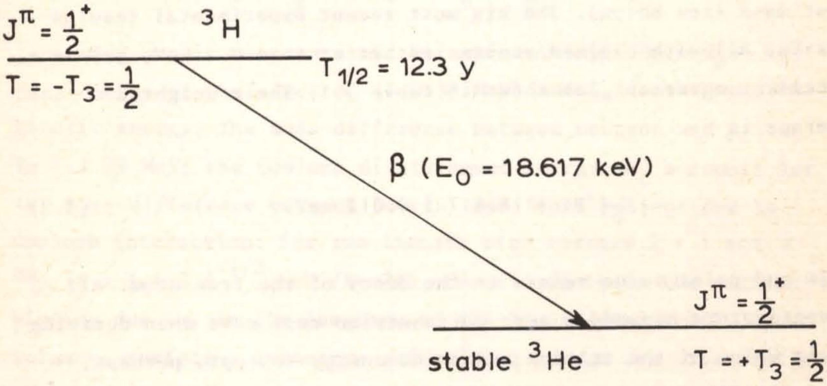

Fig. 3.1. Decay scheme of the tritium β^--transition.

^3H and ^3He are mirror nuclei in the sense that the numbers of protons and neutrons are interchanged ($N_i = Z_f$ and $Z_i = N_f$; thus, for a β^--transition: $N_i = Z_i + 1$ and $N_f = Z_f - 1$, the suffices i and f denoting the initial and final state, respectively). This implies that the ground states form an isospin doublet with isospin quantum number $T = \frac{1}{2}$. The third component of the isospin $T_3 = (Z - N)/2$ (following the convention that a proton has $T_3 = +\frac{1}{2}$ and a neutron $T_3 = -\frac{1}{2}$) is $-\frac{1}{2}$ for ^3H and $+\frac{1}{2}$ for ^3He. The assignment $T = \frac{1}{2}$ for both ground states is based on the rule that the isospin quantum number of the ground state of a light nucleus takes the lowest possible value: $T = |T_3|$.

Since $\Delta J = \Delta T = 0$ and $\pi_i = \pi_f$, the tritium transition is a mixed allowed transition: both Fermi and Gamow-Teller decay modes participate. Because of its low ft-value ($\log ft = 3.06$, see sect. 3.4) the transition is commonly classified as "superallowed". The allowed statistical shape of the tritium β-spectrum has been established down to about 1 keV (Cur52, Lew70), the lowest β-energy ever studied.

3.2. End-point energy

The end-point energy E_0 of the tritium β-spectrum is well established, thanks to numerous investigations on the antineutrino rest mass (see below). The six most recent experimental results for E_0, all with claimed accuracies better than 0.1 keV, are in excellent agreement, as shown in table 3.1. Their weighted average is

$$E_o(^3H) = 18.617 \pm 0.012 \text{ keV}. \tag{3.2}$$

This end-point value refers to the decay of the free atom. All investigators assumed a zero antineutrino rest mass when deriving their value of the tritium end-point energy (except, perhaps, Piel (Pie73), who is not clear on this point). Bergkvist (Ber72) claims that his result is practically independent of this assumption.

The liquid-drop model may be used to demonstrate why the tritium decay has a low end-point energy. According to this model the maximum total energy W_0 of a β^--particle emitted in a transition between mirror nuclei is given by

Table 3.1

Recent experimental results for the tritium end-point energy.

Author(s)	Method	End-point energy E_0 (keV)
Salgo and Staub (Sal69)	electrostatic spectrometer	18.70 ± 0.06
Daris and St-Pierre (Dar69a)	magnetic spectrometer	18.570 ± 0.075
Lewis (Lew70)	^3H implantation	18.540 ± 0.095
Bergkvist (Ber72)	magnetic spectrometer	18.610 ± 0.016
Piel (Pie73)	magnetic spectrometer	18.578 ± 0.040
Röde (Röd74)	magnetic spectrometer	18.648 ± 0.026
Weighted average[a)]		18.617 ± 0.012

a) Chi-square per degree of freedom is 1.10.

$$W_0 = m_e c^2 + E_0 \simeq (m_n - m_p)c^2 - \Delta W_C \tag{3.3}$$

(assuming a zero rest mass of the antineutrino). Here $m_e c^2$ is the rest energy of the electron ($\simeq$ 0.51 MeV) and E_0 is the maximum kinetic energy; the mass difference between neutron and proton is $\simeq$ 1.29 MeV; the Coulomb displacement energy ΔW_C accounts for the mass difference between initial and final nucleus due to Coulomb interaction: for two isobars with charges $Z + 1$ and Z ΔW_C is $\simeq 1.4\, Z\, A^{-1/3}$ MeV (Fra74). Contributions to the nuclear binding due to, in the language of the liquid-drop model, the volume-, surface-, symmetry- and pairing-energy are essentially the same for parent and daugther nucleus and cancel in the expression for W_0. For the simplest β^--transition between mirror nuclei, the decay of the neutron into a proton, $\Delta W_C = 0$ and $E_0 \simeq 1.29 - 0.51 = 0.78$ MeV. Next in simplicity is the tritium mirror transition: for this decay ΔW_C is already so large that only a small amount of energy is available as kinetic energy of the electrons. Actually, in this case the above approximation gives $\Delta W_C \simeq 1$ MeV, so that eq. 3.3 gives E_0 (^3H) $\simeq$ -0.2 MeV; a more precise treatment, including charge symmetry breaking interactions (Shl75), is needed to explain that the tritium end-point energy is still slightly positive. For higher Z the Coulomb term is so large that β^--transitions are energetically prohibited: with the exception of the neutron and tritium decay all transitions between mirror nuclei are β^+-decays. This is in accordance with the well known fact that radioactive nuclei with $N \approx Z$ lie, for not too low Z, on the β^+-active side of the valley of β-stability.

Because of the extremely low end-point energy the shape of the tritium β-spectrum in the neighbourhood of the end point is very sensitive to the influence of any finite rest mass of the antineutrino. A recent compilation of results of investigations on this subject has been given by Piel (Pie73). The most accurate result is claimed by Bergkvist (Ber72): he gives an upper limit for the antineutrino rest mass of 55-60 eV at a confidence level of 90%.

Also the longitudinal polarization of the β-particles depends on the rest mass of the antineutrino. However, this dependence disappears after averaging over the emission direction of the antineutrino, as has been discussed in some detail by Bergkvist (Ber72). Hence, no information on this rest mass can be derived from the tritium β-polarization measurement described in this thesis.

3.3. Half-life

A compilation of results of measurements of the tritium half-life is given by Piel (Pie73). The data with by far the highest claimed accuracies are those of Jones (Jon55: $T_{\frac{1}{2}} = 12.262 \pm 0.004$ y) and of Eichelberger et al. (Eic63: $T_{\frac{1}{2}} = 12.355 \pm 0.010$ y), both obtained by measuring the growth of ^3He in a known amount of ^3H. These values differ by about 10 to 20 times their stated errors. The results of calorimetric determinations of the tritium heat output show better consistency. Lewis (Lew70) demonstrated that these data strongly favour the $T_{\frac{1}{2}}$-determination of Eichelberger et al.

3.4. *ft*-value

With E_0 and $T_{\frac{1}{2}}$ known, the comparative half-life or *ft*-value of the tritium decay can be calculated in principle (eq. 1.30). Bergkvist (Ber72) gave a detailed analysis of the various corrections which are needed (e.g. influences of bound-state decay, outer radiative effects and screening). Using the half-life value obtained by Jones (see above) and his own result for the tritium end-point energy (see table 3.1), which agrees well with the weighted average presented in eq. 3.2, he arrived at: $ft = 1148 \pm 3$ sec. Use of the probably more reliable half-life result of Eichelberger (see above) leads to a 0.8% higher value

$$ft(^3\mathrm{H}) = 1157 \pm 4 \text{ sec}, \tag{3.4}$$

which corresponds to log ft = 3.06.

3.5. Nuclear matrix elements

Since the tritium β-decay is a transition between two members of an isospin multiplet, the value of the Fermi matrix element can be calculated with the aid of eq. 1.29. Inserting $T = -T_3^{\mathrm{i}} = T_3^{\mathrm{f}} = \frac{1}{2}$ one obtains $|M_{\mathrm{F}}(^3\mathrm{H})| = 1$. For a nucleus as light as tritium the magnitude of isospin impurity corrections (see subsect. 1.2.2) is expected to be smaller than 0.1% (Ram75). The magnitude of the Fermi matrix element is not influenced by strong interactions (see subsect. 1.2.2).

As remarked in subsect. 1.2.2 the Gamow-Teller matrix element depends on nuclear structure and is affected by strong interactions (pion exchange). The matrix element can be expressed as: $|M_{\mathrm{GT}}| = |M^{\mathrm{o}}_{\mathrm{GT}}|(1+\delta_{\mathrm{e}})$. The parameter δ_{e} accounts for the strong interaction effects. Comparison of experimental values of $|M_{\mathrm{GT}}|$ with a calculated $|M^{\mathrm{o}}_{\mathrm{GT}}|$-value may provide a check of the validity of the PCAC-theory. Extensive studies on this subject were presented by Primakoff (Pri70) and by Blin-Stoyle (Bli73). The ^{3}H-^{3}He case is especially suited for this approach because it is after the neutron decay the simplest β-transition, so that the wave functions of the initial and final state are known rather reliably. Hence, $|M^{o}_{GT}|$ can be calculated. In the single particle model, the $|M^{o}_{GT}|$-values of the tritium and neutron decay are equal: $|M^{o}_{GT}|^2 = 3$ (Wu66). Using more realistic ^{3}H and ^{3}He wave functions, the theoretical values of $|M^{o}_{GT}|^2$ vary between about 2.5 and 2.9 (Bli73). The rather broad range reflects uncertainties in the wave functions.

An experimental value of $|M_{GT}|$ for the tritium transition can be obtained from a comparison of the ft-value of the tritium decay with those of $0^+ \rightarrow 0^+$ transitions and the neutron decay, using $|M_F(^3\text{H})| = 1$ and, as discussed in subsect. 1.2.2, $|M_F(0^+ \rightarrow 0^+)|^2 = 2$, $|M_F(\text{n})| = 1$ and $|M_{GT}(\text{n})|^2 = 3$. Eqs. 1.31 and 1.32 yield:

$$|M_{GT}(^3\text{H})|^2 = \frac{1}{\lambda^2}\left(\frac{2ft(0^+ \rightarrow 0^+)}{ft(^3\text{H})} - 1\right) = 3\frac{ft(\text{n})}{ft(^3\text{H})}\left[\frac{2ft(0^+ \rightarrow 0^+) - ft(^3\text{H})}{2ft(0^+ \rightarrow 0^+) - ft(\text{n})}\right]. \quad (3.5)$$

Upon inserting $ft(^3\text{H}) = 1157 \pm 4$ sec (eq. 3.4), $ft(\text{n}) = 1093.3 \pm 16.5$ sec (Kro74) and for $ft(0^+ \rightarrow 0^+)$ the value 3085 ± 5 sec, adopted in subsect. 1.2.2, one obtains $|M_{GT}(^3\text{H})|^2 = 2.80 \pm 0.04$, which is not much smaller than $|M_{GT}(\text{n})|^2$. Clearly, more accurate theoretical $|M^{o}_{GT}|$ values for the tritium transition demanding more precise ^{3}H and ^{3}He wave functions, are needed to obtain conclusions about the magnitude of the PCAC-correction δ_e.

The present polarization measurement yields no information about the Gamow-Teller matrix element of the tritium decay. As may be seen from inspection of eq. 1.36, the degree of longitudinal polarization for allowed transitions is completely independent of nuclear matrix elements if the (V-λA)-theory with two-component left-handed neutrinos (implying equality of the parity-conserving and the parity-violating coupling constants: $C_V = C'_V$ and $C_A = C'_A$) is valid.

In ch. 8 we consider the ratios C'_V/C_V and C'_A/C_A. The result of the present polarization measurement is combined there with information about the nuclear matrix elements of tritium.

CHAPTER 4 THE TRITIUM SOURCES

4.1. Introduction

Source conditions are essential for β-polarization measurements at low electron energies. In the present investigation a compromise had to be found between the two following requirements: i) the amount of source material, which includes carrier and backing, should be small and of low atomic number in order to avoid large and uncertain depolarization corrections; ii) the source strength should be sufficient for reasonable counting statistics. The first requirement is especially severe at low electron energies since depolarization corrections exhibit approximately an E^{-2} energy dependence (see ch. 6). The second requirement becomes a serious limitation in the neighbourhood of the end-point energy of tritium.

In sect. 4.2 we describe the composition of the sources used and in sect. 4.3 their energy spectra.

4.2. Composition of the sources

Tritium sources made by so called thermal occlusion of tritium in titanium or zirconium layers are commercially available. This kind of sources finds widespread use as targets for the production of neutrons by bombardment with deuterium. Typically the layers have thicknesses of some mg/cm^2 and usually they are deposited on a thick backing of aluminium, nickel or, if optimum cooling is required, of copper. Sources on lower-Z backings, for example of beryllium, are not commercially obtainable.

For our purposes we chose, of course, the lower-Z carrier titanium and a backing of aluminium. The two sources used for the main experiments were made according to our specifications by Nukem (Hanau, W. Germany). They consist of tritiated titanium layers of 23 ± 2 and 120 ± 12 μg/cm^2 on 1 mm thick aluminium disks with a diameter of 10 mm.

The production process of the sources consists of several steps. First, titanium is deposited on the Al backing by vacuum evaporation. Then, the tritiation is performed by heating the titanium plus aluminium assembly for about 15 min at 400^{o}C in a tritium atmosphere. The source is cooled in the tritium atmosphere in about 2 hours to a temperature of about 80^{o}C. During this cooling some tritium is trapped in the titanium layer. Finally, the assembly is cooled to room temperature. The tritium to titanium ratio of these sources may range from 1:1 to 1:2. According to the specifications of the manufacturer the tritium remains occluded in the titanium up to temperatures of about 200^{o}C (in vacuo).

The main advantage of sources of the tritiated titanium type is their very high specific activity: the above atomic ratios correspond to specific activities ranging between 450 and 900 Ci/g. Such high values can, as far as we know, not readily be obtained with other source preparation techniques. The specific activity of, for example, tritiated organic-compound sources is limited by the chemical nature of the compound and by problems of self-radiolysis. With tritiated silanol, a very stable compound, sources with specific activities up to about 40 Ci/g can be obtained (Dar68).

A drawback of tritiated titanium sources is that the high temperatures involved in the production process rule out ultra thin backings. The minimum backing is 200 $\mu g/cm^2$ aluminium. However, in the upper part of the tritium β-spectrum, where the more accurate polarization measurements were performed, the depolarization caused by such a backing is practically the same as for an "infinitely" thick aluminium backing: the energy loss of 15 keV electrons, for instance, traversing 200 $\mu g/cm^2$ Al twice, amounts already to about 4 keV. We, therefore, could use an easier to handle backing of 1 mm thickness just as well. We show in ch. 6 that depolarization by the backing is of minor influence at energies not too far below the end-point energy.

We made an autoradiogram of the thicker source with aid of a photographic emulsion which was sensitive for the X-rays produced by the tritium β-particles in the titanium layer. The source image was perfectly homogeneous.

The strength of both sources is in the order of 10 mCi as estimated from observed counting rates in a double-focusing spectrometer (see below) and in our polarimeter. For the thinner source, with which the final polarization measurements were performed, this strength corresponds to a tritium to titanium ratio of 1:0.8, roughly in accordance with the limits quoted above. It is not clear why the thicker source is weaker than expected. Actually, we obtained a third source, with a tritiated titanium layer of 12 $\mu g/cm^2$. This source, however, was about a factor six weaker than the other ones and was hardly used.

The variation with depth of the tritium concentration in the source material is not accurately known. Most probably the aluminium backing was covered with a thin oxide film before being used in the production process of the source. Since tritium diffuses difficultly through aluminium oxide, as observed for example by Daris and St-Pierre (Dar69) (see also ref. Ber63), we expect that only a small fraction of the tritium activity resides in the backing. The titanium layer may be oxidized or nitridized on either side due to atmospheric oxidation or absorption of rest gases from the evaporation chamber. This is at least indicated by tritium profiles in thick sources as determined by Gunnersen and James (Gun60; Kab73). Their results suggest that the tritium concentration increases somewhat with depth in our titanium layer. We estimate that the average depth of the tritium is 0.7 ± 0.2 times the thickness of the titanium layer. This estimate is confirmed, within error limits, by measurements with the double-focusing spectrometer, described below.

Any dead layer on the surface of the source should be avoided since it would depolarize the emerging beam. During preliminary polarization measurements with the 120 $\mu g/cm^2$ source we noticed a gradually growing contamination on the source. Presumably this is due to rest-gas molecules that adhere on the surface after decomposition and immobilization by the intense β-radiation. Before starting the polarization measurements with the 23 $\mu g/cm^2$ source we placed several nitrogen-cooled vapour traps in the apparatus to reduce source contamination (see subsect. 5.2.1). After finishing these measurements we demonstrated with the double-focusing spectrometer that contamination can be neglected for this source (see next section).

4.3. Energy spectrum

The energy spectrum of the β-particles emerging from the sources was measured with the Groningen double-focusing spectrometer†. A description of this spectrometer has been given by Pleiter (Ple72). The β^--particles are detected by a Geiger-Muller counter with a thin gold-coated formvar window, supported by a platinum mesh. The transmission curve of this window has been measured by Pleiter. For electron energies above 15 keV the transmission was independent of energy; the transmission at 8 keV was half of that at 15 keV. We calibrated the spectrometer with L_I and M_I conversion electrons from the 39.86 keV level of ^{208}Tl that have kinetic energies of 24.510 keV ("Th-A line") and 36.155 keV ("Th-B line"), respectively (Led67). The Th(B+C+C'') calibration source was recoil-collected in an aluminium foil. The accuracy of the energy determination in the neighbourhood of the tritium end point is 65 eV. The observed shape of the conversion lines is approximately Gaussian, with a FWHM resolution $\Delta p/p$ = 0.6%. This momentum resolution corresponds in the tritium end-point region with a FWHM energy width of 220 eV ($\Delta E/E$ = 1.2%). The resolution could have been improved by using a different adjustment of the spectrometer. This, however, was not necessary since the line broadening due to the depth distribution of the activity and to energy-loss straggling amounts already to about 200 eV for the 23 μg/cm² source (see below). Furthermore, the smaller transmission, inherent in improved resolution, would give more severe background problems in the end-point region.

For an undistorted allowed β-spectrum with end-point energy E_0, the intensity distribution is given by (see eq. 1.20)

$$N(E) \sim p\, W\, F(Z,W)\, (E_0 - E)^2. \qquad (4.1)$$

Here, $N(E)$ denotes the number of electrons emitted by the atoms per

† In co-operation with Mr. R. Spanhoff.

unit of time, energy and solid angle with kinetic energy E; p and W are momentum and total energy of these electrons, respectively; $F(Z,W)$ is the Fermi function. For the tritium transition, the shape of the spectrum above, say, 1 keV is mainly determined by the product $\sqrt{E}(E_0-E)^2$, since in this energy region F (Beh69) and W are practically energy independent, while p is approximately proportional to $\sqrt{E}$. The intensity $N(E)$ has its maximum at about 3.7 keV.

The end-point energy of a β-spectrum can be determined with the aid of a Kurie plot, plotting $\left[N_{obs}(E)/pWF\right]^{\frac{1}{2}}$ vs. E. $N_{obs}(E)$ is the intensity observed at an energy setting E of the spectrometer, corrected for background and for variation of energy resolution of the spectrometer. In the neighbourhood of the end point, corrections for instrumental resolution due to finite resolution of the spectrometer and to finite source thickness, may be necessary. For an allowed transition the Kurie plot is expected to be a straight line which intersects the energy axis at E_0.

In fig. 4.1 we show a Kurie plot for the 23 μg/cm^2 tritium source at energies above 17 keV, where the spectrum distortion due to scattering in the titanium layer and in the backing is expected to be small. The observed intensities were corrected for background and for variation of energy resolution, but not yet for instrumental resolution. The Kurie plot is essentially straight, ascertaining that the influence of scattering is indeed small in the energy region concerned. The intersection with the energy axis occurs at 18.63 ± 0.07 keV. The error is mainly due to the uncertainty of the energy calibration. This measurement with the double-focusing spectrometer was performed after the final polarization measurements. The surface of the source was still clean: no traces of contamination were visible. A similar Kurie plot (not shown) of the visibly contaminated 120 μg/cm^2 source, yielded 17.8 ± 0.1 keV as intersection with the energy axis. Comparison with the value E_0 = 18.617 ± 0.012 keV of eq. 3.2 indicates that the influence of the titanium layer and of contamination is small for the 23 μg/cm^2 source, but becomes more important for the thicker source.

Until now the influence of finite spectrometer resolution and

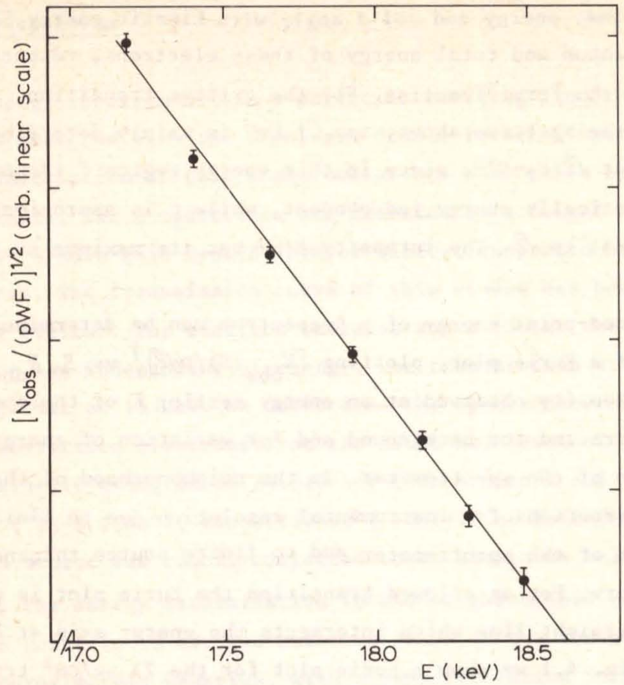

Fig. 4.1. Kurie plot of the 23 μg/cm² tritium source obtained with the double-focusing spectrometer. The straight line represents a least-squares adjustment: chi-square per degree of freedom is 1.09.

broadening in the source was disregarded. In the following discussion these effects are taken into account in order to obtain better information on the average depth of the tritium activity. Neglecting, for a moment, scattering in the source, we write for the number of electrons emitted per unit of time, energy and solid angle with energy E' in a direction perpendicular to the surface of the source:

$$N_s(E') \sim \int_0^{t_0} \int_{E'}^{E_0} n(t)\, N(E)\, w(E,t;E')\, dt\, dE. \qquad (4.2)$$

Here, $n(t)$ gives the depth distribution of the tritium activity between $t = 0$ and the maximum depth t_0; $N(E)$ is the undistorted spectrum as emitted by the tritium atoms (eq. 4.1); $w(E,t;E')$ is the probability (neglecting scattering) per unit of solid angle and energy that an electron, emitted by a tritium atom at depth t, with inital energy E, in a direction perpendicular to the surface of the source, leaves the source in that direction with final energy E'. For small t we can write in good approximation (Kno65): $w(E,t;E') \sim G_n[E';E-\Delta(t),\sigma_\ell(t)]$, a normalized Gaussian distribution centered at an energy $E-\Delta(t)$ with standard deviation $\sigma_\ell(t)$; $\Delta(t)$ is the mean energy loss in a layer with thickness t; the variation in the energy loss is due to straggling. Using the series developments

$$\int_{-\infty}^{+\infty} f(x) G_n(x;x_m,\sigma)\,dx = f(x_m) + \frac{1}{2}\sigma^2\left(\frac{d^2f}{dx^2}\right)_{x_m} + \frac{1}{8}\sigma^4\left(\frac{d^4f}{dx^4}\right)_{x_m} + \ldots \quad (4.3)$$

(the odd derivates vanish by virtue of the symmetry of the Gaussian distribution) and

$$N(E'+\Delta(t)) = N(E') + \left(\frac{dN}{dE}\right)_{E'} \Delta(t) + \tfrac{1}{2}\left(\frac{d^2N}{dE^2}\right)_{E'} \Delta^2(t) + \ldots \quad (4.4)$$

eq. 4.2 yields for values of E_0-E' which are at least a few times larger than $\bar{\Delta}$:

$$N_s(E') \sim N(E') + \left(\frac{dN}{dE}\right)_{E'} \bar{\Delta} + \tfrac{1}{2}\left(\frac{d^2N}{dE^2}\right)_{E'} (\overline{\Delta^2} + \overline{\sigma_\ell^2}) + \ldots \quad (4.5)$$

The bars denote averaging over the depth distribution. This equation can be written in a form which is more easy to interprete:

$$N_s(E') \sim N(E'+\bar{\Delta}) + \tfrac{1}{2}\left(\frac{d^2N}{dE^2}\right)_{E'} \left[\overline{(\Delta-\bar{\Delta})^2} + \overline{\sigma_\ell^2}\right] + \ldots \quad (4.6)$$

The first term on the right-hand side indicates that into first order the spectra N and N_s are shifted with respect to each other over an energy interval $\bar{\Delta}$. In the end-point region, where $(d^2N/dE^2)/N \simeq 2(E_0-E)^{-2}$ becomes large, the second term may be important. In this term, $\overline{(\Delta-\bar{\Delta})^2}$ accounts for the finite width of the distribution of the tritium in the source, while $\overline{\sigma_\ell^2}$ accounts for energy-loss straggling in the source material.

The intensity distribution actually observed with the spectrometer is obtained by applying the so called Owen-Primakoff correction (Owe48) on the distributions 4.5 or 4.6. This correction accounts for the finite resolution of the spectrometer. If the window curve of the spectrometer is Gaussian with mean energy E'' and standard deviation σ_w, eq. 4.3 may be used to obtain for $E - E'' \gg \sigma_w$:

$$N_{obs}(E'') \sim N_s(E'') + \tfrac{1}{2}\sigma_w^2\left(\frac{d^2N_s}{dE^2}\right)_{E''} + \ldots \qquad (4.7)$$

The relation between σ_w and the FWHM width ΔE is $\sigma_w = \Delta E/(8\ \ln 2)^{\frac{1}{2}} \simeq 0.42\ \Delta E$, so that $\sigma_w \simeq 90$ eV in the end-point region.

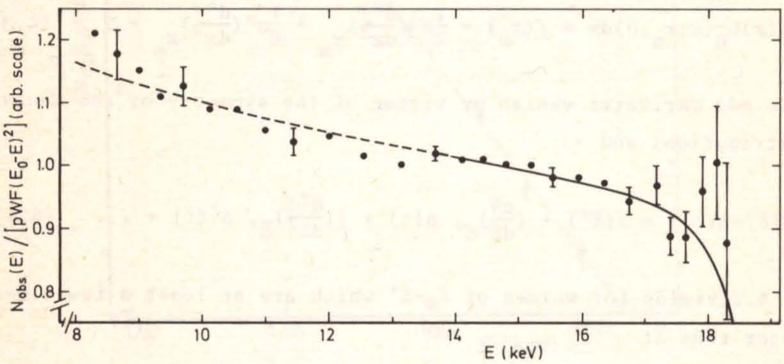

Fig. 4.2. Shape factor of 23 μg/cm² source versus energy setting of the double-focusing spectrometer. Indicated uncertainties do not include errors in E_o and E. The result of a least-squares adjustment is shown (see text).

In fig. 4.2 we show the shape factor N_{obs}/N for the 23 μg/cm² source after correction for the finite transmission of the GM-window. At energies above 14 keV this correction is of little influence. We performed a least-squares adjustment for the data between 14 and 18.3 keV with three adjustable parameters C_1, C_2 and $\bar{\Delta}$ to:

$$N_{obs}(E'') = C_1 N(E'') \times \qquad (4.8)$$

$$\left[1 + \frac{\bar{\Delta}}{N(E'')}\left(\frac{dN}{dE}\right)_{E''} + \frac{1}{2N(E'')}\left(\frac{d^2N}{dE^2}\right)_{E''}(\overline{\Delta^2} + \overline{\sigma_\ell^2} + \sigma_w^2) + C_2(E_0 - E'')^2\right]$$

Here, source thickness and instrumental resolution are accounted for according to eqs. 4.5 and 4.7; C_1 is a normalization factor; the term with C_2 is a phenomenological correction for the influence of scattering in source and backing. The term with the second derivate is relatively small: we used σ_w = 90 eV and the realistic estimate: $\overline{\Delta^2} + \overline{\sigma_\ell^2} \simeq 0.7(\bar{\Delta})^2$. The end-point energy E_0 was held fixed at the value 18.617 keV of eq. 3.2. The results of this adjustment (with a chi-square per degree of freedom of 1.14) were C_2 = 0.0015 ± 0.0012 per keV^2 and $\bar{\Delta}$ = 50 ± 70 eV. The errors include the uncertainty of the energy calibration and of the end-point energy.

The observed mean energy loss $\bar{\Delta}$ can be converted to the average depth t_{av} of the tritium in the titanium layer. Assuming that the source was not contaminated and taking a value of 8 ± 2eV/ μg/cm^2 (Ber64; Ber72) for the mean energy loss of 18.6 keV electrons in titanium we find: t_{av} = 6 ± 10 μg/cm^2. Similarly, for the 120 μg/cm^2 source: t_{av} = 100 ± 30 μg/cm^2. These results prove that the penetration of tritium into the aluminium backing is minute, as was anticipated in the previous section.

As remarked, we shall neglect the influence of contamination for the 23 μg/cm^2 source. The above result for $\bar{\Delta}$ shows that a possible low-Z contamination layer is thinner than about 10 μg/cm^2. Even for such an unrealistically thick layer, the depolarization would not exceed 0.7% (see ch. 6).

It follows from the above value of C_2 that the influence of scattering in source and backing is small in the neighbourhood of the end point. At 15 keV, for example, the $C_2(E_0-E'')$ term of eq. 4.8 amounts to about 2%, while, at 10 keV, its magnitude is still only about 11%. In ch. 6 we discuss depolarization due to scattering in source and backing: the above value of C_2 agrees roughly with intensity calculations presented there.

CHAPTER 5 INSTRUMENTATION

5.1. Introduction

For the polarization measurements presented in this thesis we made use of the Mott scattering method, which is by far the most accurate method for electrons with energies below, say, 500 keV. This method was briefly described in sect. 2.1. Our polarimeter had been calibrated by means of a double-scattering experiment at electron energies between 46 and 261 keV, as described by van Klinken (Kli65,66a). Its best performance falls in the upper half of this range. The tritium β-particles were accelerated before being analysed in the polarimeter. This acceleration does not affect the degree of longitudinal polarization of the beam, as shown by Tolhoek (To156). Originally we intended to accelerate the β-particles to a fixed final energy of 128 keV (v/c = 0.6): at this energy a calibration accuracy of better than 1% had been achieved. Because of difficulties with field emission (subsect. 5.2.4) this final energy was lowered to 79 keV (v/c = 0.5), at which energy a calibration accuracy of about 1.3% is still possible. The recalibration of the polarimeter at 79 keV is described in sect. 5.4.

The investigation was performed with two different arrangements, which are sketched in fig. 5.1. We started with arrangement I, but changed later to arrangement II, for reasons to be explained hereafter. In following the electrons from source to detector we distinguish: the source which can be replaced by a source simulator (subsect. 5.2.2); a preaccelerator and a lens L_1 for primary energy selection; a deflector followed by the main accelerator (fig. 5.1.I) or the main accelerator followed by a deflector (fig. 5.1.II); intermediate lenses L_2 and L_3; and the Mott polarimeter with scattering foil and four scintillation detectors. Lenses, deflector and detectors are all energy selective. By applying an accelerating or retarding bias voltage V_p to the source various parts of the tritium spectrum could be investigated with a fixed setting of other parts of the equipment.

In the electrostatic deflector the spin orientation of the electrons remains approximately the same, while their direction of motion changes. Thus the polarization of the beam is transformed from longitudinal to transverse.

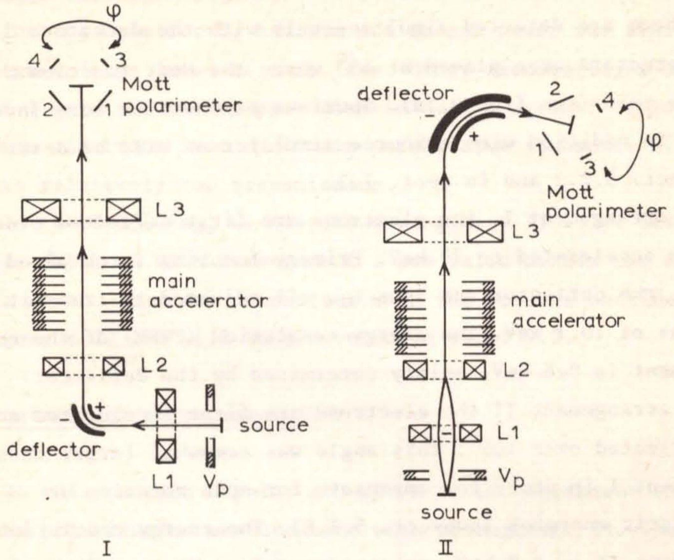

Fig. 5.1. The two basic arrangements: I with deflection before acceleration and II with deflection after acceleration. Arrangement II has been used for the main measurements.

As discussed in sect. 2.1, the polarization analysis is based on the spin dependence of Coulomb scattering of the transversely polarized electrons. The detectors 1 and 2, at scattering angles of 117°, measure the left-right asymmetry in the plane normal to the polarization vector of the electrons incident on a gold foil. Neglecting corrections for instrumental asymmetries the relation between the left-right asymmetry, the degree of transverse polarization P_T and the efficiency S_{an} of the polarimeter is

$$(L - R)/(L + R) = P_T S_{an}. \tag{5.1}$$

Here, L and R are the counting rates for the "left" and "right" detector, respectively. The calibration of the polarimeter by a double-scattering experiment (sect. 5.4) gives a value for S_{an} which includes the influence of foil thickness, angular spread, scattering from walls, etc. The effect of possible differences between the detectors 1 and 2 is eliminated by interchanging the detectors periodically by rotating the polarimeter over 180°. Instrumental asymmetries connected with a possible misalignment of the beam are detected simultaneously with the detectors 3 and 4. These detectors were placed at 45° where the Mott function S is close to zero (see fig. 2.1a). Spurious asymmetries were investigated in addition with a source simulator as will be described in subsect. 5.2.2 and in sect. 7.2.

In arrangement I the electrons are first deflected over 90° and then accelerated to 79 keV. Primary focusing is obtained with lens L_1, the deflector and lens L_2, all adjusted to transmit electrons of 10.1 keV. The energy resolution (FWHM) of the total arrangement is 0.6 keV, mainly determined by the deflector.

In arrangement II the electrons are first accelerated and then deflected over 105°. This angle was somewhat larger than in arrangement I in order to compensate for spin rotation at relativistic energies (subsect. 5.2.6). The energy resolution of arrangement II is 2.8 keV, mainly determined by L_1 and the deflector. At $V_P = 0$ the transmission window is centered at 15.5 keV, which corresponds to a mean energy of the transmitted tritium electrons of 14.5 keV.

We preferred arrangement II because there the polarization asymmetry is measured in a plane perpendicular to the plane of electrostatic deflection. This plane of deflection is a symmetry plane of the apparatus. (The detectors in fig. 5.1.II must be rotated over $+90^{\circ}$ or -90° for being in their actual counting position). In arrangement I the symmetry was less perfect, because lens L_2 rotated the transverse polarization and the beam profile at a difference rate. As shown by Tolhoek (To156) the spin of an electron moving along the z-axis in a magnetic field B, precesses around this axis over an angle

$$\alpha = (B\rho)^{-1} \int B_z(o,o,z)\, dz, \qquad (5.2)$$

where the so called $B\rho$-value of the electron is proportional to its momentum. The intensity distribution of the beam, however, is rotated over an angle $\alpha/2$ (Rus50). In principle it is possible to construct a lens which rotates neither the spin nor the beam profile, namely by using two coils with equal but opposite fields. Lens L_3 in arrangement I was constructed in such a way, but this could not be done for L_2 because not enough power was available at the high-voltage level of this lens. Other disadvantages of arrangement I were the rather poor discrimination against field-emission electrons from the main accelerator (subsect. 5.2.5) and its relatively low transmission.

In the following, we discuss arrangement II only. Still, the results obtained with arrangement I are valid within the error limits given. They are consistent with the results obtained with arrangement II and will be presented in sect. 7.2.

5.2. Details of arrangement II

In this section details are given of the equipment employed for the polarization measurements with arrangement II. The basic parts are shown in fig. 5.2 and an overall view of the arrangement is presented by a photograph (fig. 5.3).

The arrangement is a succession of energy selective devices placed in series and adjusted to each other: magnetic lenses, main accelerator, deflector and the scintillation detectors. In the course of the polarization experiments the setting of the various devices remained constant, apart from small corrections. An energy interval from the source spectrum was selected with the accelerating or retarding voltage V_p between the electrodes of the preaccelerator. The advantage of this set-up is evident: once adjusted, the total arrangement can be used for various parts of the tritium β-spectrum, without tedious readjustments of the beam alignment.

At low energy level the transmission window, as determined by L_1, is centered at 15.5 keV (somewhat varying in the course of the measurements), while the devices after the main accelerator are adjusted to about 79 keV.

The polarimeter is at ground potential. An isolation transformer provides 200 Watt power for instrumentation at the high-voltage side (-63.5 kV) of the arrangement. The vertical component

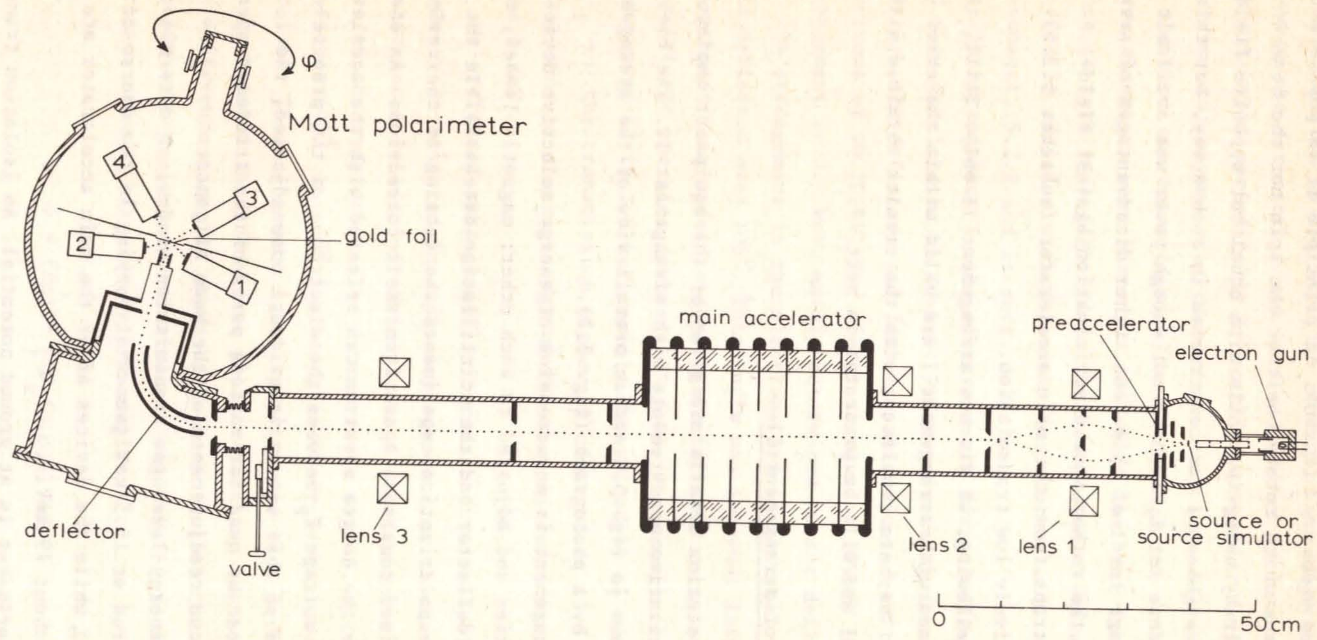

Fig. 5.2. Arrangement II in more detail. The system is operated with a tritium source or with a source simulator plus electron gun. The polarimeter is shown in a position rotated over 90° from the plane in which the polarization asymmetry is observed.

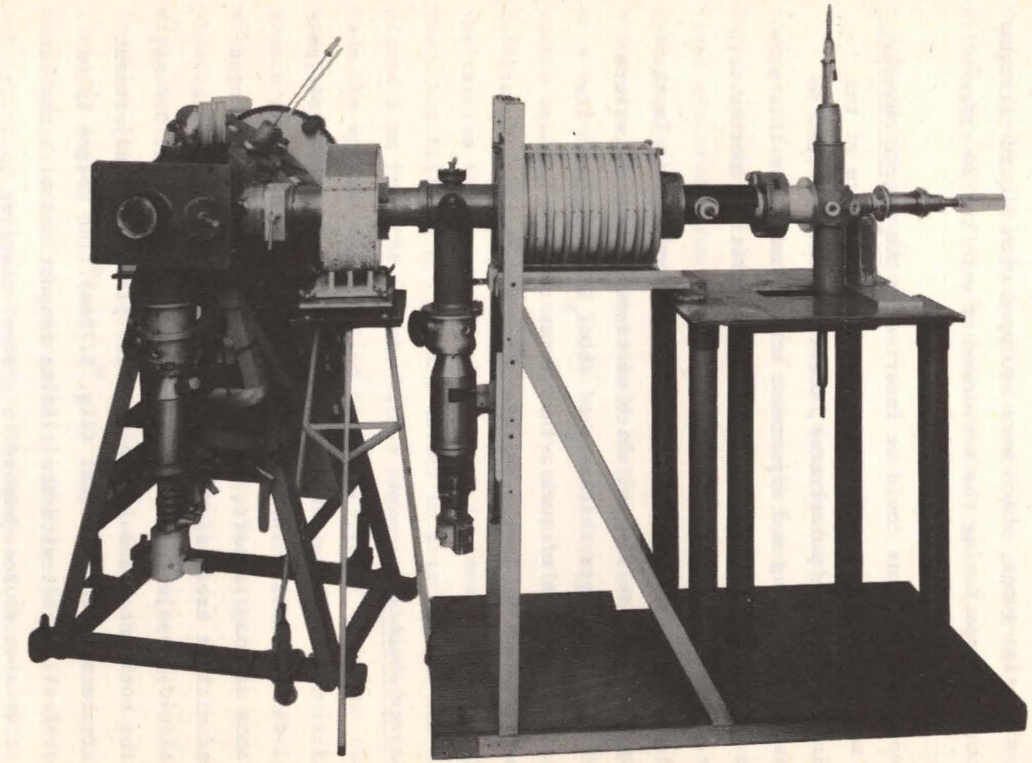

Fig. 5.3. Photograph of arrangement II. Parts of the vacuum and high-voltage facilities were removed. Photograph: Mr. R.J. van Zanten .

of the earth magnetic field was reduced by an order of magnitude with a set of Helmholtz coils. The magnetic lenses L_1, L_2 and L_3 provide energy selection, beam focusing and possibilities for geometrical adjustment. The lenses have soft-iron shields to reduce stray fields. A vacuum of about 10^{-5} Torr was maintained by two oil-diffusion pumps, which were equipped with liquid nitrogen cooled vapour traps during the measurements with the 23 $\mu g/cm^2$ source.

Fluorescent screens could be inserted in the source chamber, between main accelerator and lens L_3, and at the place of the scattering foil in the polarimeter, offering possibilities to check visually focusing and adjustment of the beam. For this purpose the source simulator was used since the tritium sources were too weak.

The distance from the source to the scattering foil in the polarimeter amounts to 210 cm, which corresponds, at a pressure of 10^{-5} Torr, to a layer thickness of about 0.004 $\mu g/cm^2$. The depolarizing influence of such a thin layer can be entirely neglected, even at the lowest energies involved in this investigation (see ch. 6).

5.2.1. Source chamber

A tritium source (see ch. 4 for a description of the tritium sources), the source simulator and a fluorescent screen were mounted on a sliding support, so that they could be interchanged easily and without breaking the vacuum. The position of these devices should be adjusted and reproduced to within about 0.1 mm, both in the horizontal and in the vertical plane. This adjustment appeared to be not very critical (fig. 5.7 e). The source is in good electrical contact with the sliding support and with the surrounding aluminium source chamber to prevent charging up.

During the measurements with the 23 $\mu g/cm^2$ source we reduced source contamination by placing 17 mm in front of the source a diaphragm ring of copper (inner diameter 25 mm), connected through a thermally isolated copper rod with an external liquid nitrogen bath. We checked with a thermocouple that the source, which was in good thermal contact with the sliding support and the source chamber, remained approximately at room temperature.

Background contributions could be measured by placing a thick copper absorber in front of the source. This absorber could be manipulated externally without breaking vacuum or high-voltage. Similarly depolarization measurements were performed by placing silver or carbon foils in front of the source (subsect. 6.3.2).

5.2.2. Source simulator

To detect possible residual instrumental asymmetries, not corrected for by the forward detectors 3 and 4, we made a device for replacing the source by a source simulator, emitting unpolarized electrons from a similar area and with approximately the same angular and energy distribution. The electrons are emitted by a tungsten filament (the cathode of the electron gun in fig. 5.2) at a variable voltage V_g with respect to the potential of the source housing and are scattered by two parallel gold foils. One foil, of 0.7 mg/cm^2 weight, could be mounted at the position of the tritium source on a diaphragm with an inner diameter of 10 mm. The other foil, of 0.3 mg/cm^2, serves as prescatterer and was placed 5 mm from the former. With a somewhat defocused primary beam the spatial distribution of the scattered electrons could be made homogeneous inside the diaphragm ring. The electrons leave the source simulator with a roughly Gaussian angular distribution and with a broad energy distribution. We estimate that the root mean square scattering angle is about 20° (Mo147), so that the angular distribution approaches isotropy inside the effective solid angle in which the electrons are transmitted towards the Mott polarimeter (between angles of 5° and 14° with respect to the beam axis). The mean energy loss of the electrons in the two foils is about 10 keV for typical V_g values of -20 kV. The shape of the energy distribution could be made similar to the shape of the tritium spectrum in the energy region of interest by a proper choice of V_g. A typical energy spectrum of the simulator is compared in fig. 5.4 with the spectrum of the tritium source.

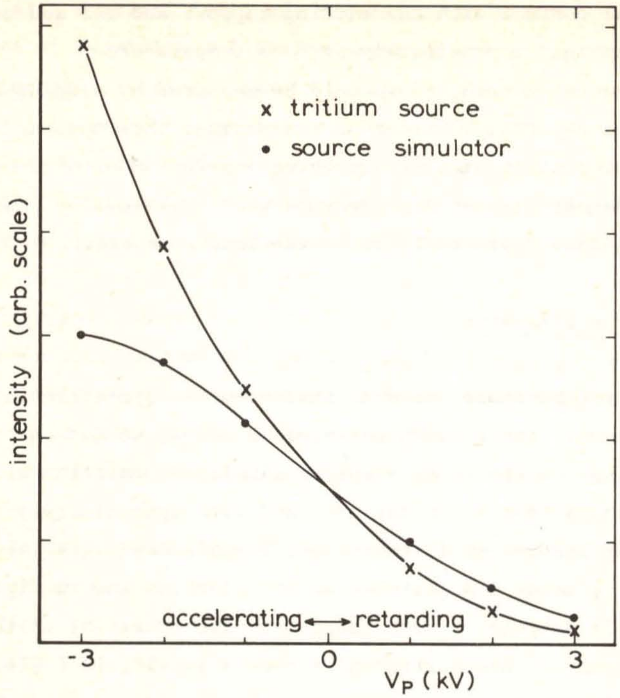

Fig. 5.4. Comparison of the intensity distributions of source simulator (V_g = -26 kV) and 23 μg/cm² tritium source in the neighbourhood of V_P = 0.

5.2.3. Preaccelerator

The preaccelerator consists of two aluminium electrodes placed at a distance d = 12 mm from each other. The first electrode (inner diameter 24 mm) at a distance of 34 mm from the source, is in electrical contact with the source chamber. The second electrode (inner diameter 28 mm) is in electrical contact with the first electrode of the main accelerator. The potential difference V_P, i.e. the potential of the first electrode with respect to that of the second one, could be adjusted between +10 and -10 kV. The focusing action of the preaccelerator is weak; the focal distance is given approximately by (Zwo45)

$$f = \frac{8d}{3}\left[(E_{out}/E_{in})^{\frac{1}{2}} - 1\right]^{-1}\left[1 - (E_{in}/E_{out})\right]^{-1}, \qquad (5.3)$$

where E_{in} and E_{out} are the kinetic energies of the electrons before and after the preacceleration ($E_{out} = E_{in} - V_p$). For instance, at E_{out} = 15.5 keV (the usual value) and E_{in} = 10 keV we find a focal distance as large as 370 mm. Only at energies below 10 keV the focusing may become disturbing. Indeed one may notice later (in fig. 5.6) that the energy calibration shows a deviation from linearity for the ^{57}Fe-line at 7.3 keV.

5.2.4. Magnetic lenses L_1 and L_2

The focal distance of lens L_1 is given by the expression

$$f = 4(B\rho)^2 \left[\int B_z(o,o,z)\ dz \right]^{-1} \tag{5.4}$$

and amounts to 90 mm for the chosen current setting. The distance between L_1 and the source is 180 mm, so that electrons of 15.5 keV are roughly focused on a diaphragm with inner diameter of 25 mm between L_1 and L_2 (see fig. 5.2).

A central absorber with a diameter of 32 mm, placed inside a ring with inner diameter of 90 mm, and various diaphragms were inserted inside lens L_1 to improve its energy selectivity and to reduce the possible influence of scattering in various parts of the arrangement, especially in the deflector. Due to this diaphragm system only electrons emitted by the source at angles between 5^o and 14^o with respect to the normal on the surface of the source are transmitted towards the deflector (solid angle $\simeq$ 0.17 steradian).

Lens L_2 is identical to L_1 apart from the fact that it has no soft-iron shield on its side towards the main accelerator. It serves for focusing purposes, but it plays an additional role in reducing field emission of electrons from the main accelerator (see below).

5.2.5. Main accelerator

The main accelerator† consists of eight ceramic sections with

† Made available by the Groningen Van de Graaff group.

stainless-steel electrodes over which a voltage of 63.5 (= 79 - 15.5) kV was equally distributed with the aid of a number of high-voltage resistors (100 MΩ; type Welwyn). In arrangement I the field emission of these electrodes caused a troublesome fluctuating background, sometimes amounting to about 40% of the total counting rate. The energy resolution of lens L_3 was insufficient to separate β-particles and field-emission electrons. To reduce field emission we introduced three precautions: i) the inner diameters of the electrodes inside the main accelerator were chosen such to defocus field-emission electrons coming from the first electrodes; ii) the electrodes were highly polished, ultra-sonically cleaned in a freon bath† and plated†† with a gold layer of about 30 $\mu g/cm^2$ to enlarge the work function; and iii) lens L_2 was placed close to the main accelerator, without a soft iron shield on its side oriented towards the main accelerator, so that its stray magnetic field deflects electrons that are field emitted by the first, most critical, electrode.

In arrangement II field emission in the main accelerator is of no concern, mainly because of the energy selectivity of the deflector.

5.2.6. Magnetic lens L_3 and deflector

The beam is focused on the entrance of the deflector by lens L_3. This deflector has been described by van Klinken (Kli65,66a). For the present experiment it was adjusted for optimum performance at 79 keV, with voltages on the spherical deflector plates of + and -9.8 kV.

The deflection angle $\zeta = 105^{\circ}$ gives a longitudinal-to-transverse conversion ratio 0.9999 at 79 keV, according to the relation given by Tolhoek (Tol56) for spin rotation in macroscopic electric fields (no spin-orbit coupling)

$$\eta = E\zeta/(E + m_e c^2). \qquad (5.5)$$

† The freon bath of the Groningen "Instituut voor Ruimteonderzoek".

†† Thanks are due to Mr. J.A. Reinders and Mr. L. Venema for performing this plating.

Here, η is the spin rotation angle, E the kinetic energy of the β-particles and $m_e c^2$ their rest energy.

5.2.7. Polarimeter

The polarimeter has also been described in detail by van Klinken (Kli65,66a). For the tritium experiment it was equipped with two 160 ± 10 μg/cm^2 gold scatterers on 30 ± 5 μg/cm^2 formvar backings† and with four detectors having aluminized (for minimizing light losses) plastic scintillators of 0.1 mm thickness: this thickness is chosen only slightly larger than the maximum range of 79 keV electrons in the scintillation material to minimize the background of the detectors. Detectors 1 and 2 (fig. 5.2), with an effective area of 20 × 25 mm^2, were placed at a mean scattering angle of 117° at 45 mm from the centre of the scatterer. For simultaneous zero-measurements the detectors 3 and 4, with scintillators of 6 × 15 mm^2, were placed 50 mm from the centre of the scatterer at a mean scattering angle of 45°. In fig. 5.5 a typical scintillation spectrum is shown.

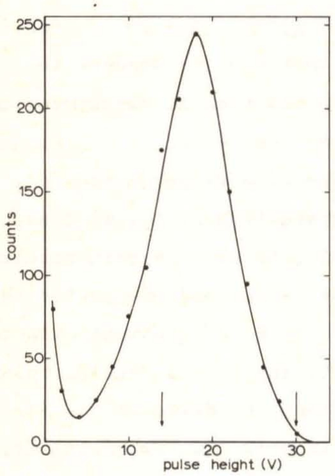

Fig. 5.5. Scintillation spectrum of detector 2; arrows indicate the discriminator setting.

The limiting diaphragm in front of the scattering foil was

† Both foils were made by vacuum evaporation by Mr. J.A. Reinders and Mr. L. Venema.

connected to the polarimeter chamber, so that it rotates with this chamber. This reduces instrumental asymmetries caused by a possible small misalignment of the diaphragm system.

For the present investigation the polarimeter was recalibrated, as will be described in sect. 5.4.

5.3. Energy calibration

The energy calibration of the system of fig. 5.2 was performed with a number of conversion lines. We have used the 7.3 keV K and the 13.6 keV L_I conversion lines of the 14.4 keV transition of ^{57}Fe, with a source of ^{57}Co electroplated on platinum; the 17.2 keV L lines and the 23.8 keV M lines (average energies) of the 25.7 keV transition of ^{161}Dy, with a ^{161}Tb source ion-implanted in iron†, and the 24.5 keV Th-A line using a Th(B+C+C'') source recoil-implanted in aluminium. The calibration sources have the same dimensions as the tritium sources and are sufficiently homogeneous; source thickness effects are small as was checked with the double-focusing spectrometer.

The results of the energy calibration are shown in fig. 5.6. In the inset of this figure the line profile observed for the Th-A line is shown. This profile could be least-squares fitted to a Gaussian function with a quadratic background (due to β-transitions in the calibration source): the FWHM energy width amounts to 2.8 ± 0.1 keV. The same value was obtained from an adjustment to the profile of the 13.6 keV ^{57}Fe-L line (not shown).

In fig. 5.7 the energy selectivity of various devices is illustrated. We estimate for the separate FWHM energy widths: 4.3 keV for lens L_1, 13 keV for lens L_2, 42 keV for main accelerator plus lens L_3, 3.8 keV for the deflector and 50 keV for the scintillation counters (see fig. 5.5), in good agreement with the observed overall resolution of 2.8 keV. The system resolution was thus mainly determined by the lens L_1 and the deflector.

The transmission of the total system is low. For instance, the probability that an electron which is emitted by a tritium atom with an energy of 15.5 keV, is detected in one of the backward-angle

---

† We thank Mr. L. Niesen for making available this source, which had been used in a Mössbauer experiment.

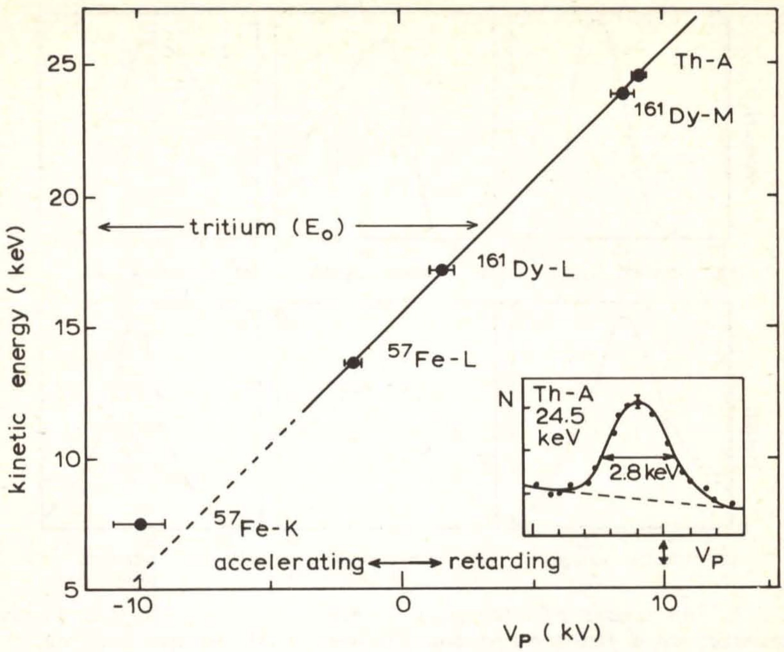

Fig. 5.6. Energy calibration of the preaccelerator with conversion lines; V_P is the voltage of the source housing with respect to the potential of the first electrode of the main accelerator. The straight line shown, with a slope of about 1 keV/kV, represents a fit to the data above 10 keV. The inset shows a line profile at 24.5 keV plotting the relative number of electrons incident on the gold scatterer versus V_P.

detectors amounts, for the optimum energy setting, using $V_P = 0$, to about 10^{-6}.

The energy width of 2.8 keV is rather large. A better energy resolution could easily have been achieved, for example by using narrower diaphragms in lens L_1. However, this would have reduced the true counting rates near the end-point energy to unacceptably low values. The v/c-resolution, in which we are mainly interested, is about a factor two smaller than the energy resolution and amounts at, for example, 15 keV to 9%. The influence of the finite resolution on the observed degree of longitudinal polarization is discussed in sect. 7.2.

In fig. 5.8 a Kurie plot of the 23 $\mu g/cm^2$ tritium source, obtained with the system of fig. 5.2 by varying the voltage V_P,

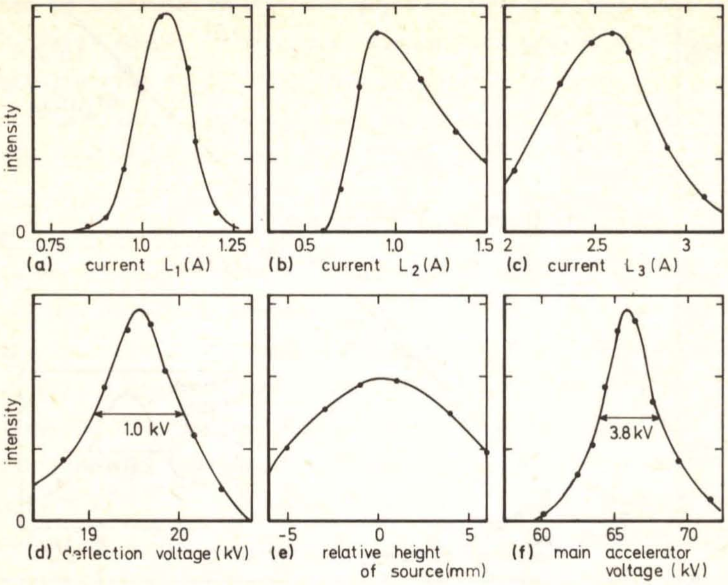

Fig. 5.7. The number of electrons incident on the gold foil in the polarimeter as a function of the adjustment of various devices. For each curve only one parameter was varied, while the others remained fixed at their optimum values. The thinner source was used as electron source.

is shown. The observed counting rates were corrected for the energy resolution of the system with the aid of eq. 4.7. Below about 14 keV the Kurie plot shows an increasing excess of electrons. Only a part of this excess can be attributed to scattering in source and backing: for comparison we indicated in the figure also the Kurie plot obtained with the double-focusing spectrometer (sect. 4.3). The discrepancy may be related to the applied method of energy selection and preacceleration. At energy settings below 15.5 keV accelerating voltages V_P were used. It cannot be excluded that secondary electrons, induced by the β-radiation, were extracted from the preaccelerator section by this accelerating potential. Though of low energy these electrons may pass lens L_1 and the deflector. Because of this uncertainty we finally disregard polarization measurements obtained with accelerating voltages V_P

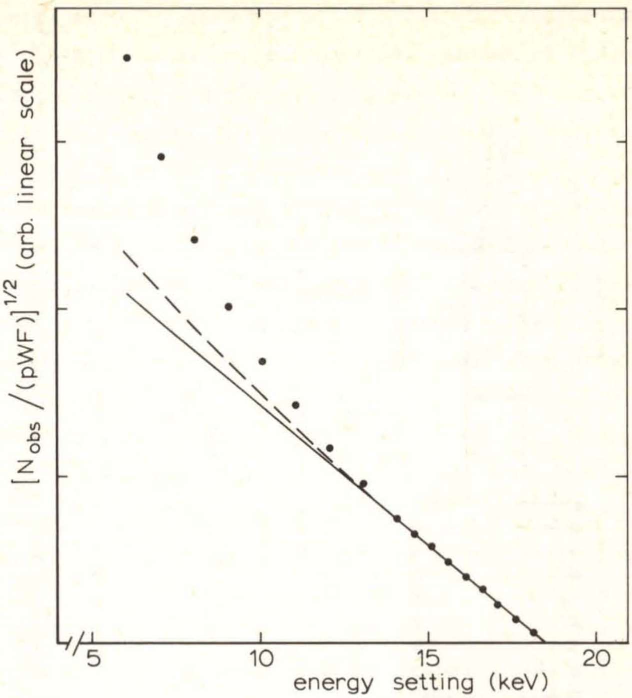

Fig. 5.8. Kurie plot of the 23 μg/cm² tritium source obtained with arrangement II. A correction for energy resolution has been applied. Statistical errors are smaller than the size of the points. The straight solid line has been based on the data above 15 keV. The dashed line gives the Kurie plot obtained with the double-focusing spectrometer (normalized to the same scale). Comment is given in the main text.

(see sect. 7.3).

5.4. Calibration of the Mott polarimeter

The efficiency S_{an} of the polarimeter had been determined earlier by Van Klinken (Kli65,66a) by means of a double-scattering experiment. In such an experiment an initially unpolarized beam is polarized transversely by the first scattering. The degree of transverse polarization is analysed in the second scattering. If all conditions (geometry, scatterer thickness) of both scatterings are the same, the observed asymmetry equals in essence the square of the effective S-value (see sect. 2.1). In such a way van Klinken has

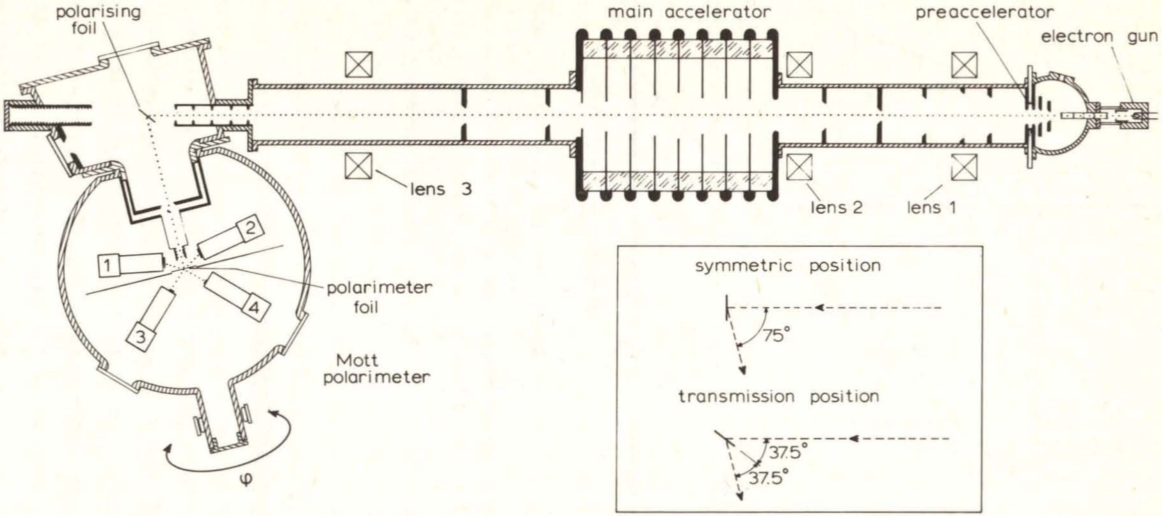

Fig. 5.9. Configuration for the recalibration of the polarimeter. The inset shows the two positions of the polarising foil.

measured effective S-values S_{1S} and S_{1T} for 105° scattering on 150 $\mu g/cm^2$ gold foils at various energies between 46 and 261 keV. The scattering foils were placed in symmetric (S) or in transmission (T) position with respect to the incoming and the scattered beam (see inset of fig. 5.9).

We have redetermined the efficiency S_{an} of the polarimeter at 79 keV with the aid of such foils with known values for S_{1S} and S_{1T}. This recalibration was undertaken because the previous calibration by van Klinken had been performed rather long ago and because the geometry inside the polarimeter had been slightly changed since then.

For the recalibration the equipment of fig. 5.2 was rearranged to the configuration of fig. 5.9. The electron gun was used as source of unpolarized electrons; the central absorber in lens L_1 was removed; the position of the deflector chamber was altered, while the deflector was replaced by a 150 $\mu g/cm^2$ gold foil, as used by van Klinken; the position of the polarimeter was also changed. During this calibration the geometry inside the polarimeter was exactly the same as during the tritium β-polarization measurements. Thus, the asymmetry observed during the calibration amounts essentially to $S_{1S}S_{an}$ or $S_{1T}S_{an}$ (compare eq. 5.1). During the calibration the supports of the polarising foil and of the foil in the polarimeter were regularly shifted up and down to eliminate the influence of inhomogeneities of the foils. In this way the effect of cracked vacuum oil adhering to the polarising foil was also reduced. This polarising foil could be shifted externally, so that the position of the beam spot on the foil could be adjusted in such a way that the asymmetry for the forward detectors in the polarimeter was close to zero. More details of the calibration procedure can be found in refs. Kli65,66a.

The recalibration was performed at an energy of 79.4 ± 0.4 keV. Results are shown in table 5.1. We used the values S_{1S} = 0.184 ± 0.0045 and S_{1T} = 0.211 ± 0.003 obtained by van Klinken. A weighted average of the results presented in the table gives S_{an} = −0.2055 ± 0.0028 for polarimeter foil **a** and S_{an} = −0.2058 ± 0.0030

Table 5.1.

Results for the calibration of the polarimeter [a].

Polarimeter foil	$S_{1S}S_{an}$ [b]	$S_{1T}S_{an}$ [b]	S_{an}	Number of cycles [c]	χ^2_ν [d]	$\text{Prob}_>$ [e]
a	-0.03742(52)		-0.2034(57)	6	0.21	0.96
a		-0.04351(27)	-0.2062(32)	10	0.66	0.75
b	-0.03641(65)		-0.1979(60)	9	1.37	0.20
b		-0.04400(36)	-0.2084(34)	22	1.30	0.17

a) *See text for details.*

b) *Errors in least significant figures, given in parentheses, are the largest of internal and external errors.*

c) *Each cycle consists of two runs with alternate counter positions (see sect. 7.1).*

d) *Chi-square divided by the number of degrees of freedom, which is in this case the number of cycles minus one.*

e) *The probability that a larger chi-square is found when the experiment is repeated (from ref. Bev69).*

for polarimeter foil b. These results are essentially the same, as is expected, since the preparation procedure of the two foils was exactly the same. We thus use for both foils the overall average

$$S_{\mathrm{an}}(79.4\ \mathrm{keV}) = -0.2056 \pm 0.0027. \tag{5.6}$$

The error is mainly due to the errors of S_{1S} and S_{1T}. The result 5.6 agrees well with the value -0.200 ± 0.004 obtained by van Klinken for a slightly different energy and geometry. Due to the shape of the β-spectrum and to small readjustments, the mean energy of the electrons during the β-polarization measurements was 1.0 to 2.4 keV lower than 79.4 keV. We derived from the measurements of van Klinken that the fractional variation with energy of S_{an} amounts to 1.3 ± 0.2% per keV in this energy region. With this correction the actual S_{an}-values for the tritium β-polarization measurements were obtained (table 7.1).

CHAPTER 6 DEPOLARIZATION IN THE SOURCE

6.1. Introduction

In the source, β-particles are isotropically emitted in all directions. Therefore, also the polarization vectors of these particles are isotropically oriented in space. For an infinitely thin source, only electrons that are initially emitted into the small acceptance angle of the polarization analyser will be detected. Since these electrons make small angles with the beam axis, almost their full polarization will be detected. In a thick source, on the other hand, electrons emitted into directions that make considerable angles with the beam axis may be scattered into the beam direction. These will show a smaller longitudinal polarization in the beam direction. Thus, the effective degree of longitudinal polarization is reduced by scattering in the source. This effect will be called depolarization in the source. It may cause serious systematic errors in β-polarization experiments.

The scattering phenomena usually involve a mixture of single, plural and multiple scattering processes with atomic nuclei and may be accompanied by inelastic collisions with atomic electrons. The longitudinal depolarization is essentially due to the fact that during the elastic scattering processes the electron spins, which are initially oriented longitudinally, are rotated less than the momentum vectors. This implies that the longitudinal component of the beam polarization is reduced. The transverse beam polarization will be zero on the average if, as is usually the case, the source is symmetric with respect to the beam axis.

In the next section we give a short survey of theories on depolarization in the source. These theories, however, are not well suited for our tritium sources on infinitely thick backings. In section 6.3 the procedure for obtaining the depolarization correction for these sources is discussed. It will be shown that the correction is small for energy settings close to the tritium end-point energy.

6.2. Survey of theories on depolarization in the source

6.2.1. General

In general, the polarization vector of a beam of electrons changes magnitude as well as direction during Coulomb scattering through atomic nuclei or electrons. The change of magnitude is due to spin-orbit coupling, affecting the component of the polarization normal to the scattering plane (see sect. 2.1), while the change of direction is due to spin rotation in the scattering plane. The behaviour or the polarization vector is commonly described with the complex scattering functions f and g, mentioned in sect. 2.1, that depend on the energy of the electrons, the atomic number Z of the scatterer and the scattering angle θ. For the specific case of an initially longitudinally polarized beam, the ratio of the longitudinal components of the polarization vectors after and before the scattering is (Mot64)

$$\frac{P'}{P} = \frac{(fg^* + f^*g)\sin\theta + (|f|^2 - |g|^2)\cos\theta}{|f|^2 + |g|^2}. \qquad (6.1)$$

Depolarization in the source is usually treated in first Born approximation $[Z/(137\beta) << 1$, where $\beta = v/c]$. In this approximation f and g are real and their ratio is (Mot65)

$$\frac{g}{f} = \frac{1}{2}\,\frac{(1 - \sqrt{1-\beta^2})\sin\theta}{1 - \sin^2(\frac{\theta}{2})(1 - \sqrt{1-\beta^2})}. \qquad (6.2)$$

In first Born approximation no spin-orbit coupling is found: the Mott function S (eq. 2.4) is zero for real f and g. Thus, the component of the polarization vector in the scattering plane rotates without change of magnitude. The rotation angle η is found by combining eqs. 6.1 and 6.2:

$$\frac{P'}{P} = \cos(\theta - \eta) = \frac{\cos\theta + \beta^2\sin^2(\theta/2)}{1 - \beta^2\sin^2(\theta/2)}. \qquad (6.3)$$

At relativistic velocities ($\beta = 1$) $\eta = \theta$: the polarization vector follows the momentum vector completely, whereas in the non-relativistic limit ($\beta = 0$) $\eta = 0$: the polarization vector does not rotate at all. At small scattering angle eq. 6.3 gives: $\eta = \theta(1-\sqrt{1-\beta^2})$, the same relation as applies for the case of deflection in a macroscopic transverse electric field (eq. 5.5).

As discussed by Mühlschlegel (Müh59) depolarization in thin sources without backing is mainly due to two types of scattering events (see also the inset of fig. 6.1): (i) small-angle plural and multiple scattering processes with high probability but small depolarization per event of electrons initially emitted approximately into the direction of the analysed beam (assumed to be perpendicular on the surface of the source); ii) single large-angle scattering processes over about 90° with small probability but large depolarization per event of electrons initially emitted parallelly to the surface layer and deflected into the beam direction mainly by large-angle single scattering.

6.2.2. Small-angle scattering

Mühlschlegel estimated the fractional depolarization of β-particles by small-angle scattering in a thin homogeneous source of thickness t_0. Using the small-angle approximation for the spin-rotation angle η (eq. 6.3) he obtained straightforwardly

$$\frac{\Delta P}{P_0} = \frac{(1-\beta^2)}{2t_0} \int_0^{t_0} \overline{\theta^2}(t)\, dt, \qquad (6.4)$$

where t denotes the depth of the activity and P_0 the initial degree of longitudinal polarization of the β-particles. The mean square scattering angle had been taken from Molière's theory of multiple scattering (Mol47): $\overline{\theta^2}(t) \simeq B(t)\ \theta_2^2(t)$. Here B is the so called Molière parameter which is related to the mean number of scattering events m as $B = \ln(0.857Bm)$. In the multiple scattering region B varies usually from 2 to 12. The angle $\theta_2(t)$ is a characteristic angle: on the average an electron makes only one collision in a layer of thickness t for which the scattering angle exceeds $\theta_2(t)$. In first Born approximation (Kei60; Oms68)

$$\theta_2^2(t) = 0.60\ \frac{Z(Z+1)}{A}\ \frac{(1-\beta^2)}{\beta^4} t\ \left[\mathrm{rad}^2\right], \ (t \text{ in g/cm}^2). \qquad (6.5)$$

Combination of eqs. 6.4 and 6.5 and integration yields:

$$\frac{\Delta P}{P_0} \simeq \tfrac{1}{4}(1 - \beta^2)\, \theta_2^2(t_0)\, B(t_0). \tag{6.6}$$

Mühlschlegel gave as region of validity of this expression

$$10^{-3}\, \beta^2 \lesssim t_0\,[\mathrm{g/cm^2}] \lesssim \frac{A\, \beta^4}{3B(t_0)\, Z(Z+1)\, (1-\beta^2)}. \tag{6.7}$$

The lower limit corresponds to a mean number of scattering events of about 7, while the upper limit corresponds to a root mean-square scattering angle of about 25°.

Mühlschlegel's estimate may be compared with an expression obtained by Passatore (Pas60; Bra67,68) for the depolarization of a *beam* normally incident on a scattering foil. Passatore investigated the longitudinal depolarization by multiple scattering of the total emerging beam: the spin component of each forwardly scattered electron was taken along its final direction of motion. By using an iteration procedure of the matrices connecting the polarization states before and after each single scattering event, he arrived, in first Born approximation, at the rather complicated expression

$$\frac{\Delta P}{P_0} \simeq 1 - \left[1 - \frac{2(1 - \beta^2)\ln\left(\frac{1 - \cos\theta_2}{1 - \cos\theta_1}\right)}{2\frac{\cos\theta_1 - \cos\theta_2}{(1 - \cos\theta_1)(1 - \cos\theta_2)} - \beta^2 \ln\left(\frac{1 - \cos\theta_2}{1 - \cos\theta_1}\right)} \right]^{m-1}. \tag{6.8}$$

In this expression m is the mean number of collisions in the foil, θ_1 is the screening angle accounting for screening by atomic electrons and θ_2 is the characteristic angle of the foil, according to eq. 6.5.

We remark that eq. 6.8 can be transformed into a form similar to that of eq. 6.6 if the depolarization is small. In first Born approximation we can substitute $\theta_1^2 = \theta_2^2/m$ (see for example refs. Kei60 and Oms68, where also expressions for θ_1 and m are given).

Then, eq. 6.8 becomes to first order in foil thickness t_f:

$$\frac{\Delta P}{P_0} \simeq \tfrac{1}{2}(1 - \beta^2)\ \theta_2^2(t_f)\ \ln m(t_f). \qquad (6.9)$$

The geometrical conditions underlying the depolarization relations 6.6 and 6.9 are completely different. However, for small thicknesses scattering probabilities are very forwardly peaked with respect to the direction of incidence. Then, eq. 6.9 can be applied also for the depolarization by small-angle multiple scattering in a source. Integration of the right-hand side of eq. 6.9 between $t_f = 0$ and $t_f = t_0$ yields

$$\frac{\Delta P}{P_0} \simeq \tfrac{1}{4}(1 - \beta^2)\ \theta_2^2(t_0)\ \left[\ln \{m(t_0)\} - 0.5\right], \qquad (6.10)$$

which is in reasonable agreement with Mühlschlegel's expression 6.6. For example, for m = 10 or 100 the value of B is 3.4 or 6.3, whereas the value of $[\ln(m) - 0.5]$ is 1.8 or 4.1, respectively. Differences may be due to various simplifications and approximations in both theories. For example, Mühlschlegel suggests to account for single-scattering contributions by using in eq. 6.6 $(B - \varepsilon)$ instead of B, where ε is of order unity.

6.2.3. Large-angle scattering

The degree of longitudinal polarization of β-particles that are singly scattered over about 90° is approximately $P_0\beta^2/(2-\beta^2)$ (see eq. 6.3). The contribution of these electrons to the depolarization in the source is difficult to estimate since they are emitted nearly in the plane of the source, so that the path lengths may become very large. A limitation of the path lengths is caused, however, by the fact that after some distance a large fraction of these electrons will be scattered out of the source layer by multiple scattering. This effect is taken into account by Mühlschlegel (Müh59) by introducing a small angle δ_c: the path lengths of electrons emitted at depth t at angles between $90^\circ-\delta_c$ and $90^\circ+\delta_c$, with respect to the normal on the source, are assumed to be t/δ_c. He obtained for the fractional depolarization by large-angle scattering

$$\frac{\Delta P}{P_0} \simeq \tfrac{1}{2}(1 - \beta^2)^{\frac{1}{2}} \; \theta_2^2(t_0) \; \ln \frac{1}{2\delta_c} \, . \tag{6.11}$$

It appears that the depolarization is rather insensitive to the value of δ_c. Mühlschlegel took $\delta_c = 0.1$ rad ($\simeq 5^{\circ}$) as a plausible estimate.

A similar but more complicated expression was obtained by Wegener (Weg58; Bie59) who adopted a delta-function for the 90° scattering probability. The limitation in path length was taken into account by introducing a convergence factor into the calculations.

6.2.4. Discussion

The estimate of Mühlschlegel for the total longitudinal depolarization in a homogeneous source is found by summing the contributions of eqs. 6.6 and 6.11:

$$\frac{\Delta P}{P_0} = 0.30 \; \frac{Z(Z+1)}{A} \; \frac{(1-\beta^2)^{\frac{3}{2}}}{\beta^4} \times \left[\frac{B(t_0)}{2} \, (1-\beta^2)^{\frac{1}{2}} + \ln \frac{1}{2\delta_c}\right] t_0 \qquad (t_0 \text{ in g/cm}^2) \, . \tag{6.12}$$

It is assumed that the source has no backing and that the influence of energy losses may be neglected. As anticipated no depolarization occurs at extremely relativistic energies, since then the electron spins follow the momentum vectors completely during the scattering processes. Going towards lower energies the depolarization increases since (i) scattering probabilities increase strongly and (ii) spin rotation angles decrease.

Mühlschlegel's estimate seems to predict the right order of magnitude of the depolarization. Van Klinken (Kli65a) found that the observed and the calculated depolarizations are not very different: the estimate of Mühlschlegel was found to be somewhat too small, especially at higher Z. For gold sources Schwarz et al. (Sch68) observed depolarizations up to about a factor three larger than was estimated from eq. 6.12. On the other hand, Lazarus and Greenberg (Laz70) measured a depolarization more than a factor three lower than expected.

6.3. Depolarization in the tritium sources

6.3.1. Introduction

For the tritium sources used in our investigation depolarization occurs by diffuse scattering in the aluminium backing and by scattering in the titanium layer. The various processes are indicated in fig. 6.1.

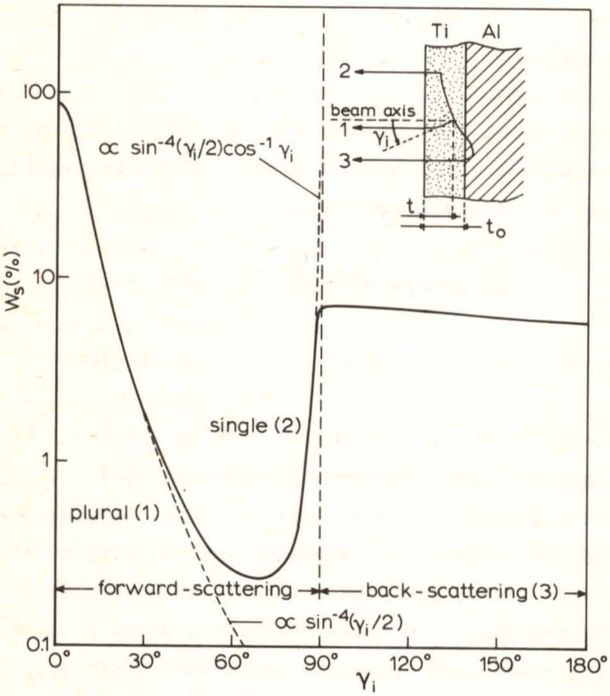

Fig. 6.1. Classification of scattering processes in the 23 μg/cm² tritium source for electrons initially emitted with an energy E_i = 15 keV and angle γ_i (see inset) at a depth t = 16 μg/cm². Plotted is an estimate of the probability (per unit of solid angle) W_s that such electrons leave the source in a direction normal to the source plane with final energy ≤ 15 keV. The estimate was based on measurements of Kanter (Kan57) and on calculations of Keil et al. (Kei60). We distinguish: plural and multiple scattering over small angles, single scattering over 90° and diffuse back-scattering. In the forward-scattering region path lengths increase as $\cos^{-1}\gamma_i$.

Because of the low kinetic energies involved, the spins of the electrons are hardly rotated by these scattering processes (eq. 6.3). Thus, the degree of longitudinal polarization $P_s(E)$ of the beam of electrons that leave the source nearly perpendicularly on its surface plane with energy E, can be written as

$$P_s(E) = \overline{P(E_i) \cos \gamma_i}, \qquad (6.13)$$

where the bar denotes an average over the scattering histories of the contributing electrons. These electrons are emitted by the tritium atoms with initial energy E_i ($E \leq E_i \leq E_0$), with degree of longitudinal polarization $P(E_i)$ and with angle γ_i with respect to the beam axis (inset fig. 6.1). The cosine function projects the initial spin direction on the final direction of the beam. The polarization $P_s(E)$ can be larger or smaller than the initial degree of polarization $P(E)$ of electrons emitted by the tritium atoms with energy E. This depends on a balance between scattering and energy loss. If energy losses are relatively unimportant $[P(E_i) \simeq P(E)]$, $|P_s(E)|$ will be smaller than $|P(E)|$ due to depolarization by scattering. This is the case for the tritium sources used in the present experiment. However, if energy losses are so large that, on the average, $|P(E_i)|$ is considerably larger than $|P(E)|$ and if $\bar{\gamma}_i$ is small (low-Z source), then it is possible that a polarization enhancement is observed: $|P_s(E)| > |P(E)|$. Indeed, we encountered such an effect when placing a 200 $\mu g/cm^2$ carbon foil in front of the 23 $\mu g/cm^2$ tritium source (subsect. 6.3.3): with the carbon foil the absolute magnitude of the observed polarization proved to be larger than without.

The complexity of the scattering processes accompanied with energy losses precludes finding an analytic expression for the depolarization with the aid of eq. 6.13. The theoretical estimates presented in the foregoing section are of limited utility since back-scattering through thick backings is not accounted for. We therefore used a semi-empirical method: $P_s(E)$ was written to first order in t_{av}, the average depth of the tritium atoms in the titanium layer, as

$$P_s(E,t_{av}) = P(E)D_s(E,t_{av}) = P(E)\ [1-d_0(E)]\ [1-d_1(E)\ t_{av}]. \quad (6.14)$$

The factor $D_s(E,t_{av})$ is the depolarization factor of the source; the fractional depolarization equals $1 - D_s(E,t_{av})$. The coefficients $d_0(E)$ and $d_1(E)$ account for back-scattering and for scattering in the titanium layer, respectively. We estimated $d_0(E)$ from measured back-scattering probabilities (subsect. 6.3.2). The coefficient $d_1(E)$ was determined experimentally by varying t_{av} as described in subsect. 6.3.2.

For clarity we point out explicitly that $P_s(E,t_{av})$ refers to electrons that emerge from the source with energy E but were emitted by the tritium atoms with, on the average, higher energies. $P(E)$, on the other hand, refers to electrons emitted by the atoms with energy E, but emerging from the source at, on the average, lower energies.

6.3.2. Depolarization by back-scattering

The depolarization of electrons scattered by thick backings has hardly been investigated experimentally or theoretically. We only know of the work of Braicovich et al. (Bra66) who performed measurements on this effect for various materials at electron energies between 0.3 and 2.0 MeV and at back-scattering angles between about 140° and 170°. Their results, however, are hardly applicable in our case because of the high energies and the limited angular interval.

For obtaining the coefficient d_0 in eq. 6.14 we consider the titanium layer as infinitely thin: the tritium activity is assumed to be direct on the aluminium backing. In that case the number of electrons $N_s(E)$ emitted per unit of time, energy and solid angle with energy E in a direction perpendicular to the surface of the source, can be written as

$$N_s(E) = N(E) + \int_{\pi/2}^{\pi}\int_{E}^{E_0} 2\pi \sin\gamma_i\ w_b(E_i,\gamma_i;E)\ N(E_i)\ d\gamma_i\ dE_i . \quad (6.15)$$

Here, $N(E_i)$ accounts for the statistical shape of the tritium β-spectrum and includes a trivial intensity factor; $w_b(E_i,\gamma_i;E)$ is the probability per unit of solid angle and energy that an electron with initial energy E_i and emission angle γ_i (see inset fig. 6.1) leaves the aluminium backing perpendicularly with final energy E. The first term on the right-hand side of eq. 6.15 corresponds to the unscattered fraction: these electrons are emitted by the tritium atoms directly in the beam direction. The second term corresponds to electrons that have suffered one or more scatterings in the backing. Neglecting spin rotation the "amount of polarization" carried away by the beam in the angular, time and energy interval concerned is:

$$N_s(E)\, P_s(E,0) = N(E)\, P(E) + \int_{\pi/2}^{\pi}\int_{E}^{E_0} 2\pi \sin\gamma_i\, w_b(E_i,\gamma_i;E)\, N(E_i)\, P(E_i) \cos\gamma_i\, d\gamma_i\, dE_i . \tag{6.16}$$

Combination of eqs. 6.14 (with $t_{av} = 0$), 6.15 and 6.16 yields:

$$d_0(E) = \frac{\int_{\pi/2}^{\pi}\int_{E}^{E_0} \left[1-\cos\gamma_i\, P(E_i)/P(E)\right] 2\pi \sin\gamma_i\, w_b(E_i,\gamma_i;E)\, N(E_i)\, d\gamma_i\, dE_i}{N(E) + \int_{\pi/2}^{\pi}\int_{E}^{E_0} 2\pi \sin\gamma_i\, w_b(E_i,\gamma_i;E)\, N(E_i)\, d\gamma_i\, dE_i} . \tag{6.17}$$

We deduced values for $w_b(E_i,\gamma_i;E)$ from experimental results of Kanter (Kan57) and of Kulenkampff and Rüttiger (Kul54; Kul58) on yields and energy distributions of back-scattered electrons.

Kanter measured energy- and angular distributions of initially mono-energetic electrons with primary energies of 10, 30, 50 and 70 keV, back-scattered by thick targets of Al, Cu, Ag or Au. The energy analysis of the scattered electrons was performed with two electrostatic spectrometers. Various directions of the incident and the emerging beam with respect to the normal on the target surface were investigated (see fig. 6.2). The angles of incidence were $\gamma_i = 100^\circ$, 125°, 145° and 180°, while several angles of emergence γ_f between -60° and 80° were selected.

Kulenkampff and Rüttiger performed similar measurements at normal incidence ($\gamma_i = 180^\circ$) with primary energies of the electrons

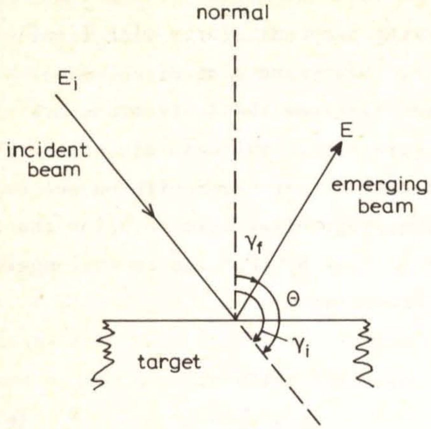

Fig. 6.2. Scattering geometry for back-scattering experiments from literature (Kan57; Kul54,58).

between 20 and 40 keV. Targets of Al, Cu, Ag and Pt were used and the selected scattering angles were $\theta = 97^o$, 117^o and 137^o ($\gamma_f = 83^o$, 63^o and 43^o, respectively). Energy distributions were investigated with the so called "Gegenfeld" method.

In the following we briefly describe how we deduced $w_b(E_i, \gamma_i; E)$-values from figures presented by Kanter and by Kulenkampff and Rüttiger.

Fig. 6.3 shows the energy integrated probability of normal emergence from an Al-target as a function of the angle of incidence, for E_i = 10 and 50 keV. These plots were constructed from fig. 9 of ref. Kan57, showing angular distributions of electrons back-scattered from aluminium. Apparently the probabilities are rather insensitive to the initial energy of the electrons. Upon numerical integration over γ_i of the probabilities presented in fig. 6.3 we obtained the back-scattering contribution at normal emergence for a thin, isotropic and mono-energetic source on a thick aluminium backing. At E_i = 10 keV, 7.8% of the electrons emitted in backward directions leave the backing in a unit solid angle around the normal on the source (at E_i = 50 keV: 6.5%). These values agree with calculated results of Kanter (Kan57; fig. 11). Thus, the ratio of the numbers of scattered and unscattered electrons amounts, for the normal direction, to $2\pi \cdot 0.078 = 0.49$ at E_i = 10 keV. The scattered fraction, however, has an appreciably lower average energy.

For obtaining $w_b(E_i, \gamma_i; E)$ we have to know the energy distribution of the perpendicularly emerging electrons as a function of the incidence parameters E_i and γ_i. As far as we know no direct measurements of these distributions are available. However, Kanter

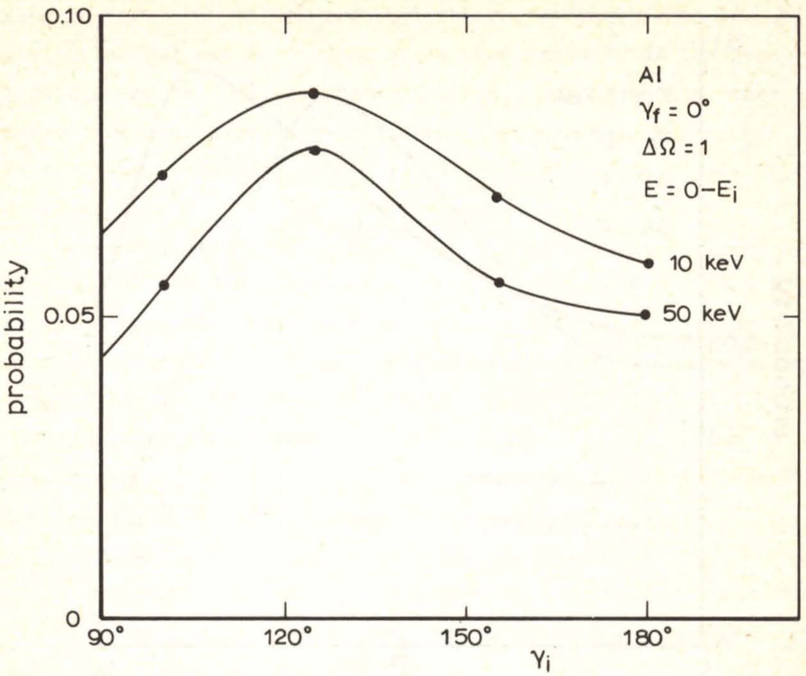

Fig. 6.3. Probability that electrons with initial energies of 10 and 50 keV are back-scattered from a thick Al-target into a direction normal to the target plane, as a function of the angle of incidence γ_i. Points refer to data taken from ref. Kan57.

observed that the mean and the most probable energy losses of back-scattered electrons are determined only by the scattering angle $\theta = \gamma_i - \gamma_f$ (see fig. 6.2) in the case that the emerging beam lies in the plane determined by the incident beam and the normal on the target. These losses are within Kanter's error limits, independent of γ_i and γ_f. Assuming that, in good approximation, the whole energy distribution depends only on θ, the energy distribution of the normally emerging electrons can be derived from measurements with a different geometry, but with the same scattering angle θ. In this way we constructed the energy distributions of perpendicularly emerging electrons at four angles of incidence: $\gamma_i = 97^o$, 117^o, 137^o (using refs. Ku154,58) and 170^o (using ref. Kan57). The energy integrated probability for normal emergence was normalized for each value of γ_i and E_i to values shown in fig. 6.3. The results for $\gamma_i = 97^o$ and 170^o,

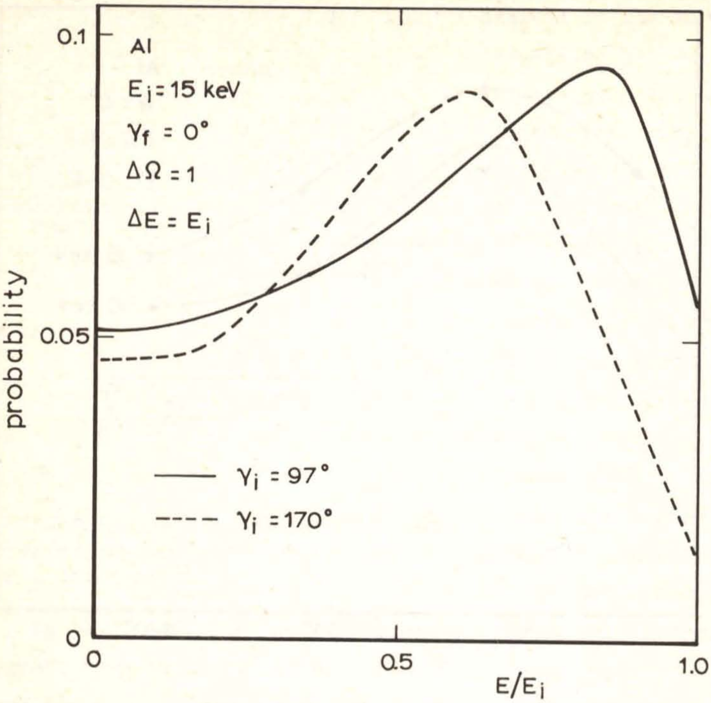

Fig. 6.4. Energy distributions, for two values of γ_i, of electrons (E_i = 15 keV) that are back-scattered from a thick Al-target into a direction normal to the target plane. The construction of these plots is explained in the text.

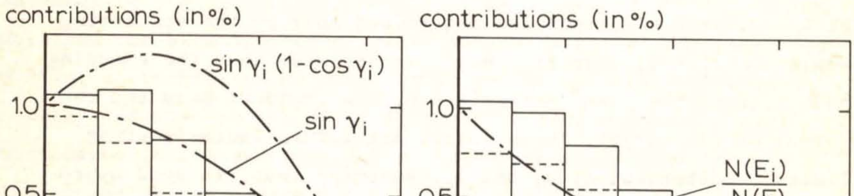

Fig. 6.5. Histograms showing contributions of back-scattering to intensity (---) and depolarization (—) of the beam emerging from the tritium source at E = 15 keV in a direction normal to the source plane. In (a) the dependence on γ_i is shown; for comparison also plots of sin γ_i and sin γ_i(1-cos γ_i) are given (using the same scale). In (b) the dependence on E_i is compared with the shape of the tritium β-spectrum (also on the same scale).

shown in fig. 6.4, illustrate that the energy integrated probability for normal emergence does not depend strongly on the angle of incidence (as appears also from fig. 6.3), while, on the other hand, energy losses increase strongly with increasing γ_i. From these four distributions values for $\omega_b(E_i,\gamma_i;E)$ were obtained directly or by interpolation.

The integrals of eq. 6.17 were calculated numerically with intervals of 15^o for γ_i and using energy steps of 0.2 or 0.5 keV. For calculating the numerator we assumed that $P(E_i)$ is proportional to v/c. In table 6.1 we show some details of the calculation of $d_0(E)$ for E = 15 keV using energy steps of 0.5 keV. In fig. 6.5 two histograms pertinent to this calculation are shown. A similar calculation for E = 15 keV with energy steps of 0.2 keV gives a slightly larger d_0-value (4.3% instead of 3.9%).

The results of the back-scattering calculations are presented in table 6.2 and fig. 6.6. As anticipated, the depolarization due to back-scattering is small near the tritium end-point energy but becomes large at lower energies.

The average energy loss $\overline{E_i - E}$ of the back-scattered electrons can be calculated similarly. As expected, it is small near the end-point energy (for example, 0.6 keV at E = 16 keV) but becomes considerable at lower energies (for example, 2.4 keV at E = 10 keV and 2.9 keV at E = 6 keV).

The estimated relative accuracy of the calculated d_0-values is about 25%. This estimate includes the experimental errors of Kanter and of Kulenkampff and Rüttiger (5-10%), read-off errors from their graphs and errors due to approximations in the calculations.

As remarked, we assumed that the spin direction of the electrons remains unchanged during the scattering processes: i.e. we treated the spin-rotation in the non-relativistic limit. The error in the calculated d_0-values caused by this assumption is estimated as follows. In second Born approximation $[Z^2/(137\beta)^2 \ll 1]$ the ratio of the longitudinal components of the polarization vectors of an initially longitudinally polarized beam after and before single Coulomb scattering over an angle θ is (Mot64)

Table 6.1

Illustration of the calculation of $d_0(E)$ for $E = 15$ keV. For each angular interval of 15^o around γ_i and energy interval of 0.5 keV around E_i three numbers are given: in italics the probability $w_b(E_i,\gamma_i;E)$ in $^o/oo$ (see text) and above and beneath it the contributions (in $^o/oo$) to intensity and depolarization of the beams, respectively. Summation of the contributions of all angular and energy intervals yields an intensity contribution of 27.4 $^o/oo$ and a depolarization of 38.6 $^o/oo$. See also fig. 6.5.

E_i (keV) \ γ_i	97.5^o	112.5^o	127.5^o	142.5^o	157.5^o	172.5^o
15.25	2.9 *4.0* 3.3	2.1 *3.6* 2.9	1.3 *2.4* 2.1	0.7 *1.6* 1.2	0.4 *1.3* 0.7	0.1 *1.2* 0.2
15.75	2.4 *4.6* 2.7	2.1 *4.1* 2.9	1.2 *3.2* 1.9	0.7 *2.2* 1.3	0.4 *1.9* 0.8	0.1 *1.7* 0.2
16.25	1.8 *5.0* 2.0	1.6 *4.8* 2.2	1.1 *3.8* 1.8	0.6 *2.8* 1.2	0.3 *2.4* 0.6	0.1 *2.1* 0.2
16.75	1.2 *5.3* 1.4	1.1 *5.2* 1.5	0.8 *4.2* 1.2	0.5 *3.3* 0.8	0.2 *2.7* 0.5	0.1 *2.4* 0.1
17.25	0.7 *5.4* 0.8	0.6 *5.4* 0.9	0.5 *4.5* 0.7	0.3 *3.7* 0.5	0.2 *3.1* 0.3	0.1 *2.8* 0.1
17.75	0.3 *5.4* 0.3	0.3 *5.5* 0.4	0.2 *4.7* 0.3	0.1 *3.9* 0.2	0.1 *3.4* 0.1	0.0 *3.0* 0.0
18.25	0.1 *5.2* 0.1	0.1 *5.4* 0.1	0.0 *4.8* 0.1	0.0 *4.1* 0.0	0.0 *3.6* 0.0	0.0 *3.3* 0.0

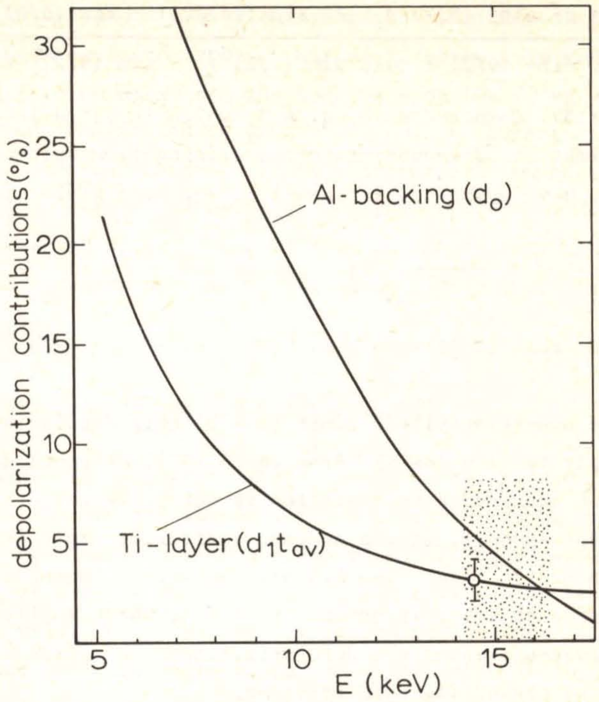

Fig. 6.6. Depolarization by the Al-backing (d_0) and by the Ti-layer ($d_1 t_{av}$) of electrons from the 23 μg/cm^2 source. The drawn d_0 -curve is an absolute estimate. The shape of the $d_1 t_{av}$-curve was calculated (see text). This curve was normalized to the measured value at 14.5 keV. For the final result for the tritium β-polarization use has been made only of the hatched region, where the corrections are small.

Table 6.2.

Depolarization factors, as defined in eq. 6.14, for the 23 μg/cm^2 tritium source at energy settings used for the polarization measurements. Uncertainties in least significant figures are given in parentheses.

E (keV)	$1 - d_0(E)$	$1 - d_1(E)t_{av}$	$D_s(E, t_{av})$
16.0	0.970(8)	0.973(11)	0.944(13)
15.3	0.961(10)	0.972(11)	0.933(14)
14.5	0.947(13)	0.969(11)	0.918(16)
12.8	0.910(22)	0.960(14)	0.874(25)
11.0	0.85(4)	0.95(2)	0.80(4)
9.1	0.78(5)	0.92(3)	0.72(5)
7.3	0.70(7)	0.89(4)	0.62(7)
6.3	0.64(9)	0.85(7)	0.54(9)
5.5	0.58(10)	0.80(9)	0.47(9)

$$\frac{P'}{P} = \frac{\cos\theta + \beta^2 \sin^2(\theta/2) + \pi\alpha Z\beta \sin(\theta/2)\left[1 - \sin(\theta/2)\right]}{1 - \beta^2 \sin^2(\theta/2) + \pi\alpha Z\beta \sin(\theta/2)\left[1 - \sin(\theta/2)\right]}, \tag{6.18}$$

where $\alpha \approx 1/137$. Compared with eq. 6.3, which is valid in first Born approximation, Z-dependent terms, arising from spin-orbit interaction, have appeared. For small β, eq. 6.18 gives

$$\frac{P - P'}{P} \approx (1 - \cos\theta) \times \left[1 - \beta^2 \cos^2(\theta/2) - \pi\alpha Z\beta \sin(\theta/2)\{1 - \sin(\theta/2)\}\right], \tag{6.19}$$

while in the non-relativistic limit ($\beta \to 0$) this depolarization amounts simply to $(1 - \cos\theta)$. From eq. 6.19 it is concluded that spin rotation can indeed be neglected in our back-scattering calculations. For example, at the average scattering angle for E = 15 keV of about 120° (see fig. 6.5 a), the second factor in the right-hand side of eq. 6.19 amounts to 0.975, which implies that we perhaps over-estimated the depolarization with a factor of about 1.025 by neglecting spin rotation.

During the slowing-down of the β-particles in the backing material, exchange interactions with atomic electrons may occur. We estimated the influence of these interactions on the d_0-values using theoretical studies on electron-electron scattering (Møller scattering) of Ford and Mullin (For57) and of Batygin and Toptygin (Bat60). From their work and from a discussion given by Rebel et al. (Reb64) we estimated that the fractional reduction of the d_0-values due to these exchange effects is much smaller than 0.1% at 16 keV, 5% at 10 keV and 30% at 6 keV. These reductions were neglected.

During the polarization measurements only electrons that emerge from the source with angles between 5° and 14° with respect to the normal on the source plane reach the polarimeter (see subsect. 5.2.4). The calculated d_0-values, however, refer to electrons that emerge perpendicularly from the source. Errors due to this difference are negligible in comparison with the 25% error assigned above (see for instance fig. 9 of ref. Kan57). For the same reason we did not allow for the fact that the tritium activity is not deposited directly on the aluminium backing: on the average a layer of about 7 μg/cm^2 titanium is present between the tritium atoms and the backing (for the 23 μg/cm^2 source).

To check the procedure described in this subsection we performed similar depolarization calculations for a ^{147}Pm source (E_0 = 225 keV) on a thick gold backing. For this source the depolarization has been measured by van Klinken (Kli66b). For d_0-values up to 0.5 calculation and experiment agree within the estimated error of 25%.

6.3.3. Depolarization by the titanium layer

In order to estimate the $d_1 t_{av}$-term in eq. 6.14, we calculated the fractional depolarization for a homogeneous 23 μg/cm^2 ^{3}H-Ti source without backing with the aid of Mühlschlegel's relation eq. 6.12. It must be remarked that this thickness is below the limit for validity of the Molière approximation (the left-hand side of eq. 6.7 amounts to 60 μg/cm^2 at 15 keV). Taking B = 1 as an extrapolation of Molière's theory and δ_c = 0.1 rad as in an example given by Mühlschlegel, eq. 6.12 gives for $\Delta P/P_0$: 3.4% at 17 keV, 5% at 14 keV, 10% at 10 keV and 28% at 6 keV. These values indicate the magnitude of the quantity $d_1 t_{av}$ for the source used. However, the influence of the aluminium backing, of energy losses, and of the inhomogeneity of the tritium distribution is not accounted for. Furthermore, the choice of B and δ_c is rather arbitrary. A probably better estimate for $d_1 t_{av}$ was obtained experimentally by placing various foils directly in front of the 23 μg/cm^2 source, effectively changing the depth of the tritium activity. Results of polarization measurements at E = 14.5 keV with a silver foil of 50 ± 5 μg/cm^2 (on 22 ± 2 μg/cm^2 formvar) and with a carbon foil of 200 ± 20 μg/cm^2 in front of the tritium source are shown in fig. 6.7 together with results for the 23 μg/cm^2 and 120 μg/cm^2 (used in arrangement I) sources. For a realistic mutual comparison t_{av} was converted to an equivalent titanium depth by applying the factor $Z(Z+1)/A$ of eq. 6.12: thus, 1 μg/cm^2 of silver corresponds to 2 μg/cm^2 of titanium, while 1 μg/cm^2 of carbon is converted to 0.33 μg/cm^2 of titanium. The

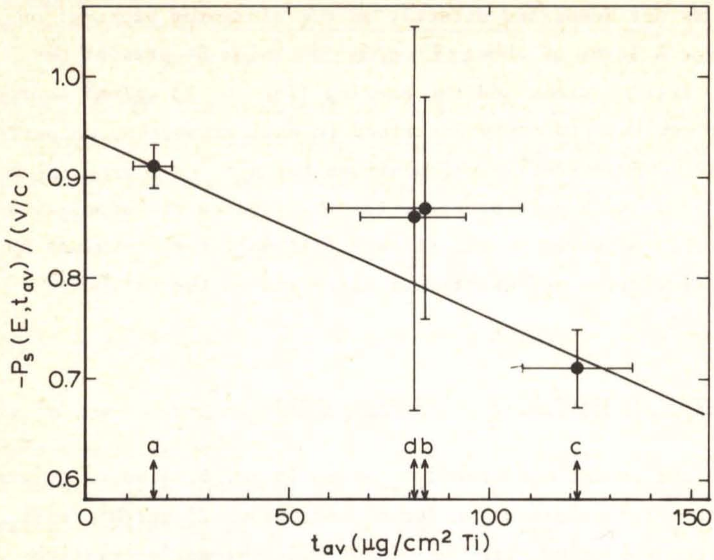

Fig. 6.7. Decrease of the measured degree of polarization at 14.5 keV with increasing depth t_{av} of the tritium activity. Point (a) refers to a polarization value obtained with the 23 μg/cm² source; (b) to a value obtained with the 120 μg/cm² source; (c) and (d) to values obtained with a silver and a carbon foil, respectively, in front of the 23 μg/cm² source. The thickness of these foils was expressed in Ti-equivalents, as explained in the text. The straight line is a least-squares fit.

magnitude of t_{av} for the 23 and 120 μg/cm² sources is 16 ± 5 and 84 ± 24 μg/cm², respectively (sect. 4.2). Because energy losses in the actual silver and carbon foils and in the corresponding equivalent titanium layers differ, the influence of polarization enhancement (subsect. 6.3.1) is different. We applied a first-order correction for this difference, using tabulated stopping powers (Ber64). The correction is small for the silver data (2.7% at 14.5 keV; 6.1% at 9.1 keV) but considerable for the results with the carbon foil (11% at 14.5 keV; 25% at 9.1 keV). With the values of $d_1(E)$ derived from linear fits to similar data as presented in fig. 6.7, we obtained for the 23 μg/cm² source: $d_1 t_{av}$ = (3.1 ± 1.1)% at 14.5 keV, (3.1 ± 1.3)% at 12.8 keV, (2.8 ± 1.1)% at 11.0 keV and (2.4 ± 1.2)% at 9.1 keV. These results are somewhat smaller than the estimates given above, but at 14.5 keV the experimental result agrees rather well with the estimated value of about 4.6%. However, the measured values are less energy dependent than expected from eq. 6.12. This may be related to the method of energy selection and preacceleration. For mean energies below 14.5 keV an accelerating voltage V_p was applied. As discussed in sect. 5.3, it cannot be excluded that secondary electrons, induced by the β-radiation, are extracted from the preaccelerator section by this accelerating voltage. Because of this uncertainty we have finally disregarded the depolarization measurements performed with an accelerating voltage V_p. The measured depolarization contribution $d_1 t_{av}$ = (3.1 ± 1.1)% at 14.5 keV (V_p = 0) was accepted and values at other energies (fig. 6.6; table 6.2) were deduced from this result using the energy dependence of eq. 6.12 and allowing for some polarization enhancement due to energy loss (≈ 0.3 keV).

It should be noted that at lower energies accurate values for the depolarization contribution by the titanium layer are hardly needed because of the inaccuracy due to the rapidly increasing depolarization by back-scattering. Only results for β-energies larger than 14.5 keV, which are obtained with zero or retarding voltage V_p, will be used in ch. 7 for comparison with theory. At these energies the depolarization correction is small and secondary electrons do not contribute.

CHAPTER 7 POLARIZATION MEASUREMENTS

7.1. Experimental procedure

The longitudinal polarization of β^--particles from the decay of tritium has been investigated at energies between 5.5 and 16.0 keV. Before the start of these measurements the Mott polarimeter was recalibrated, as described in sect. 5.4. After finishing the actual polarization measurements the influence of depolarization in the source was investigated both experimentally and numerically, as described in sect. 6.3.

During the polarization measurements we performed at each energy setting a series of asymmetry measurements with the tritium source as well as with the source simulator. The tritium measurements were interrupted regularly for background counting.

Before starting polarization measurements at a certain energy setting, the electron beam was aligned with the aid of the forward-angle detectors 3 and 4 that monitor the asymmetry $\delta(45^o)$. The deflector position and voltage were adjusted so that $|\delta(45^o)| < 0.1$ in the plane of deflection ($\phi = 0^o, 180^o$). Then, more critically, $|\delta(45^o)|$ in the plane in which the polarization asymmetry is measured ($\phi = 90^o, 270^o$) was reduced to less than 0.03 by small adjustments of current and position of lens L_3.

At each energy setting a number of measurement cycles was collected, each consisting of two runs with alternate counter positions. The duration of the cycles ranged from 20 to 80 minutes. The counting rates for the polarization sensitive detectors 1 and 2 ranged between 210 c/s at the lowest and 2 c/s at the highest energy setting.

Background measurements were performed in various ways: usually by measuring with the source covered by an absorber, but also by measuring without high voltage on the main accelerator or by closing a valve (fig. 5.2) between lens L_3 and the deflector. All three methods gave the same result within statistical accuracy amounting to about 0.6 c/s for detectors 1 and 2. This is only about 30% of the total counting rate at the highest energy setting. The background was constant in time and independent of the preacceleration voltage V_p. A part of the background may be attributed to some radioactive contamination of the polarimeter chamber by previous experiments with ^{147}Pm. The background contribution for detectors 3 and 4 was 3% at most.

Zero-measurements with the source replaced by a source simulator were performed with the same adjustments of the apparatus as during the tritium measurements. The simulator gave the same forward asymmetry $\delta(45^o)$ as the tritium source within a difference of about 0.005 for all azimuthal angles ϕ. This indicates that the simulator replaced the source properly.

Data storage and polarimeter rotation were automatized, so that non-stop measurements could be performed. Read out occurs when the content of a timer exceeds a preselected number. This number, the position of the polarimeter and the content of the four counters are recorded by a Sodeco printer and by a paper tape puncher. After each run the polarimeter is rotated automatically over 180^o and a new counting period is started. The information on the paper tape was put on punch cards by means of an external interface system. The data on the punch cards were further processed at the TR4 computer of the Rekencentrum of the Groningen University (see next section).

Several times a day the stability of the various currents and voltages was checked. Sometimes small readjustments of the current through lens L_3 (fig. 5.2) and the deflection voltage were necessary in order to keep the forward asymmetry $\delta(45^o)$ within acceptable limits (see above). Runs for which $\delta(45^o)$ was too large were skipped. Regularly, scintillation spectra of the detectors were collected and spectra of the tritium source (see fig. 5.4) were measured in order to check the proper functionating of the various components of the apparatus. The consistency of the results presented in the subsequent section indicates that the influence of instabilities is small compared with statistical fluctuations.

7.2. Data analysis and results

Following the procedure sketched in the previous section we performed polarization measurements at nine settings between -10 kV (accelerating) and +2 kV (retarding) of the preacceleration voltage V_p, using the 23 μg/cm^2 source (see ch. 4) and arrangement II (see ch. 5). The analysis of the data obtained during these measurements is explained in this section; results are presented in table 7.1.

The average energy of the analysed β⁻-particles ranged from 5.5 to 16.0 keV. Values of E_{av} shown in column 1 of table 7.1, were calculated from the relation:

$$E_{av}(E') = \frac{\int E\, N_s(E)\; G_a(E;E',\sigma_a)\; dE}{\int N_s(E)\; G_a(E;E',\sigma_a)\; dE} \; . \qquad (7.1)$$

Here, $N_s(E)$ refers to the energy distribution of the β-particles when they leave the source. The integrals were calculated numerically with the aid of a computer program, using the source spectrum N_s measured with the double-focusing spectrometer (sect. 4.3) and using the window curve G_a of the apparatus, discussed in sect. 5.3 (see the inset of fig. 5.5). At an energy setting E' = 15.5 keV (V_p = 0), for example, the calculated average energy is 14.5 keV. Similarly, the average value of the velocity v/c was calculated: results are given in column 2 of table 7.1.

The observed degree of polarization is also an average over the transmitted energy window and depends on the quantity

$$P_{av}(E') = \frac{\int P_s(E)\; N_s(E)\; G_a(E;E',\sigma_a)\; dE}{\int N_s(E)\; G_a(E;E',\sigma_a)\; dE} \; , \qquad (7.2)$$

where $P_s(E)$ refers to the polarization of the β-particles when they leave the source (see eq. 6.14). Upon expanding $P_s(E)$ in the neighbourhood of E' as a Taylor series, eq. 7.2 can be written as:

$$P_{av}(E') = P_s(E') + \left(\frac{dP_s}{dE}\right)_{E'} (E - E')_{av} + \\ + \tfrac{1}{2}\left(\frac{d^2P_s}{dE^2}\right)_{E'} \left[(E - E')^2\right]_{av} + \ldots.. \qquad (7.3)$$

$P_s(E_{av})$, the polarization of electrons leaving the source with energy E_{av}, can be expanded as:

$$P_s(E_{av}) = P_s(E') + \left(\frac{dP_s}{dE}\right)_{E'} (E_{av} - E') + \\ + \tfrac{1}{2}\left(\frac{d^2P_s}{dE^2}\right)_{E'} (E_{av} - E')^2 + \ldots.. \tag{7.4}$$

The zeroth- and first-order terms of the expansions 7.3 and 7.4 are equal. We checked by calculation that the second-order terms are approximately equal; it turns out that

$$P_{av}(E') = P_s(E_{av}) \tag{7.5}$$

to within about 0.3%, for the entire energy range under consideration. A correction for this small difference was included in the depolarization factor D_a, to be introduced in eq. 7.9.

From the numbers of counts observed during the polarization measurements, asymmetries were calculated with the aid of a computer program. The observed asymmetry $\delta_{obs}(117^o)$ was obtained from

$$\delta_{obs}(117^o) = \frac{(N_{1A}N_{2B}/N_{2A}N_{1B})^{\frac{1}{2}} - 1}{(N_{1A}N_{2B}/N_{2A}N_{1B})^{\frac{1}{2}} + 1}, \tag{7.6}$$

where N_{1A} is the number of electrons, corrected for background, registered by detector 1 while the polarimeter chamber is in the position 'A' ($\phi_1 = 90^o$, $\phi_2 = 270^o$; ϕ_1 and ϕ_2 being the azimuthal positions of the detectors 1 and 2, respectively), N_{1B} is this number with the polarimeter chamber in position 'B' ($\phi_1 = 270^o$, $\phi_2 = 90^o$) etc. The asymmetries $\delta_{obs}(45^o)$ for the source and $\delta^0_{obs}(117^o)$ and $\delta^0_{obs}(45^o)$ for the source simulator were calculated from relations similar to eq. 7.6. As shown in refs. Kli65,66a, errors due to differences between the detectors are eliminated by using these expressions.

Values for $\delta_{obs}(117^o)$ are given in column 3 of table 7.1. These values, like most of the data of the table, are averages for the various measurement cycles collected at the energy setting under consideration.

A correction for instrumental asymmetries due to a possible small misalignment of the incident beam and the rotation axis of the polarimeter was obtained from the observed asymmetry for the forward detectors. The corrected asymmetry, tabulated in column 4 of table 7.1, is given by (Kli65,66a; Dui69)

$$\delta_{corr}(117^o) = \delta_{obs}(117^o) - C\,\delta_{obs}(45^o). \qquad (7.7)$$

Here $C = a(117^o)/a(45^o)$, where $a = (dI/d\theta)/I$ is a measure for the dependence of the scattering probability on angle. We used the experimentally determined value $C = 0.29 \pm 0.01$ (fig. 7.1).

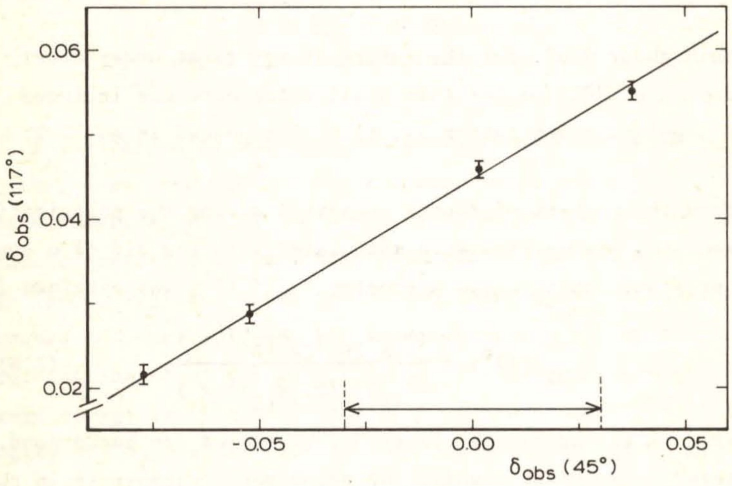

Fig. 7.1. Dependence of $\delta_{obs}(117^o)$ on $\delta_{obs}(45^o)$, as observed by varying the adjustment of the electron beam. During the polarization measurements $\delta_{obs}(45^o)$ was restricted to the region indicated by the arrow.

A tentative theoretical estimate, using screened relativistic single-scattering cross sections (Lin64 ; Büh68) gave $C \simeq 0.25$. However, the influence of plural and multiple scattering processes in the polarimeter foil is not taken into account for this estimate. Expression 7.7 is correct in first order up to a small residual term (Dui69), which, for the geometry of the present experiment, amounts to about $0.003\ y$ (y in mm). The quantity y denotes the component in the measuring plane of the shift between the axis of

TABLE 7.1.

Results of tritium β-polarization measurements with the 23 μg/cm² source and arrangement II [a].

Average energy (keV)	Average velocity v/c	Observed asymmetry $\delta_{obs}(117^{o})$	Corrected asymmetry $\delta_{corr}(117^{o})$	Corrected zero-asymmetry $\delta^{o}_{corr}(117^{o})$	Polarimeter efficiency $-S_{an}$	Depolarization factor D_sD_a	Degree of longitudinal polarization $-P$	$-P/(v/c)$	Consistency information [b]
16.0(2)	0.2445(15)	0.0556(10)	0.0493(10)	0.0033(6)	0.1992(29)	0.925(14)	0.2496(84)	1.021(35)	0.79/113/0.95
15.3(2)	0.2394(16)	0.0507(11)	0.0487(11)	0.0047(5)	0.2000(29)	0.914(15)	0.2407(84)	1.005(36)	1.15/48/0.23
14.5(2)	0.2333(16)	0.0449(6)	0.0435(6)	0.0018(7)	0.2005(29)	0.900(17)	0.2311(72)	0.991(32)	0.97/78/0.55
12.8(2)	0.2197(17)	0.0382(8)	0.0384(8)	0.0025(10)	0.2013(28)	0.86(3)	0.208(10)	0.95(5)	0.67/11/0.75
11.0(2)	0.2042(19)	0.0311(3)	0.0314(3)	0.0024(7)	0.2019(28)	0.79(4)	0.182(11)	0.89(5)	0.92/33/0.60
9.1(2)	0.1862(20)	0.0240(4)	0.0253(4)	0.0033(7)	0.2021(28)	0.70(5)	0.156(13)	0.84(7)	0.71/31/0.88
7.3(3)	0.1672(34)	0.0244(4)	0.0196(4)	0.0036(6)	0.2027(28)	0.61(7)	0.129(16)	0.77(10)	0.68/15/0.80
6.3(3)	0.1556(37)	0.0229(6)	0.0184(6)	0.0041(5)	0.2027(28)	0.53(9)	0.133(24)	0.85(15)	1.43/6/0.21
5.5(4)	0.1455(53)	0.0170(3)	0.0152(3)	0.0032(4)	0.2029(28)	0.46(9)	0.128(26)	0.88(18)	1.15/27/0.28

a) This table is explained in detail in sect. 7.2. Uncertainties in least significant figures are given in brackets.

b) Presented are: reduced chi-square value/number of cycles/probability that a larger chi-square is found when the experiment is repeated.

rotation and the centre of the beam spot on the scattering foil. This and possible other residual correction terms were measured in the additional zero-measurements with the source simulator.

The degree of transverse polarization of the beam entering the polarimeter, P_T, is deduced from

$$P_T S_{an} = \delta_{corr}(117^o) - \delta^0_{corr}(117^o). \tag{7.8}$$

Here, $\delta^0_{corr}(117^o)$ is the corrected asymmetry for the source simulator, calculated from a relation similar to eq. 7.7. These additional zero-measurements are necessary for high-precision experiments. Most values of $\delta^0_{corr}(117^o)$ (see column 5 of table 7.1) are positive and of order 0.003. This size, though small with respect to $\delta_{corr}(117^o)$, is not completely understood. A beam shift y of about 1 mm would explain it, but shifts larger than 0.5 mm seem rather unrealistic. For the result 7.11 (see later) which is compared with theory, the magnitude of $\delta^0_{corr}(117^o)$ is, on the average, about 7% of $\delta_{corr}(117^o)$.

The values of S_{an} given in column 6 of table 7.1 were deduced from the calibration value 5.6, applying small corrections for energy differences, as explained in sect. 5.4.

The degree of longitudinal polarization P_s of the analysed β-particles at the moment of leaving the source follows from

$$P_T(E') = D_a P_s(E_{av}) \tag{7.9}$$

(see eqs. 7.2 and 7.5). The factor D_a accounts for depolarization in the apparatus. We concluded from relations given by Tolhoek (Tol56) for the motion of polarized particles in electromagnetic fields, that the longitudinal electrostatic fields in preaccelerator and main accelerator and the longitudinal magnetic fields of the lenses leave the electron polarization unchanged. Transverse magnetic field components due to fringing fields of the lenses rotate the direction of the electrons at the same rate as the longitudinal electron spin and leave the degree of longitudinal polarization of the beam unaffected. The influence of incomplete spin rotation in the deflector is smaller than 0.1%. Thus, depolarization in the apparatus is mainly due to the aperture of the diaphragm system of lens L_1 (subsect. 5.2.4). By averaging the longitudinal spin component over this aperture we obtained D_a = 0.980 ± 0.005 (including the small correction discussed in connection with eq. 7.5).

Our results for P_s (not given explicitely in table 7.1) are presented in fig. 7.2.

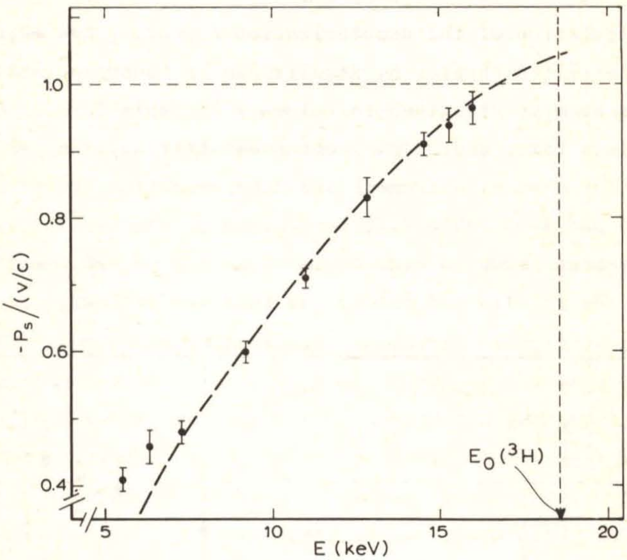

Fig. 7.2. Results for the polarization P_s of the β-particles at the moment of leaving the source, as function of energy. Indicated errors are statistical. The curve represents a least-squares fit of the data to a quadratic function. For comments, see main text.

Originally, we intended to extrapolate these results to the tritium end-point energy, having in mind that at this energy depolarization in the source is practically absent, so that the thus obtained polarization value can be directly compared with theory. For example, the fit to a quadratic function shown in fig. 7.2 gives as extrapolated polarization value (divided by $-v/c$): 1.04 ± 0.04. We abandonned this approach for two reasons. In the first place, the extrapolated result depends on polarization measurements at lower energies which are not very reliable, as discussed in sect. 5.3 and subsect. 6.3.3. Furthermore, the result of the extrapolation depends rather sensitively on the adopted functional dependence of P_s on E, which dependence is not sufficiently well known beforehand.

Instead, we applied a correction for depolarization in the source. According to eq. 6.14 the polarization P of the β-particles at the moment of emission by the tritium atoms follows from

$$P_s = D_s P. \tag{7.10}$$

The calculation of the depolarization factor D_s has been explained in detail in chapter 6. Results can be found in table 6.2, while values of $D_s D_a$ are given in column 7 of table 7.1.

The values for P and $P/(v/c)$ obtained after applying the above corrections for beam misalignment and depolarization are presented in columns 8 and 9 of table 7.1, respectively. The results for P have already been shown in fig. 2.2 as function of v/c. In fig. 7.3 we show the results for $P/(v/c)$ as function of energy.

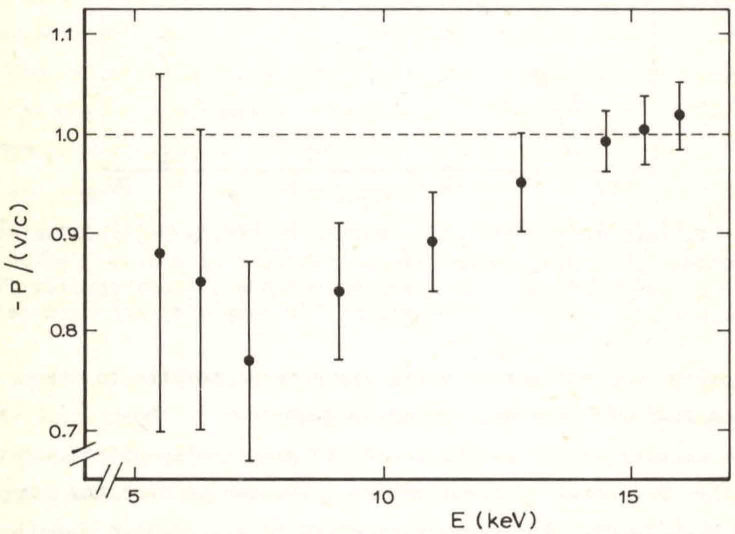

Fig. 7.3. Results for the polarization P of the β-particles at the moment of emission by the tritium atoms, as function of energy. Indicated errors include all known sources of error.

In the last column of table 7.1 an indication is given of the statistical consistency of the results for P of the various measurement cycles collected at one and the same energy setting.

Tabulated is: (i) the reduced chi-square value, i.e. the value of chi-square divided by the number of degrees of freedom, which is in our case one less than the number of cycles; (ii) the number of cycles and (iii) the probability that a larger chi-square is obtained when the experiment is repeated (taken from ref. Bev69). All these probabilities lie between 0.21 and 0.95, which is acceptable.

The values for $-P/(v/c)$ obtained with arrangement I and the 120 $\mu g/cm^2$ source are: 1.12 ± 0.14 at 15.8 keV; 1.08 ± 0.14 at 14.1 keV; 1.02 ± 0.15 at 12.1 keV and 1.10 ± 0.25 at 10.1 keV. Within error limits the results obtained with arrangements I and II are consistent, but the errors with arrangement I are much larger.

7.3. Comparison with theory and with other polarization results

For comparison with theory we only use the three polarization values obtained with the 23 $\mu g/cm^2$ source and arrangement II at the highest energy settings (see table 7.1). For these results the depolarization correction is small and sufficiently accurate. At lower energies it becomes large and less accurate. Besides, spurious electrons may interfere at lower energies, as discussed in sect. 5.3 and subsect. 6.3.3. Therefore, we give as our final result for the longitudinal polarization of β-particles emitted in the decay of tritium the weighted average of the values at the three highest energies only:

$$P(^3H) = -(1.005 \pm 0.026)\ v/c, \tag{7.11}$$

at a mean energy of 15.2 keV and a corresponding mean velocity of 0.24 c. The given error is one standard deviation and includes all known sources of error (see table 7.1): counting statistics (1.4%) and errors in the polarimeter efficiency S_{an} (1.4%), in the depolarization correction (1.6%) and in the energy calibration of the apparatus (0.7%). The various errors were added quadratically.

The two-component neutrino theory discussed in subsect. 1.2.3 predicts for allowed transitions: $P = -v/c$ (for β^--particles), apart from corrections for higher-order transitions, finite nuclear size and screening by atomic electrons. These corrections can be completely neglected in our experiment (see sect. 2.2). Thus, our result 7.11, obtained with a calibrated polarimeter, with extensive checks on instrumental asymmetries and from measurements near the end point of the spectrum, agrees excellently with the theoretical prediction. In the next chapter we discuss the magnitude of the ratios C'_V/C_V and C'_A/C_A, using the result 7.11.

Most of the earlier measurements on other allowed and first-forbidden transitions yielded too low polarization values at intermediate velocities ($0.4 \lesssim v/c \lesssim 0.6$), as shown in the compilation of data of fig. 2.2. The intermediate-velocity data refer to the decays of ^{60}Co (E_o = 313 keV), ^{147}Pm (E_o = 225 keV) and ^{198}Au (E_o = 962 keV); details on energy settings can be found in this figure. Because our result 7.11 confirms the relation $P = -v/c$ at much lower velocities, we propose to ascribe these earlier deviations to instrumental effects rather than to fundamental shortcomings of the theory. The most obvious cause of the deviations may be an underestimate of the depolarization in the source material. However, several investigators (Eck64; Kli66) used thin sources in which depolarization can hardly be disastrous. Nevertheless, measurements close to the end-point energy and with preselection of energy are safer in view of scattering and straggling of unwanted higher-energy electrons in the source or in other parts of the arrangement. The use of calculated values for the polarimeter efficiency S_{an} may also cause too low polarization results at intermediate velocities because it can not be excluded that the theoretical Mott asymmetry functions S, from which the calculated S_{an}-values are derived, are too large at intermediate velocities: double-scattering experiments (Mik63; Kli65,66a; Boe71) at intermediate velocities yield lower S-values than expected theoretically, while at higher velocities theory and experiment agree.

We do not know how to explain the low polarization values of Eckardt et al. (Eck64). Their results have been obtained with one and the same polarimeter setting at 100 keV by changing the source potential. Their data were not corrected for depolarization in the source material, but we agree with the authors that the given source conditions do not suggest large corrections.

We also have no certain explanation for the previous Groningen results (Kli66) at intermediate velocities obtained with an absolutely calibrated polarimeter, but we remark that these lower values have a large error margin and that these results have not been checked with a precise source simulator. We note that a part of the deviations for the high-Z nuclei ^{147}Pm and ^{198}Au may be caused by an underestimate of the screening factor Λ (see sect. 2.2).

Bienlein et al. (Bie59) were among the first investigators who obtained precise results at higher energies. They proposed to ascribe a deviation of 16% at 120 keV for ^{60}Co to the influence of screening on their calculated S_{an}-value. However, the calculations of Lin (Lin64) and Bühring (Büh68) showed that this effect is less than 3% and offers no explanation.

Lazarus and Greenberg (Laz70) are the only investigators who report $P \approx -v/c$ at intermediate velocities (fig. 2.2). However, their data contain an unexplained discrepancy between the (large) intensity of back-scattered and consequently depolarized electrons and the (small) correction for depolarization by the source backing, given by the authors. We remark that their polarimeter was equipped with two polarization sensitive detectors at $\theta = 70^{\circ}$. Instrumental asymmetries were measured using unpolarized conversion electrons. In our experience the sensitivity to instrumental asymmetries is much larger at forward angles than at backward angles: for decreasing scattering angles the magnitude of instrumental asymmetries increases as ctg $\frac{\theta}{2}$ (Kli65,66a), while polarization asymmetries become relatively small (especially at lower energies) since the polarimeter efficiency S_{an} decreases. For an accurate determination of instrumental asymmetries we prefer two extra detectors placed at $\theta \approx 45^{\circ}$ combined with the use of a precise source simulator.

8.1. Introduction

As discussed in sect. 1.2 the experimental features of β-decay are consistent with lepton conservation, time-reversal invariance, V,A-interaction and two-component neutrino theory with left-handed neutrinos. The latter implies that the parity-conserving and the parity-violating coupling constants in the interaction hamiltonian are equal: $C_i = C'_i$, with i = V (vector) or A (axial vector).

Information about the ratios C'_i/C_i can be obtained from experimental results for the degree of longitudinal polarization of β-particles or neutrinos and for the β-γ circular polarization correlation. The observables due to parity violation contain C'_i/C_i in a form

$$x_i = 2C_iC'_i/(C_i^2 + C_i'^2) \tag{8.1}$$

($-1 \leq x_i \leq +1$). For $C'_i \approx C_i$, this "parity factor" x_i is insensitive to the value of C'_i/C_i (see fig. 8.1). Therefore, a high precision is needed to set even modest limits on possible deviations of C'_i/C_i from unity. For pure Fermi or Gamow-Teller transitions these limits are independent of assumptions on the magnitude of the nuclear matrix elements.

In a survey study published in 1965 Steffen and Frauenfelder (Ste65) suggested the limits:

$$0.4 < C'_V/C_V < 2.5 \quad \text{and} \quad 0.85 < C'_A/C_A < 1.15 \,. \tag{8.2}$$

The limits for C'_V/C_V came from positron polarization measurements on pure Fermi transitions, while the limits for C'_A/C_A were derived from β-γ circular polarization correlation data. We have to remark that the statistical interpretation of these limits is not clear. For instance, the range for C'_A/C_A was based on β-γ circular polarization correlation experiments for ^{60}Co which yielded x_A = 1.020 ± 0.030 and for ^{22}Na yielding x_A = 1.038 ± 0.054. Since the

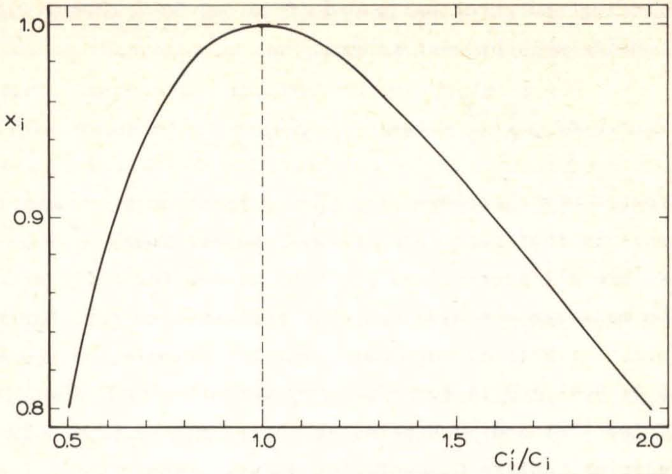

Fig. 8.1. Dependence of $x_i = 2C_iC_i'/(C_i^2 + C_i'^2)$ *on the ratio* C_i'/C_i $(i = V,A)$ *around* $C_i'/C_i = 1$.

theoretical value of x_A cannot be larger than 1, the C_A'/C_A-range was obtained from the lower limit for x_A of about 0.99. The range given is only indicative, since it is strongly determined by the "lucky circumstance" that the experimental x_A-values lie rather far above the extreme value 1. A more accurate experimental result $x_A = 0.99 \pm 0.02$, for instance, would give a considerably broader range for C_A'/C_A. In the following section we give a somewhat more detailed account on confidence levels for error limits of coupling-constant ratios.

Paul (Pau70) reported in 1970 from an extensive least-squares adjustment procedure to data from the literature:

$$C_V'/C_V = 0.82 {}^{+0.40}_{-0.13} \quad \text{and} \quad C_A'/C_A = 1.10 \pm 0.06 . \qquad (8.3a)$$

The range for C_A'/C_A might give a suggestion that C_A'/C_A deviates from unity. However, as remarked already in subsect. 1.2.1, Paul's error limits are external errors which are about 2.4 times smaller than the internal ones. Later, Kropf and Paul (Kro74) felt it safer (as we do) to use the larger of the internal and external errors. Enlarging the error estimates of (8.3a) by a factor 2.4 gives the considerably broader ranges:

$$C'_V/C_V = 0.82 \begin{smallmatrix}+\,0.97\\-\,0.32\end{smallmatrix} \quad \text{and} \quad C'_A/C_A = 1.10 \pm 0.15. \qquad (8.3b)$$

The reason why the ranges for C'_V/C_V are so much braoder than the C'_A/C_A-ones is that pure Fermi decays (superallowed $0^+ \to 0^+$ transitions) are all short-lived positron decays for which accurate polarization measurements have not been performed so far. Experimental results for $P/(v/c)$ were obtained, for example, by Deutsch et al. (Deu57: 0.95 ± 0.14 for ^{34}Cl), by Gerhart et al. (Ger59: 0.73 ± 0.17 for ^{14}O) and by Hopkins et al. (Hop61: 0.97 ± 0.19 for ^{14}O). In addition, unlike Gamow-Teller decays, Fermi transitions show no β-asymmetry and no β-γ circular polarization correlation.

In the next section we show that narrower limits for C'_V/C_V follow from our tritium β-polarization measurement.

8.2. Limits obtained from the present investigation

If lepton conservation, time-reversal invariance and V,A-interaction are assumed and if the influence of screening, finite nuclear size and higher-order transitions is neglected, the theoretical expression for the degree of longitudinal polarization of β^--particles emitted in an allowed transition is (rewriting eq. 1.36 and using eq. 8.1)

$$\begin{aligned} -P/(v/c) &= 1 - \rho_m (C_V - C'_V)^2/(C_V^2 + C_V'^2) - (1-\rho_m)(C_A - C'_A)^2/(C_A^2 + C_A'^2) \\ &= \rho_m x_V + (1-\rho_m) x_A \,. \end{aligned} \qquad (8.4)$$

Here, the mixing parameter

$$\rho_m = (C_V^2 + C_V'^2)\, |M_F|^2 \Big/ \Big[(C_V^2 + C_V'^2)\, |M_F|^2 + (C_A^2 + C_A'^2)\, |M_{GT}|^2 \Big] \qquad (8.5)$$

is a measure for the relative strengths of the Fermi and the Gamow-Teller contributions to the transition under consideration: its value lies between 0 (pure Gamow-Teller transition) and 1 (pure

Fermi transition). It is seen from eq. 8.4 that for any set of values of the coupling constants the theoretical value of $-P/(v/c)$ is restricted to the interval $-1 \leq -P/(v/c) \leq 1$.

The value of ρ_m for the tritium decay can be found by substituting in eq. 8.5 values for $\lambda^2 = (C_A^2 + C_A'^2)/(C_V^2 + C_V'^2)$ (subsect. 1.2.2) and for $|M_F(^3H)|$ and $|M_{GT}(^3H)|$ (sect. 3.5). More directly, however, $\rho_m(^3H)$ is found from the expression

$$\rho_m(^3H) = ft(^3H)\ |M_F(^3H)|^2 \ / \ \left[ft(0^+ \rightarrow 0^+)\ |M_F(0^+ \rightarrow 0^+)|^2\right] \quad (8.6)$$

(see eq. 1.31). Using $|M_F(^3H)| = 1$ (sect. 3.5), $ft(^3H) = 1157 \pm 4$ sec (eq. 3.4), $|M_F(0^+ \rightarrow 0^+)|^2 = 2$ and $ft(0^+ \rightarrow 0^+) = 3085 \pm 5$ sec (subsect. 1.2.2) one obtains $\rho_m(^3H) = 0.1875 \pm 0.0007$.

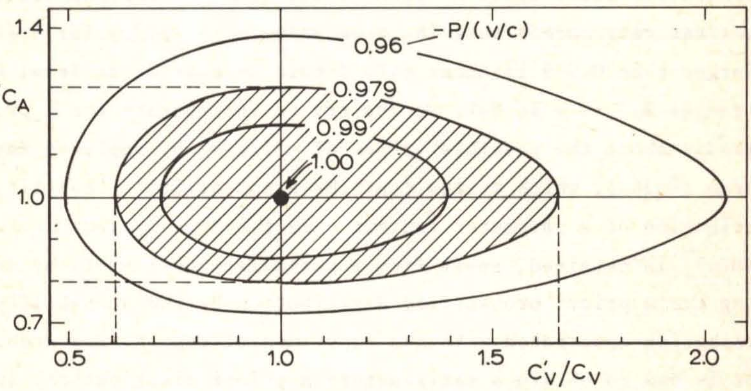

Fig. 8.2. Iso-polarization contours as calculated for various degrees of longitudinal polarization of β-particles from the tritium decay. The experimental P-value confines C_V'/C_V and C_A'/C_A to the shaded area.

In fig. 8.2 some iso-polarization contours for the tritium transition are presented which were calculated from eq. 8.4, using the above value of $\rho_m(^3H)$. In this figure we have shaded the area allowed for C_V'/C_V and C_A'/C_A if the tritium result $-P/(v/c) = 1.005 \pm 0.026$ (eq. 7.11) is interpreted as $-P/(v/c) \geq 0.979$ ($= 1.005 - 0.026$). By taking the extremes of the contour for $-P/(v/c) = 0.979$ (see fig. 8.2) we obtained

$$0.61 < C'_V/C_V < 1.65 \quad \text{and} \quad 0.80 < C'_A/C_A < 1.26. \quad (8.7)$$

These limits do not depend sensitively on the value of ρ_m. Effectively C'_A/C_A has been considered as a free parameter for obtaining the limits for C'_V/C_V, and vice versa. The C'_V/C_V-range is much narrower than in eq. 8.2 and somewhat narrower than in eq. 8.3b. The range for C'_A/C_A is somewhat broader than the ranges given in these equations.

The statistical procedure leading to the limits 8.7 is essentially the same as was used for obtaining the limits 8.2 and is, as remarked, not unambiguous. Strictly speaking, the a priori knowledge that the "true" value of $-P/(v/c)$ must lie between -1 and $+1$ should be incorporated. When this a priori knowledge is ignored, our experimental result $-P/(v/c) = 1.005 \pm 0.026$ means that the probability (in "inverse probability" sense: see ref. Hud64) that the true value of $-P/(v/c)$ for tritium is larger than 0.979 is about 84%. Then, the confidence level for the ranges 8.7 is also 84%. We may try to incorporate the a priori knowledge about the possible values of $-P/(v/c)$ by applying Bayes theorem (Hud64), which states that the a posteriori probability distribution of a parameter [in our case the "true" value of $-P/(v/c)$] is obtained, apart from a normalization factor, by multiplying the a priori probability distribution by the probability distribution associated with the experimental result. The problematic point is how to obtain a satisfactory a priori distribution. In the spirit of Bayes we may define the a priori probability density of $-P/(v/c)$ as equal to one for $|P/(v/c)| \leq 1$ and as zero elsewhere. This means that each value of $-P/(v/c)$ between -1 and $+1$ is assumed to be equally probable a priori. Because the probability distribution associated with the experimental result is Gaussian (with a mean value of 1.005 and a standard deviation of 0.026) the a posteriori probability distribution becomes a Gaussian function truncated at $-P/(v/c) = 1$. It turns out that the a posteriori probability that the true value of $-P/(v/c)$ lies between 0.979 and 1.000 is 63%, while there is a chance of 37% that this parameter has a value below 0.979. This means that, in this approach, the confidence level of the ranges 8.7 is 63%. However, the choice of the a priori probability is rather arbitrary: if one assumes that C'_i/C_i has a constant a priori probability, a confidence level of about 80% for the ranges 8.7 is found. In conclusion, we assume a confidence level for the ranges 8.7 of about 70%.

The possibility to obtain limits for C'_V/C_V from a polarization measurement on a mixed transition remains restricted to decays between mirror nuclei. The reason is that all other mixed transitions are isospin forbidden ($\Delta T \neq 0$), so that the Fermi matrix element is small (Sch66, Ram75). As discussed in sect. 3.2, all transitions between mirror nuclei are β^+-transitions, apart from the neutron and the tritium decay. The accuracy of positron polarization measurements is poor: the most accurate result was obtained using Bhabha scattering and has a claimed accuracy of 9% (Ul161). Longitudinal polarization measurements for the decay of the free neutron have not been attempted so far, and will be hardly feasible. Thus, the tritium decay remains as the only suitable mixed transition for obtaining limits on C'_V/C_V.

REFERENCES

Ava62 R.O. Avakyan, G.L. Bayatyan, M.E. Vishnevskii and E.V. Pushkin, Sov. Phys. JETP 14 (1962) 491.

Bat60 V.V. Batygin and I.N. Toptygin, Sov. Phys. JETP 37 (10) (1960) 975.

Beh69 H. Behrens and J. Jänecke, Numerical tables for beta decay and electron capture, Landolt-Börnstein, New Series (Springer, Berlin, 1969) Vol. I/4.

Ber63 I. Bergström, F. Brown, J.A. Davies, J.S. Geiger, R.L. Graham and R. Kelly, Nucl. Instr. 21 (1963) 249.

Ber64 M.J. Berger and S.M. Seltzer, in Studies in penetration of charged particles in matter (Nuclear Science Series, Report Number 39, National Academy of Sciences, Washington, 1964), p. 205.

Ber72 K.-E. Bergkvist, Nucl. Phys. B39 (1972) 317; 371.

Bev69 P.R. Bevington, Data reduction and error analysis for the physical sciences (McGraw-Hill, New York, 1969).

Bie59 H. Bienlein, K. Güthner, H. v. Issendorff and H. Wegener, Nucl. Instr. 4 (1959) 79; Z. Phys. 154 (1959) 376.

Bli73 R.J. Blin-Stoyle, Fundamental interactions and the nucleus (North-Holland, Amsterdam, 1973).

Boe71 H. Boersch, R. Schliepe and K.E. Schriefl, Nucl. Phys. A163 (1971) 625.

Bra66 L. Braicovich, B. de Michelis and A. Fasana, Nucl. Phys. 82 (1966) 645; Phys. Rev. 145 (1966) 952.

Bra67 L. Braicovich, Nuovo Cim. 52A (1967) 566.

Bra68 L. Braicovich, Nuovo Cim. 55A (1968) 609.

Bro62 A.R. Brosi, A.I. Galonsky, B.H. Ketelle and H.B. Willard, Nucl. Phys. 33 (1962) 353.

Büh68 W. Bühring, Z. Phys. 212 (1968) 61.

Cur52 S.C. Curran, Physica 18 (1952) 1161.

Cur57 R.B. Curtis and R.R. Lewis, Phys. Rev. 107 (1957) 543.

Dar68 R. Daris and C. St-Pierre, Nucl. Instr. 64 (1968) 346.

Dar69 R. Daris and C. St-Pierre, Nucl. Instr. 71 (1969) 187.

Dar69a R. Daris and C. St-Pierre, Nucl. Phys. A138 (1969) 545.

Deu57 M. Deutsch, B. Gittelman, R.W. Bauer, L. Grodzins and

A.W. Sunyar, Phys. Rev. 107 (1957) 1733.

Dui69 R.J. van Duinen, thesis, Groningen, 1969.

Eck64 V. Eckardt, A. Ladage and U.V. Moellendorff, Phys. Lett. 13 (1964) 53.

Eic63 J.F. Eichelberger, G.R. Grove and L.V. Jones, Mound Lab. progress report MLM1160 (Miamisburg, Ohio, 1963).

Fer34 E. Fermi, Z. Phys. 88 (1934) 161.

For57 G.W. Ford and C.J. Mullin, Phys. Rev. 108 (1957) 477.

Fra57 H. Frauenfelder, R. Bobone, E. von Goeler, N. Levine, H.R. Lewis, R.N. Peacock, A. Rossi and G. De Pasquali, Phys. Rev. 106 (1957) 386.

Fra68 H. Frauenfelder and R.M. Steffen, in Alpha-, beta- and gamma-ray spectroscopy, ed. K. Siegbahn (North-Holland, Amsterdam, 1968), vol. 2, ch. XXIV F.

Fra74 H. Frauenfelder and E.M. Henley, Subatomic Physics (Prentice-Hall, Englewood Cliffs, N.J., 1974).

Ger59 J.B. Gerhart, F.H. Schmidt, H. Bicksel and J.C. Hopkins, Phys. Rev. 114 (1959) 1095.

Gol58 M. Goldhaber, L. Grodzins and A.W. Sunyar, Phys. Rev. 109 (1958) 1015.

Gun60 E.M. Gunnersen and G. James, Nucl. Instr. 8 (1960) 173.

Har75 J.C. Hardy and I.S. Towner, Nucl. Phys. A254 (1975) 221.

Hol64 G. Holzwarth and H.J. Meister, Nucl. Phys. 59 (1964) 56.

Hop61 J.C. Hopkins, J.B. Gerhart, F.H. Schmidt and J.E. Stroth, Phys. Rev. 121 (1961) 1185.

Hud64 D.J. Hudson, Maximum likelihood and least-squares theory (CERN 64-18, Geneva, 1964).

Jac57 J.D. Jackson, S.B. Treiman and H.W. Wyld Jr., Phys. Rev. 106 (1957) 517; Nucl. Phys. 4 (1957) 206.

Jon55 W.M. Jones, Phys. Rev. 100 (1955) 124.

Kab73 S.M. Kabir, Nucl. Instr. 109 (1973) 533.

Kan57 H. Kanter, Ann. der Phys. 20 (1957) 144.

Kau54 S. Kaufman and W.F. Libby, Phys. Rev. 93 (1954) 1337.

Kei60 E. Keil, E. Zeitler and W. Zinn, Z. Naturf. 15a (1960) 1031.

Kes76 J. Kessler, Polarized electrons (Springer, Berlin, 1976).

Kli65 J. van Klinken, thesis, Groningen, 1965.

Kli65a J. van Klinken, Nucl. Phys. 61 (1965) 593.

Kli65b J. van Klinken, unpublished results, 1965.

Kli66 J. van Klinken, Nucl. Phys. 75 (1966) 145.

Kli66a J. van Klinken, Nucl. Phys. 75 (1966) 161.

Kno65 G. Knop and W. Paul, in Alpha-, beta- and gamma-ray spectroscopy, ed. K. Siegbahn (North-Holland, Amsterdam, 1965), vol. 1, ch. I.

Kof62 O. Kofoed-Hansen and C.J. Christensen, in Handbuch der Physik, ed. S. Flügge (Springer, Berlin, 1962), vol. XLI/2.

Kok76 F.W.J. Koks and J. van Klinken, Nucl. Phys. A272 (1976) 61.

Kro74 A. Kropf and H. Paul, Z. Phys. 267 (1974) 129.

Kul54 H. Kulenkampff and K. Rüttiger, Z. Phys. 137 (1954) 426.

Kul58 H. Kulenkampff and K. Rüttiger, Z. Phys. 152 (1958) 249.

Lad61 A. Ladage, thesis, Hamburg, 1961.

Laz70 D.M. Lazarus and J.S. Greenberg, Phys. Rev. D2 (1970) 45.

Led67 C.M. Lederer, J.M. Hollander and I. Perlman, Table of Isotopes (Wiley, New York, 1967).

Lee56 T.D. Lee and C.N. Yang, Phys. Rev. 104 (1956) 254.

Lee57 T.D. Lee and C.N. Yang, Phys. Rev. 105 (1957) 1671.

Lew70 V.E. Lewis, Nucl. Phys. A151 (1970) 120.

Lin64 S.R. Lin, Phys. Rev. 133 (1964) A965.

Lob62 V.M. Lobashov and V.A. Nazarenko, Sov. Phys. JETP 15 (1962) 247.

Mik63 L. Mikaélyan, A. Borovoi and E. Denisov, Nucl. Phys. 47 (1963) 328.

Mol47 G. Molière, Z. Naturf. 2a (1974) 133.

Mor59 M. Morita, Phys. Rev. 114 (1959) 1080.

Mot29 N.F. Mott, Proc. Roy. Soc. (London) A124 (1929) 425.

Mot32 N.F. Mott, Proc. Roy. Soc. (London) A135 (1932) 429.

Mot64 J.W. Motz, H. Olsen and H.W. Koch, Rev. Mod. Phys. 36 (1964) 881.

Mot65 N.F. Mott and H.S. Massey, The theory of atomic collisions (Clarendon Press, Oxford, 1965).

Müh59 B. Mühlschlegel, Z. Phys. 155 (1959) 69.

Nel59 D.F. Nelson and R.W. Pidd, Phys. Rev. 114 (1959) 728.

Oms68 J. Oms, P. Erman and S. Hultberg, Ark. Phys. 39 (1968) 573.

Owe48 G.E. Owen and H. Primakoff, Phys. Rev. 74 (1948) 1406.

Pas60 G. Passatore, Nuovo Cim. 18 (1960) 532.

Pau57 W. Pauli, Nuovo Cim. 6 (1957) 204.

Pau70 H. Paul, Nucl. Phys. A154 (1970) 160.

Pie73 W.F. Piel, Nucl. Phys. A203 (1973) 369.

Ple72 F. Pleiter, thesis, Groningen, 1972.

Pos57 H. Postma, W.J. Huiskamp, A.R. Miedema, M.J. Steenkamp, H.A. Tolhoek and C.J. Gorter, Physica 23 (1957) 259.

Pos58 H. Postma, W.J. Huiskamp, A.R. Miedema, M.J. Steenkamp, H.A. Tolhoek and C.J. Gorter, Physica 24 (1958) 157.

Pos60 H. Postma, thesis, Groningen, 1960.

Pri70 H. Primakoff, Springer tracts in modern physics 53 (1970) 7.

Ram75 S. Raman, T.A. Walkiewicz and H. Behrens, Atomic data and nuclear data tables, 16 (1975) 451.

Reb64 H. Rebel, G. Schatz and W. Bühring, Z. Phys. 180 (1964) 392.

Röd74 B. Röde, Z. Naturf. 29a (1974) 261.

Ros61 M.E. Rose, Relativistic electron theory (Wiley, New York, 1961).

Rus50 A.A. Rusterholz, Elektronenoptik I (Birkhäuser, Basel, 1950), p. 94.

Rut34 E. Rutherford, P. Harteck and M.L.E. Oliphant, Nature 133 (1934) 413.

Ryu75 H. Ryu, Memoirs of the faculty of engineering Hiroshima University, Vol. 5, No. 3 (Serial No. 17), febr. 1975.

Sal69 R.C. Salgo and H.H. Staub, Nucl. Phys. A138 (1969) 417.

Sch66 H.F. Schopper, Weak interactions and nuclear beta decay (North-Holland, Amsterdam, 1966).

Sch68 G.R. Schwarz, R. Löhken and H. Rebel, Z. Phys. 217 (1968) 465.

Shl75 S. Shlomo and D.O. Riska, Nucl. Phys. A254 (1975) 281.

Ste59 R.M. Steffen, Phys. Rev. 115 (1959) 980.

Ste65 R.M. Steffen and H. Frauenfelder, in Alpha-, beta- and gamma-ray spectroscopy, ed. K. Siegbahn (North-Holland, Amsterdam, 1965), vol. 2, ch. XXIV G.

Tol63 H.A. Tolhoek, Selected topics in nuclear theory (International Atomic Energy Agency, Vienna, 1963).

Tol65 H.A. Tolhoek, Rev. Mod. Phys. 28 (1956) 277.

Ull61 J.D. Ullman, H. Frauenfelder, H.J. Lipkin and A. Rossi, Phys. Rev. 122 (1961) 536.

Waa57 H. de Waard and O.J. Poppema, Physica 23 (1957) 597.

Weg58 H. Wegener, Z. Phys. 151 (1958) 252.

Wen67 H. Wenninger, J. Stiewe, H. Muusz and H. Leutz, Nucl. Phys. A96 (1967) 177.

Wey29 H. Weyl, Z. Phys. 56 (1929) 330.

Wu 57 C.S. Wu, E. Ambler, R.W. Hayward, D.D. Hoppes and R.P. Hudson, Phys. Rev. 105 (1957) 1413; 106 (1957) 1361.

Wu 66 C.S. Wu and S.A. Moszkowski, Beta decay (Wiley, New York, 1966).

Zwo45 V.K. Zworykin, G.A. Morton, E.G. Ramberg, J. Hillier and A.W. Vance, Electron optics and the electron microscope (Wiley, New York, 1945), p. 447.

SAMENVATTING

In dit proefschrift wordt een onderzoek beschreven van de longitudinale polarisatiegraad van β-deeltjes met lage snelheden. Het onderzoek werd verricht met β-deeltjes afkomstig van het toegestane verval van tritium.

Nadat in 1956 bleek dat het β-verval niet spiegelings invariant is heeft de zogenoemde twee componenten neutrino theorie algemeen ingang gevonden. Uit de experimenten volgde verder dat neutrinos linkshandig zijn en dat de interactie een (V-λA)-karakter heeft. Een twee componenten theorie met linkshandige neutrinos impliceert dat de "pariteit-behoudende" en de "pariteit-niet-behoudende" koppelingsconstanten in de interactiehamiltoniaan even groot zijn: $C'_V = C_V$ voor vector interactie en $C'_A = C_A$ voor axiale vector interactie. Een direct gevolg hiervan is dat de longitudinale polarisatiegraad van β^--deeltjes bij toegestaan β-verval in essentie gegeven wordt door de eenvoudige relatie $P= -v/c$, waarbij v de snelheid is van de electronen en c de lichtsnelheid. Deze relatie is inderdaad bevestigd door een aantal nauwkeurige experimenten voor energiewaarden boven ongeveer 120 keV, overeenkomend met snelheden groter dan $0.6c$. Voor snelheden $0.4 \lesssim v/c \lesssim 0.6$, waarvoor de experimentele moeilijkheden snel toenemen, zijn echter grote afwijkingen gerapporteerd, terwijl er tot nu toe nog geen metingen waren verricht bij energieën lager dan 40 keV ($v/c = 0.37$).

Het doel van dit onderzoek was het nauwkeurig meten van de polarisatiegraad bij zeer lage snelheden, om te zien of bij lage energieën inderdaad afwijkingen optreden.

Het tritiumverval werd gekozen voor dit onderzoek vanwege zijn zeer lage eindpuntsenergie van 18,6 keV ($v/c = 0.26$). De overgang is bovendien van belang omdat deze plaatsvindt tussen spiegelkernen, zodat zowel de Fermi als de Gamow-Teller vervalswijzen optreden. Bij voldoende nauwkeurigheid kan een polarisatiemeting van belang zijn voor het stellen van grenzen aan de verhoudingen C'_V/C_V en C'_A/C_A.

Polarisatiemetingen zijn verricht voor energiewaarden tussen 5.5 en 16.0 keV ($0.15 < v/c < 0.25$). Na energieselectie werden de electronen versneld tot een energie van 79 keV. De polarisatiegraad werd gemeten met een absoluut geijkte Mott polarimeter. Instrumentele asymmetrieën werden zoveel mogelijk gereduceerd met behulp van twee extra tellers en bovendien met behulp van een bron die ongepolariseerde electronen uitzond. Aangetoond werd dat de depolarisatie in de bron gering is in de buurt van de eindpuntsenergie.

Het uiteindelijke resultaat voor de longitudinale polarisatiegraad van de β-deeltjes met een gemiddelde energie van 15.2 keV (v = 0.24c) is

$$P(^3H) = -(1.005 \pm 0.026)\ v/c.$$

Vanwege de goede overeenstemming van dit resultaat met de theorie stellen wij voor om vroegere polarisatiemetingen aan andere toegestane overgangen die bij snelheden lager dan 0.6c afwijkingen te zien gaven te negeren. Het polarisatieresultaat leidt tot de volgende grenzen voor de verhoudingen van de koppelingsconstanten: $0.61 < C'_V/C_V < 1.65$ en $0.80 < C'_A/C_A < 1.26$. In het bijzonder de C'_V/C_V-grenzen zijn van belang omdat ze nauwkeuriger zijn dan de grenzen verkregen uit alle andere relevante pariteitsexperimenten samen.

9242
1977